AD_____

Award Number: DAMD17-02-1-0582

TITLE: In Situ Evaluation of the Role of the Small GTPase Rac3 in Breast Cancer

PRINCIPAL INVESTIGATOR: Suranganie F. Dharmawardhane, Ph.D.

CONTRACTING ORGANIZATION: The University of Texas at Austin
Austin, TX 78713-7727

REPORT DATE: July 2005

TYPE OF REPORT: Final

PREPARED FOR: U.S. Army Medical Research and Materiel Command
Fort Detrick, Maryland 21702-5012

REPORT DOCUMENTATION PAGE

Form Approved
OMB No. 0704-0188

1. REPORT DATE	2. REPORT TYPE	3. DATES COVERED
01-07-2005	Final	1 Apr 2002 – 30 Jun 2005

4. TITLE AND SUBTITLE

In Situ Evaluation of the Role of the Small GTPase Rac3 in Breast Cancer

5a. CONTRACT NUMBER

5b. GRANT NUMBER
DAMD17-02-1-0582

5c. PROGRAM ELEMENT NUMBER

6. AUTHOR(S)

Suranganie F. Dharmawardhane, Ph.D.

5d. PROJECT NUMBER

5e. TASK NUMBER

5f. WORK UNIT NUMBER

7. PERFORMING ORGANIZATION NAME(S) AND ADDRESS(ES)

The University of Texas at Austin
Austin, TX 78713-7727

8. PERFORMING ORGANIZATION REPORT NUMBER

9. SPONSORING / MONITORING AGENCY NAME(S) AND ADDRESS(ES)
U.S. Army Medical Research and Materiel Command
Fort Detrick, Maryland 21702-5012

10. SPONSOR/MONITOR'S ACRONYM(S)

11. SPONSOR/MONITOR'S REPORT NUMBER(S)

12. DISTRIBUTION / AVAILABILITY STATEMENT
Approved for Public Release; Distribution Unlimited

13. SUPPLEMENTARY NOTES

14. ABSTRACT
To test the hypothesis that the signaling protein Rac3 is critical for the initiation of breast cancer metastasis, we created stable fluorescently-tagged breast cancer cell lines that express active and inactive forms of Rac3 and its close homolog Rac1 in a highly metastatic variant of the MDA-MB-435 metastatic breast cancer cell line. Dominant active forms of Rac3 and Rac1 were stably expressed in a low metastatic variant of MDA-MB-435. High metastatic cell lines expressing dominant negative Rac1 or Rac3 demonstrated similar reduction in invasion and migration *in vitro* compared to controls. Cell lines expressing a dominant negative Rac1 or Rac3 did not show differences in proliferation; however, when implanted in nude mice, both cell lines produced smaller primary tumors that demonstrated reduced metastasis compared to controls. Expression of dominant active Rac1 or Rac3 in a low metastatic breast cancer cell variant resulted in enhanced migratory and invasive properties. The metastatic efficiency of the Rac1 or Rac3 mutant cells was analyzed in the nude mouse model of experimental metastasis. Mammary tumors from cells expressing Rac1 or Rac3 dominant active mutations were more metastatic while the mammary tumors from cells expressing dominant negative Rac1 or Rac3 were less metastatic when compared to controls. To provide a direct assessment of these mutant cell lines, we developed a fluorescence illumination system to specifically image fluorescence breast cancer progression in live mice.

15. SUBJECT TERMS
Rac3, PAK, breast cancer metastasis, live image analysis

16. SECURITY CLASSIFICATION OF:			17. LIMITATION OF ABSTRACT	18. NUMBER OF PAGES	19a. NAME OF RESPONSIBLE PERSON
					USAMRMC
a. REPORT	b. ABSTRACT	c. THIS PAGE			19b. TELEPHONE NUMBER *(include area code)*
U	U	U	UU	91	

Table of Contents

Introduction

Cancer metastasis is a complex multistep process in which malignant cells escape from a primary tumor, invade surrounding tissue, migrate through the extracellular matrix (ECM), and are transported via the circulatory system to establish secondary tumors at distant sites (1-3). Rho GTPases are key regulatory molecules that have been implicated in cell invasion and migration (4; 5). The small GTPase Rac3 is a closely related homolog of the Rho GTPases Rac1 and Cdc42, which have been shown to regulate actin cytoskeletal reorganization during cell invasion. Exhibiting an 89% and 92% identity to Rac1 and Rac2, respectively, Rac3 differs from other Rac proteins only in the C-terminus, a region essential for subcellular localization and regulatory protein binding (6). Therefore, Rac1 and Rac3 may localize to different regions even though they may have similar functions. In fact, differential localization of Rac1 and Rac3 has been demonstrated in the developing mammalian brain (7). Rac3 has been implicated in breast cancer by being constitutively active in aggressively dividing, high-metastatic breast cancer cell lines and tissues (8). Moreover, ectopic activation of Rac3 in the mammary epithelium has been shown to lead to the formation of mammary lesions (9). Transient expression of dominant active Rac3 activated DNA synthesis and conferred a highly proliferative phenotype to human mammary epithelial cells via activation of a downsteam effector, P21-activated kinase (PAK) (7). PAKs are a group of 62-68 kDa serine/threonine kinases that have been identified as targets of activated Rac and Cdc42 that been implicated in the regulation of breast cancer (10). However, a role for Rac3 and PAK as metastasis promoters *in vivo* has yet to be substantiated.

Hypothesis

We hypothesize that the signaling proteins Rac1, Rac3, and PAK are critical for the first step of metastasis when tumor cells invade the ECM and enter the circulatory system.

Results

A. Vector construction

During the first year of funding, we cloned Rac1, Rac3, and PAK mutant cDNA in to the Tet/OFF (clontech) system to achieve regulation of mutant protein expression via the control of a Tet suppressor. We used a two plasmid Tet/OFF system and successfully created cell lines that expressed the first retroviral plasmid Rev/Tet that had the tetracycline responsive inactivator but did not succeed with creation of stable cell lines that consistently expressed the second plasmid Rev-TRE that contained genes of interest. Therefore, our cloning strategy was changed to the use of bicistronic vectors that express red fluorescent protein (RFP) and the gene of interest as separate proteins (Clontech). These bicistronic vectors contain an internal ribosome entry cite to ensure expression of the gene of interest with an antibiotic resistance marker.

The following well-characterized mutant cDNA were cloned into the bicistronic expression vectors:

1. Rac1 or Rac3 cDNA containing amino acid substitutions that render the expressed protein dominant negative (T17N)
2. Rac1 or Rac3 cDNA containing amino acid substitutions that render the expressed protein dominant active (G12V)
3. Residues 83-149 or 83-149 (L107F) from the auto-inhibitory domain (AID) of PAK1. The AID of PAK has been shown to bind to and inactivate endogenous PAK in the 83-149 form but not in the presence of the L107F amino acid substitution.

B. Characterization of MDA-MB-435 metastatic variants

During the first year of the award, we created cell lines expressing dominant active Rac1 and Rac3 in the Hs578t primary breast cancer cell line, which was proposed as a model system for a non-metastatic cell line. However, we experienced unforeseen difficulties with establishment of primary tumors in the mammary fat pads of nude mice using the Hs578t parental cell line.

Therefore, during the second year of funding, we characterized metastatic variants of MDA-MB-435 cell line as a potential model system. The MDA-MB-435 metastatic variants were created according to α6 integrin expression and relative metastatic efficiency from mammary tumors established in nude mice by our collaborator Dr. Janet Price (UT-MDACC, Houston, TX), as described in (11). Selection of metastatic variants of the same cell line ensured primary tumor establishment with highly aggressive MDA-MB-435 cells and a better assessment of the effect of expressing mutant proteins in a similar genetic background. To determine if the MDA-MB-435 metastatic variants were a suitable model for the present investigation, the variants were first characterized in terms of cell functions relevant to metastasis known to be under Rac regulation. Our investigation of the role of Rac isoforms on metastatic functions of MDA-MB-435 metastatic variants *in vitro* was recently accepted for publication (12, see Appendix, Baugher, et al., 2005, Breast Cancer Research, for detailed methods for Figs. 1-10).

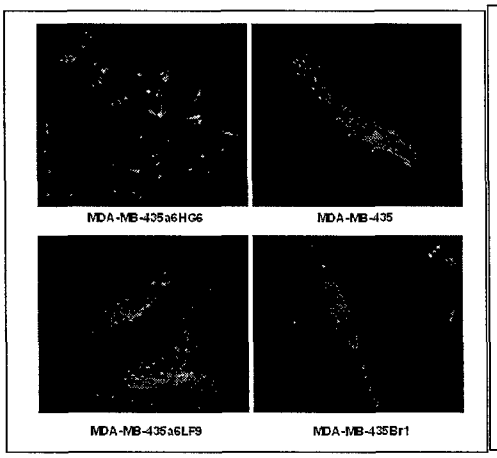

Figure 1. Characterization of cytoskeletal structures and focal adhesion distribution in MDA-MB-435 metastatic variants. Each of the MDA-MB-435 metastatic variants (MDA-MB-435 α6HG6, high metastatic variant; MDA-MB-435, parental cell line; MDA-MB-435 α6LF9, medium metastatic variant; MDA-MB-435Br1, least metastatic variant) were plated onto glass coverslips. Actin was then visualized with rhodamine phalloidin and focal adhesions were visualized with an anti-phosphotyrosine antibody followed by a FITC-conjugated secondary antibody.

As demonstrated by immunofluorescence microscopy of the MDA-MB-435 metastatic variants, the high metastatic variant MDA-MB-435α6HG6 demonstrated cells that were more spread and contained cell surface actin structures called lamellipodia that promote cell migrations and small focal adhesions with the ECM (Fig. 1). Next, the migratory efficiencies of the panel of MDA-MB-435 cell variants were tested in a haptotaxis assay by assessment of their relative efficiency to migrate through matrigel (a basement membrane substance) to the underside of the inner membrane of a Transwell. The high metastatic variant MDA-MB-435α6HG6 was more migratory and invasive *in vitro* when compared to parental or less metastatic variants of MDA-MB-435. (Fig. 2a).

Since Rac proteins have been implicated in regulation of cell migration and invasion (4-6), we tested the effect of a pan-Rho GTPase inhibitor *Clostridium difficile* Toxin B on the migratory efficiency of the MDA-MB-435α6HG6 high metastatic variant. Subsequent to treatment with Toxin B, MDA-MB-435α6HG6 cells exhibited a 50% decrease in migration to basal lamina (Fig. 2b). Therefore, increased migration in the most metastatic variant of MDA-MB-435 appears to be regulated by the Rho family of small GTPases.

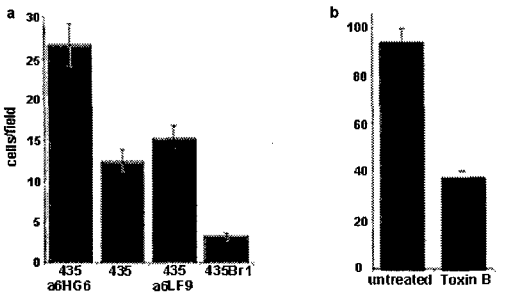

Figure 2. Haptotaxis assays of MDA-MB-435 metastatic variants. (a) Each variant was adjusted to 500,000 cells and applied to Transwell chambers in a basement membrane haptotaxis assay. Cells migrating to the underside of the chamber were stained with Propidium iodide (PI) and counted under (400X). Bars represent +/- SEM. Data is representative of three independent experiments. **(b)** MDA-MB-435 α6HG6 cells either treated with Toxin B or untreated were subjected to a haptotaxis assay. Each group was adjusted to equal cell counts and applied to Transwell chambers. Cells migrating to the underside of the chamber were stained with PI and counted under (400X). Bars represent +/- SEM.

Since high metastasis of the MDA-MB-435 variants correlated with cell functions under Rac regulation, we monitored the Rac expression levels of the metastatic variants. All four variants expressed similar levels of Rac proteins. Next, we determined that Rac activity, as monitored according to interaction of the endogenous Rac proteins with a GST-PBD (p21-binding) domain of PAK that specifically binds to the GTP bound active form of Rac, correlated with metastatic efficiency. As shown in Figure 3a, total endogenous Rac protein expression remained equal among the cell variants. However, levels of active Rac ranged from highest in the most metastatic variant, medium in parental and medium metastatic variant, and non-detectable in the least metastatic variant. Interestingly, the endogenous activity of the closely homologous protein Cdc42 was too low for detection in parental and MDA-MB-435 variants indicating that Cdc42 activity may not be as relevant in the MDA-MB-435 cell line (Fig. 3b).

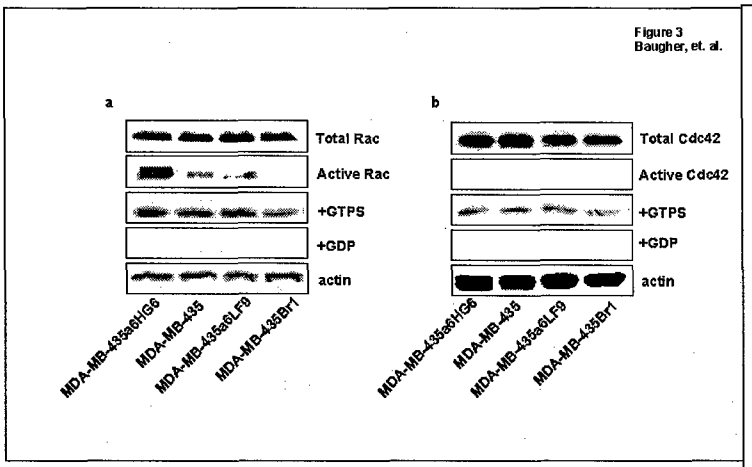

Figure 3. Rac and Cdc42 activity in MDA-MB-435 metastatic variants. Whole cell lysates of variants were subjected to SDS-PAGE followed by western blot analysis for total Rac **(a)** using an anti-Rac antibody and total Cdc42 **(b)** using an anti-Cdc42 antibody. Rac and Cdc42 activity were assayed using the PAK-PBD activity assay. A non-hydrolyzable GTP analog (GTPγS) was used as a positive control; GDP alone was used as a negative control. Equal loading of lanes was maintained by performing a total protein assay and is confirmed by western blot analysis for total actin. Results are representative of three independent experiments.

Thus, the characterization of the MDA-MB-435 metastatic variants demonstrated that metastatic efficiency could be correlated with *in vitro* functions under Rac regulation such as lamellipodia and focal adhesion formation as well as adhesion, invasion, and migration through the ECM. Moreover, the high metastatic variant MDA-MB-435 α6HG6 exhibited high endogenous Rac activity compared to less metastatic variants and the enhanced migration efficiency of the high metastatic variant can be blocked by a Rho GTPase inhibitor (Figs. 1-3). Therefore, we selected the MDA-MB-435 as a model system for our investigation of the role of Rac1 and Rac3 in breast cancer metastasis.

C. Analysis of the role of Rac1 and Rac3 in breast cancer metastasis

Since Rac activity correlated with metastatic efficiency of the MDA-MB-435 metastatic variants, we selected the high metastatic MDA-MB-435α6HG6 variant with high Rac activity and the low metastatic MDA-MB-435Br variant with little to no Rac activity for further analysis. The following stably transfected cell lines were created in MDA-MB-435Br and MDA-MB-435α6HG6 backgrounds (Fig. 4a). We have determined that the mutations are dominant by performing activity assays for endogenous Rac (Fig. 4b).

a

Dominant Active Mutants

MDA-MB-435Br1 vector	MDA-MB-435Br1 Rac1(G12V)	MDA-MB-435Br1 Rac3(G12V)

Dominant Negative Mutants

MDA-MB-435a6HG6 vector	MDA-MB-435a6HG6 Rac1(T17N)	MDA-MB-435a6HG6 Rac3(T17N)

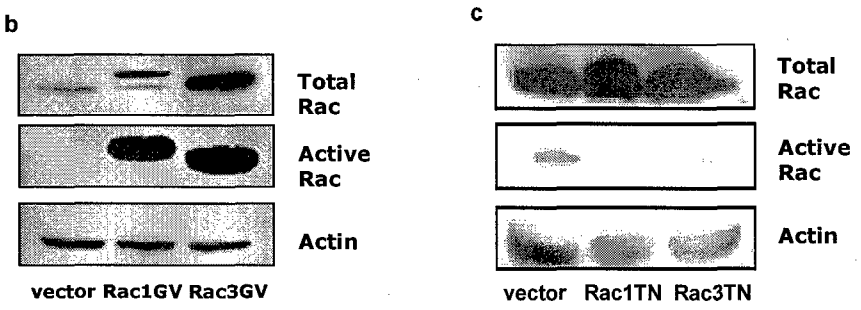

Figure 4. Characterization of stable cell lines expressing mutant Rac isoforms. Whole cell lysates of stable cell lines expressing vector alone or Rac1 or Rac3 mutants **(a)** were subjected to SDS-PAGE followed by western blot analysis for total Rac using an anti-Rac antibody. Dominant active cell lines are shown in **(b)**, dominant negative cell lines are shown in **(c)**. Rac activity was assayed using the PAK-PBD activity assay. Equal loading of lanes was maintained by performing a total protein assay and is confirmed by western blot analysis for total actin. Results are representative of three independent experiments.

In vitro analysis of MDA-MB-435 variants expressing Rac mutants:

We next investigated a role for Rac isoforms in regulation of breast cancer cell proliferation by a comparative analysis of the cell lines expressing dominant active or dominant negative Rac1 or

Rac3 with their respective controls. Interestingly, expression of dominant active Rac1 or Rac3 increased the S phase (peak between G1 and G2 phases, representative of cell cycle progression) of the low metastatic variant. In MDA-MB-435Br1 cells expressing vector alone, 43.5% of all cells assayed were in S phase while 50.4% of MDA-MB-435Br1 cells expressing Rac1(G12V) and 54.2% of MDA-MB-435Br1 cells expressing Rac3(G12V) were in S phase (Fig. 5).

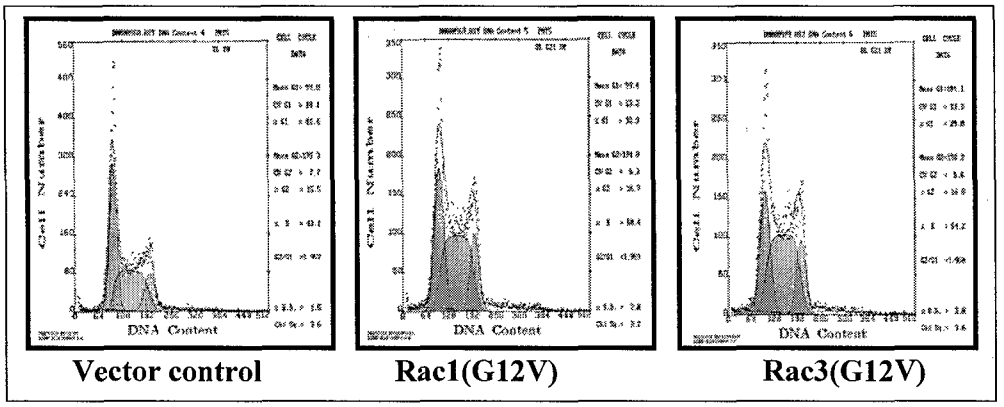

Figure 5. Cell cycle analysis of stable cell lines expressing vector alone, dominant active Rac1, or dominant active Rac3. Vector alone **(a)**, dominant active Rac1 **(b)**, or dominant active Rac3 **(c)** stable cell lines were fixed, stained with PI, and subjected to flow cytometry.

However, expression of dominant negative Rac 1 or Rac3 did not alter the cell cycle of MDA-MB-435a6HG6 where the percentage of cells in S phase for MDA-MB-435a6HG6 vector alone was 43.9%, MDA-MB-435α6HG6.Rac1(T17N) is 45.4%, and 40.9% for MDA-MB-435α6HG6.Rac3(T17N). This result indicates that cell cycle progression of this high metastatic variant is probably not under Rac regulation (Fig. 6).

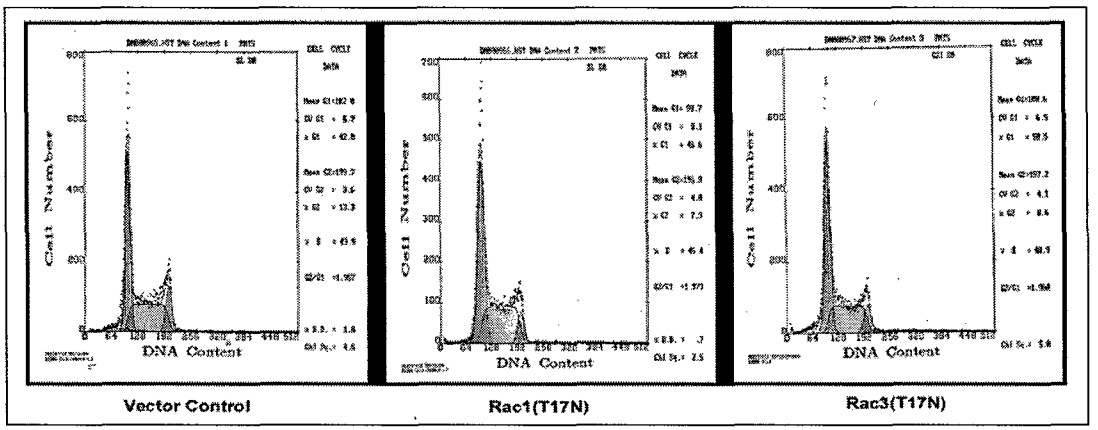

Figure 6. Cell cycle analysis of stable cell lines expressing vector alone, dominant negative Rac1, or dominant negative Rac3. Vector alone **(a)**, dominant negative Rac1 **(b)**, or dominant negative Rac3 **(c)** stable cell lines were fixed, stained with PI, and subjected to flow cytometry.

Since modulation of the actin cytoskeleton and dynamic turnover of focal adhesions is central to metastatic cancer cell invasion through the ECM, we determined the cytoskeletal morphology of MDA-MB-435 variants expressing Rac mutants. Expression of Rac1 or Rac3 dominant active constructs (G12V) in the least metastatic MDA-MB-435Br variant resulted in a

cellular morphology that was more reminiscent of a metastatic variant by exhibiting spread cells with more lamellipodia and more focal adhesions (Fig. 7). Conversely, expression of Rac1 or Rac3 dominant negative constructs (T17N) in the most metastatic MDA-MB-435α6HG6 variant resulted in a cellular morphology that was more reminiscent of a less metastatic variant by exhibiting less lamellipodia and less focal adhesions (Fig. 8).

Therefore, we assessed the role of Rac isoforms on cell functions relevant to the first step of metastasis where metastatic cells are required to interact with and invade through the surrounding ECM exhibiting motile mechanisms. As expected, low metastatic MDA-MB-435Br cells expressing dominant active Rac1 or Rac3 were more efficient than vector alone controls in adhesion, invasion, and haptotaxis assays towards matrigel (Fig. 9). Conversely, high metastatic MDA-MB-435α6HG6 cells expressing dominant active Rac1 or Rac3 were less efficient than vector alone controls in adhesion, invasion, and haptotaxis assays towards matrigel (Fig. 10).

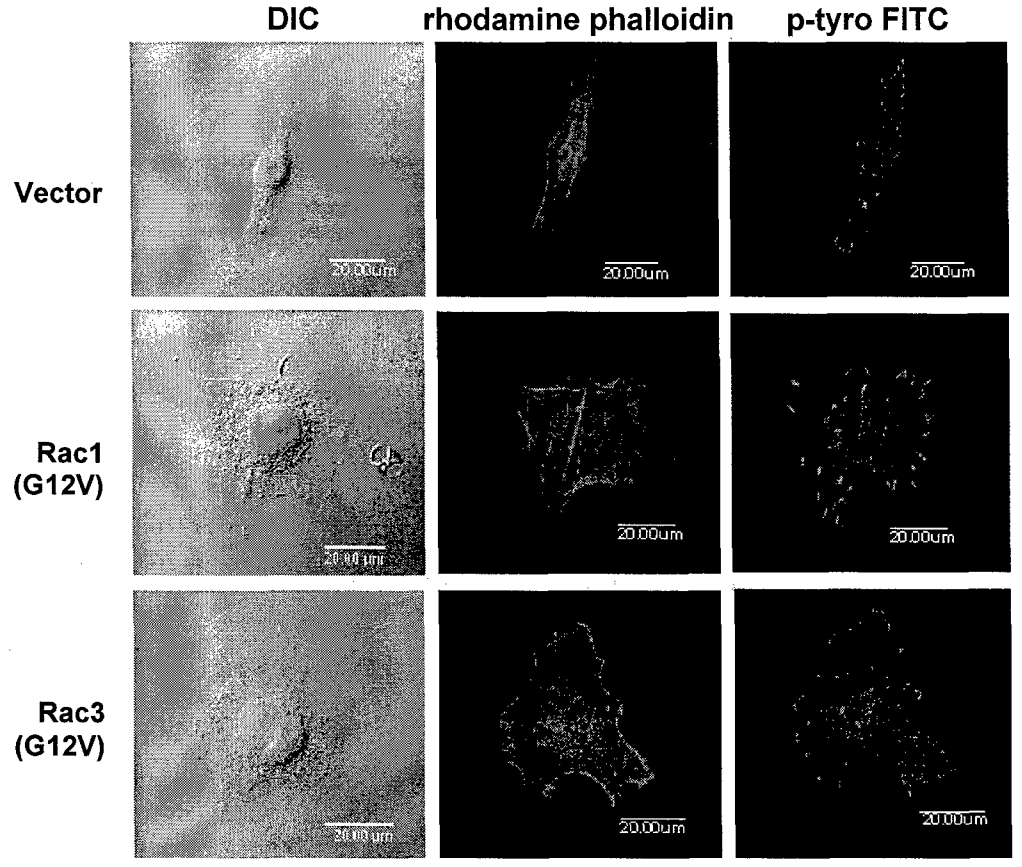

Figure 7. Effects of ectopic dominant active Rac(G12V) expression in low metastatic variant MDA-MB-435Br1 on cellular morphology. Confocal DIC and fluorescent microscopy were performed on MDA-MB-435Br1 cell variant stably expressing vector alone, myc-Rac1(G12V), or myc-Rac3(G12V). Cells were plated on glass coverslips, fixed in 3.7% formaldehyde and permeabilized with 0.2% Triton X-100. Actin was then visualized with rhodamine phalloidin and focal adhesions were visualized with an anti-phosphotyro antibody followed by an FITC-conjugated secondary antibody.

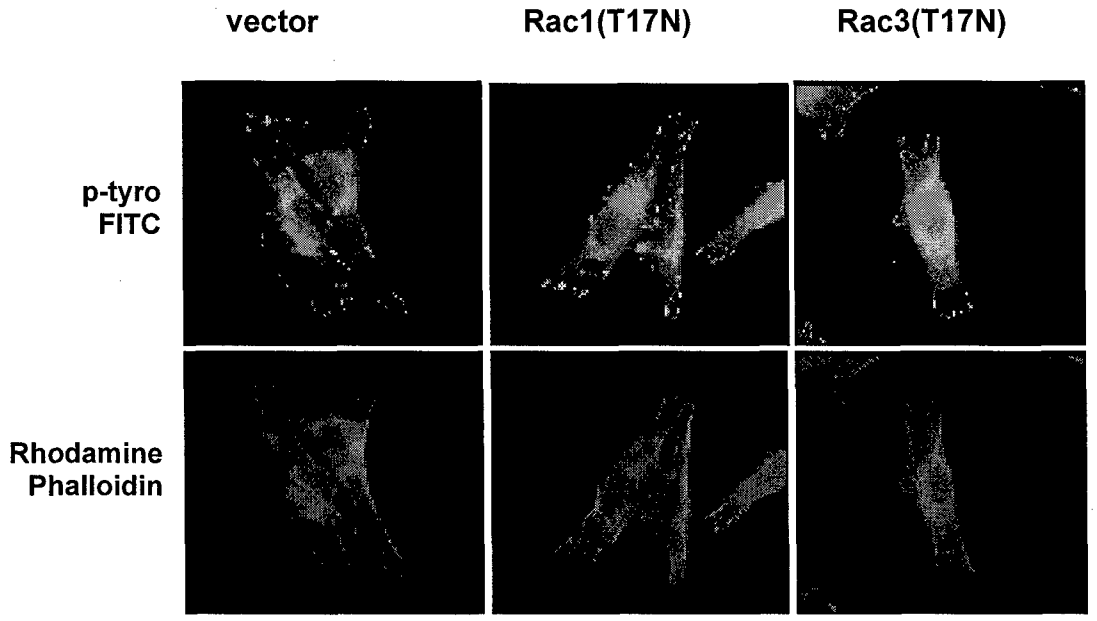

Figure 8. Effects of ectopic dominant negative Rac(T17N) expression in highly metastatic variant MDA-MB-435a6HG6 on cellular morphology. Fluorescent microscopy was performed on the MDA-MB-435a6HG6 cell variant stably expressing vector alone, myc-Rac1(T17N), or myc-Rac3(T17N). Cells were plated on glass coverslips, fixed in 3.7% formaldehyde and permeabilized with 0.2% Triton X-100. Actin was then visualized with rhodamine phalloidin and focal adhesions were visualized with an anti-p-tyro-FITC conjugate.

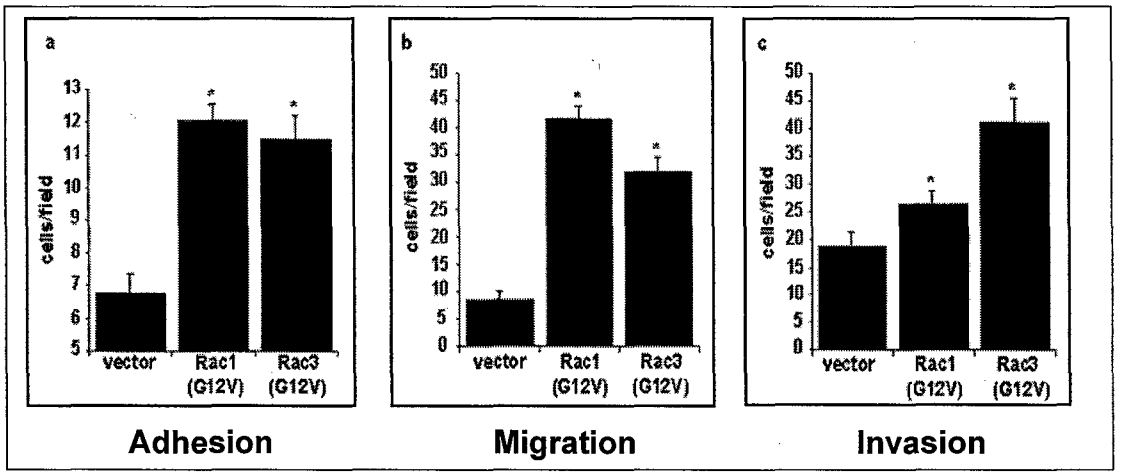

Figure 9. Effects of dominant active Rac isoforms on metastatic properties, as measured *in vitro*. MDA-MB-435Br1 cells expressing vector alone, myc-Rac1(G12V), or myc-Rac3(G12V), were subjected to adhesion **(a)**, haptotaxis **(b)**, and invasion **(c)** assays. Cells were counted under (200X) for adhesions assays, and (400X) for haptotaxis and invasion assays. Y-axis represents the number of cells/field for at least 20 microscopic fields per cell line. Bars represent standard error of the mean, and are representative of at least 3 separate experiments. An asterix indicates a statistically significant difference compared to the control (vector) as determined by a Student's *t*-test ($P<0.05$).

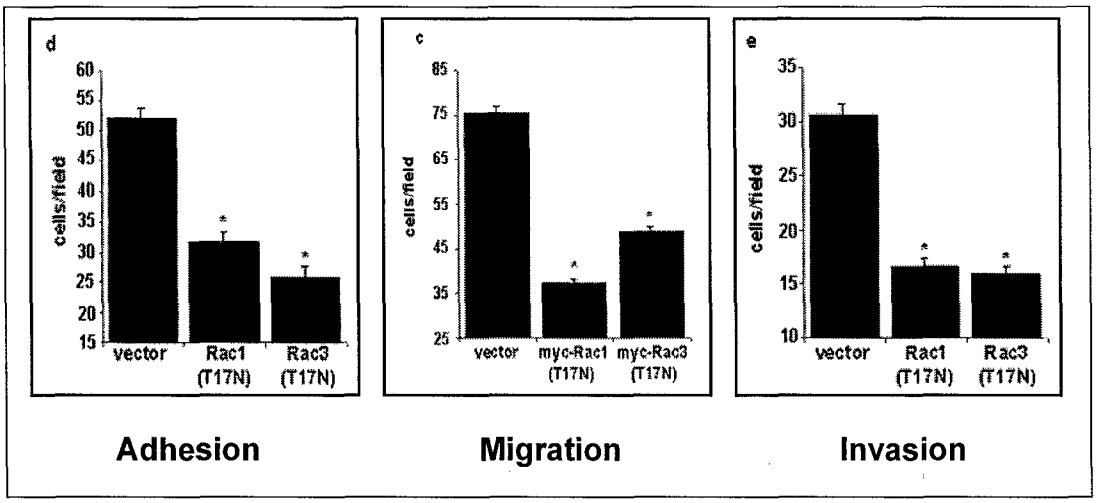

Figure 10. Effects of dominant negative Rac isoforms on metastatic properties, as measured *in vitro.* MDA-MB-435α6HG6 cells transiently expressing vector alone, myc-Rac1(T17N), or myc-Rac3(T17N), were subjected to adhesion **(d)**, migration **(e)**, and invasion assays **(f)**. Cells were counted at (200x) for adhesions assays, and (400x) for haptotaxis and invasion assays. Y-axis represents the number of cells/field for at least 20 microscopic fields per variant. Bars represent standard error of the mean, and are representative of at least 3 separate experiments. An asterix indicates a statistically significant difference compared to the control (vector) as determined by a Student's *t*-test ($P<0.05$).

In vivo analysis of MDA-MB-435 variants expressing Rac mutants:

Since cells expressing dominant active Rac1 or Rac3 demonstrated such dramatic changes in cell functions relevant to metastasis, we tested the effect of these mutations *in vivo,* using the nude mouse model of experimental metastasis. In collaboration with Dr. Janet Price (Cancer Biology Dept., MD Anderson Cancer Center, Houston, TX), we conducted a preliminary study where the mammary fat pads of 4-6 wks old female athymic nude mice (10 mice per treatment) were inoculated with control MDA-MB-435Br expressing vector alone, MDA-MB-435Br expressing Rac1(G12V) or Rac3 (G12V), control MDA-MB-435α6HG6 expressing vector alone, or MDA-MB-435α6HG6 expressing Rac1(T17N) or Rac3(T17N). All mice demonstrated tumor take with about a 90% efficiency, which reduced the sample size to about 8-9 per treatment. There were no significant differences in mammary tumor take and growth of primary mammary tumors among the different cell lines. Following 90 days or when the primary tumors reached an average size of 1.5 cm, the mice were sacrificed and the lung metastases investigated. The lungs were removed from the animal subsequent to euthanization and injected through the bronchus with a 15% India ink solution followed by Fekete's destaining solution as described in (13). Quantification of the number of metastatic foci demonstrates that expression of a dominant active Rac1 or Rac 3 in a low metastatic variant increases the number of lung metastases ~100% over vector alone controls while expression of a dominant negative Rac 1 or Rac3 dramatically reduces the number of lung metastases in a high metastatic variant.

Therefore, these data indicate a regulatory role for both Rac1 and Rac3 in breast cancer metastasis. Next, as proposed in the Task 2 of this research project, we initiated *in situ* image analysis of metastatic breast cancer progression to confirm our results and to identify the exact stage of metastasis that is regulated by Rac isoforms.

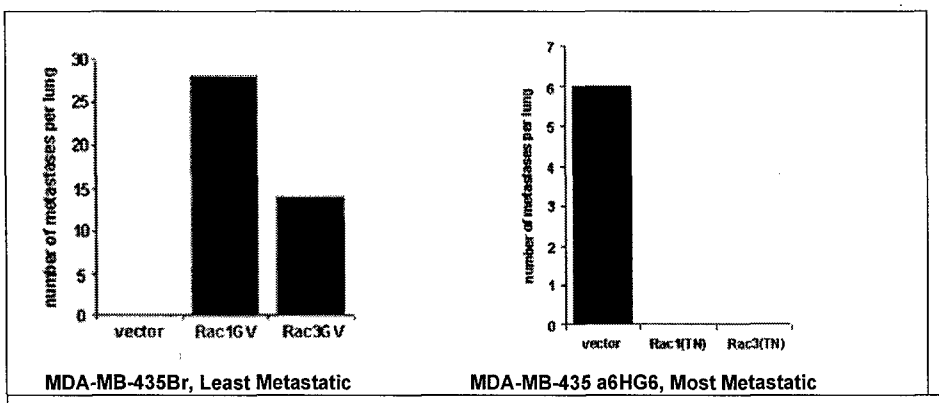

Figure 11. Effects of cells expressing mutant Rac isoforms on number of pulmonary metastasis from mammary tumors. (a) Metastases from mammary tumors established from MDA-MB-435Br cells expressing vector, Rac1(G12V), or Rac3 (G12V). **(b)** Metastases from mammary tumors established from MDA-MB-435α6HG6 cells expressing vector, Rac1(T17N), or Rac3(T17N).

D. *In situ* image analysis of breast cancer progression

Development of a macroscopic fluorescence imaging system

In collaboration with Dr. Rebecca Richards-Kortum's group (Biomedical Engineering Department, The University of Texas at Austin) we developed a macroscopic fluorescence imaging system to monitor fluorescently-tagged mammary tumor progression in mouse models in real-time with no or minimal intervention. Figure 12 represents the design of this inexpensive and portable tool to facilitate non-invasive *in situ* cancer detection with the potential to monitor fluorescent tumor formation and progression as well as investigate the efficacy of potential cancer preventatives and therapeutics (for details see Appendix, **Carlson, et al., submitted, Molecular Imaging**).

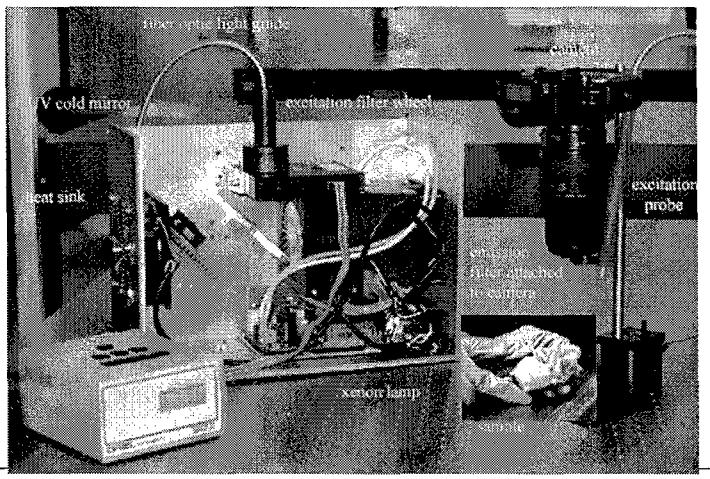

Figure 12. Macroscopic imaging system for *in situ* analysis of fluorescently-tagged tumors. This system is illuminated from a 300W Xenon arc lamp with an integrated parabolic reflector. Light is directed by a cold mirror to the excitation filter wheel. A bandpass filter centered at 545nm was used for excitation filtering. Excitation light was focused onto a flexible fiber optic light guide. Fluorescence emission from mouse with red fluorescent protein (RFP)-tagged mammary tumor was recorded using a Canon EOS-D30 digital camera fitted with two emission filters, a bandpass filter centered at 610nm and a 570nm longpass filter.

The macroscopic fluorescence imaging system was used for a direct analysis of RFP-tagged MDA-MB-435α6HG6 tumor progression in nude mice. Figure 13 represents fluorescent images of stably expressing RFP-MDA-MB-435α6HG6 human breast tumors in the mammary fat pad of female athymic, nude mice. We were able to image $1X10^5$ RFP-tagged cells prior to injection, in the syringe during injection into the mammary fat pad of a female athymic nude mouse, and under the skin of the mouse. A strength of our system is this ability to visualize inoculation and tumor take of FP-tagged cancer cells. At day one, we imaged successful tumor take and RFP-tagged MDA-MB-435 cell proliferation as increased fluorescence at the site of inoculation. This preliminary study determined system was sufficient to detect the fluorescence signal from RFP-tagged cells in the mammary fat pad at levels 6-7 times more than the autofluorescence from nude mouse skin due to artifacts such as epidermal keratin.

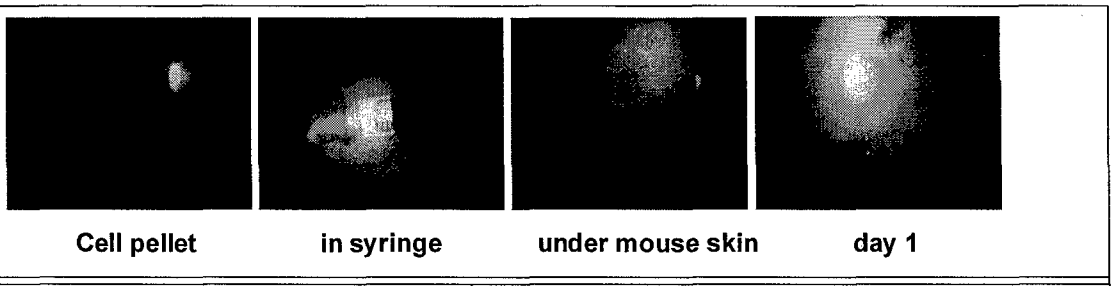

Fig. 13. Image analysis of RFP-tagged MDA-MB-435a6HG6 cells at the site of inoculation. $1X10^5$ RFP-MDA-MB-435α6HG6 cells were injected into the mammary fat pad of a female athymic nude mouse. Red fluorescence was imaged from the cell pellet, in the syringe during injection, under the mouse skin immediately following injection, and 1 day after injection.

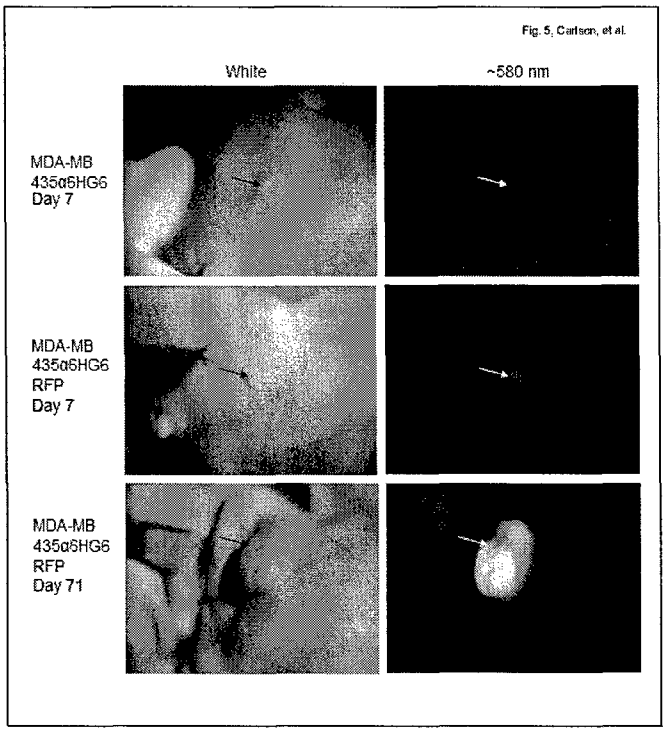

Figure 14. Images of RFP- or non-RFP-expressing MDA-MB-435α6HG6 mammary tumors in female athymic, nude mice. Left column, images under white light; right column, images at 580nm. Top row, non-RFP-tagged MDA-MB-435α6HG6 mammary tumors at day 7. Middle row, RFP-tagged MDA-MB-435α6HG6 mammary tumor at day 7, post-mammary fatpad injection. Bottom row, RFP-tagged MDA-MB-435α6HG6 mammary tumor at day 71 post-injection.

RFP-tagged MDA-MB-435 α6HG6 tumor progression at the mammary pad was followed by daily non-invasive image analysis of the same nude mouse. In the day 7 fluorescent image, RFP emission was obvious at the site of injection, indicating successful MDA-MB-435α6HG6 tumor cell take and survival in the nude mouse host. This is not so obvious when the mouse was imaged under white light using the same macroscopic imaging system. At day 71, the white light image of the same mouse showed a clearly discernable mammary tumor. The image of this tumor under RFP excitation on day 71 showed a substantial increase in fluorescence signal. In parallel, female nude mice were also injected in the mammary fat pad with non-RFP expressing MDA-MB-435α6HG6 human breast cancer cells which emitted no fluorescence above background autofluorescence of the skin (Fig. 14).

We then quantified the RFP-tagged MDA-MB-435α6HG6 mammary tumor growth in nude mice over time by analyzing increases in tumor fluorescence intensity. After normalization, tumor area was manually traced in each grayscale image using Image J software and the mean grayscale value was calculated for the traced tumor area and plotted versus time. As demonstrated in Figure 15, an increase in fluorescence intensity was evident with increased mammary tumor size in the RFP-tagged tumor but not in the control non-RFP-tagged tumor. Therefore, the macroscopic fluorescence imaging system can be used conveniently for non-invasive quantification of fluorescent tumor progression of metastatic breast cancer.

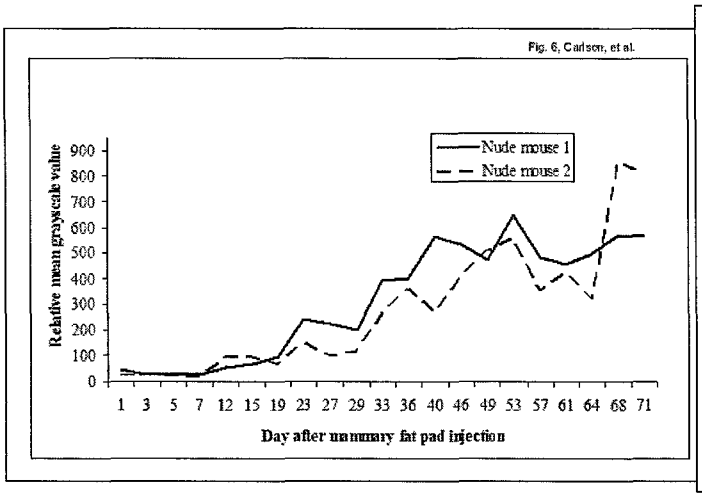

Figure 15. Fluorescence intensity RFP- or non-RFP-expressing MDA-MB-435α6HG6 mammary tumors in nude mice as a function of time. RFP- or non-RFP-expressing MDA-MB-435α6HG6 cells were injected into the mammary fat pads of two female athymic, nude mice. Tumor growth was monitored via fluorescent image analysis using the macroscopic imaging system. Images were converted to grayscale and the mean grayscale pixel value for the traced tumor area was plotted versus time.

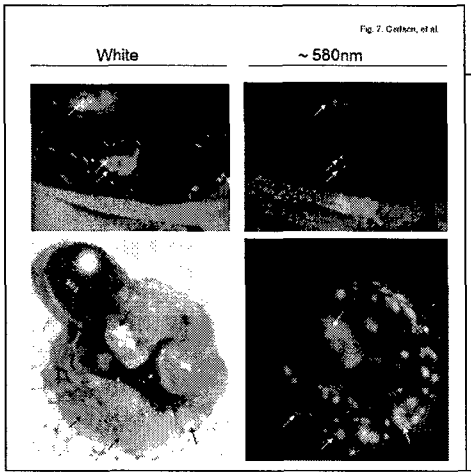

Figure 16. Images of lung metastases from RFP-tagged MDA-MB-435α6HG6 mammary tumors. RFP- tagged MDA-MB-435α6HG6 human breast cancer cells were injected into the mammary fat pad of female, nude athymic mice. The mammary tumor was allowed to grow for 71 days until necropsy. Left column, images under white light; right column, images at 580nm. Top row, mouse with open chest cavity. Bottom row, excised lung with metastases seen as white nodules (black arrows) under white light and RFP expressing metastatic lesions verified by fluorescent imaging at 580 nm (white arrows).

Once the primary tumor reached ~1.5cm at 71 days, we imaged distant metastases on the chest as faint red fluorescent patches. To confirm that these were lung metastases, the mouse was sacrificed and a skin flap created over the chest cavity. This enabled the imaging of the lung metastases as red fluorescent foci. Even though we were able to detect areas of distant metastases by whole-body imaging, intravital imaging where a skin flap is opened over the areas of interest is necessary for a complete analysis of metastatic lesions by our system in the current configuration. Following necropsy, red fluorescence signal from distant lung metastases was easily detected by our system (Fig. 16). This verified the existence of metastatic lesions, since such lesions were not obvious to the untrained, naked eye. Therefore our system can be easily used to detect and quantify metastases without prior histopathology.

Thus, the use of this macroscopic fluorescence imaging system is a viable approach for further analysis of MDA-MB-435 cell variants expressing Rac and PAK mutations. We are continuing with the investigation of the role of Rac1 and Rac3 in breast cancer metastasis. As described, we have inoculated nude mice with RFP-tagged MDA-MB-435 variants expressing vector, Rac1 or Rac3 dominant active or dominant negative constructs (10 mice per treatment). The analysis of fluorescent mammary tumors in these mice using the macroscopic imaging system is currently in progress. We expect to complete this study by December 2005 and submit a manuscript in a peer-reviewed publication such as "Cancer Research" for publication.

Adaptation of a fluorescence confocal microscope for image analysis of breast cancer progression:

To enable a more complete analysis of the role of Rac1, Rac3, and PAK in breast cancer metastasis, we have also initiated the adaptation of a fluorescence confocal microscope for *in situ* image analysis of fluorescently-tagged breast cancer progression in nude mice. During the third year of the award, we completed the adaptation of the confocal imaging system previously used by our collaborative research group for *in situ* reflectance image analysis, to include fluorescence image analysis. Using this confocal microscope to monitor reflectance, we reported image analysis of non-fluorescent cancer cells and blood vessels inside live mouse tumors up to a depth of 500 microns (14).

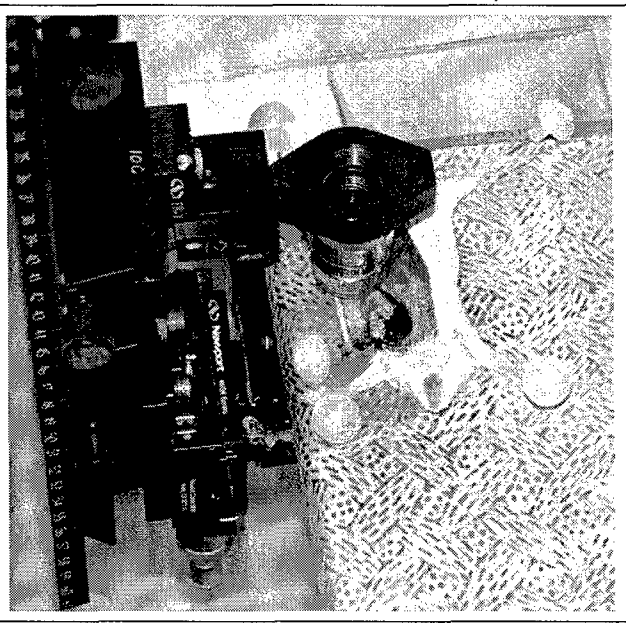

Figure 17. *In situ* analysis of breast cancer progression by confocal microscopy. The mouse is placed on a specially constructed stage. This microscope is equipped with a diode light source directed to a scanning system that creates a focused excitation field by raster scanning across the back aperture of a 25x 0.8NA water-immersion objective. The objective focuses 14-30 mW of power onto the tumor. Light reflected from the sample is focused into a pinhole aperture and collected by an avalanche photodiode detector (APD C5460, Hamamatsu). For details, see (14).

As demonstrated in Figure 17, this confocal microscope is especially designed for image analysis of small animals by containing a large stage with a long working distance. As with all confocal microscopes, this system uses a spatial filter in front of the photodetector to increase axial resolution, thus enabling the optical sectioning of thick tissues and cells and their subsequent computerized 3-D reconstruction. This system has now been adapted and optimized for scanning epifluorescence confocal imaging and demonstrates increased illumination, sensitivity, depths of detection, and spatial resolution. A filter block of 558/583 nm was installed for visualizing RFP-tagged cells. The laser source was replaced with an ultrafast and more sensitive argon laser (Coherent laser) with a variable wavelength from 476-514 nm and a power output range from 100mW to 10W. A 40X water immersion objective was purchased to gain better resolution. Two scanning mirrors driven by a pair of galvanometers produce a two-dimensional image that are detected by a 8kHz resonant scanner (Electro-Optical products, Inc.) to produce a frame rate of 15Hz. Thus, we are now capable of capturing 15 frames/sec (half-video rate) using an avalanche photodiode detector (Hamamatsu).

Preliminary studies conducted with RFP- or GFP- tagged MDA-MB-435 cells growing on tissue culture plates demonstrate that our system is capable of imaging fluorescent breast cancer cells. Studies are under way to determine the feasibility of using this system to analyze FP-tagged breast cancer cells in live nude mice. To confirm the results of this project, we plan to detect and analyze progression of RFP-tagged MDA-MB-435 variants expressing Rac1, Rac3, or PAK mutants, in live nude mice. This will enable us to validate our hypothesis Rac1, Rac3, and PAK are critical for the first step of metastasis when tumor cells invade the ECM and enter the circulatory system.

Figure 17. Fluorescence confocal microscopy of FP-tagged MDA-MB-435 cells. The epifluorescence confocal microscope that was especially designed for *in situ* analysis of fluorescently-tagged mammary tumor progression in live animal models was tested on RFP (left) - or GFP (right) -tagged MDA-MB-435 cells.

E. Analysis of the role of the red wine phytoestrogen resveratrol in regulation of breast cancer progression via Rho GTPases

Investigation of the role of the hormone estrogen and related plant-derived phytoestrogens is an exciting new direction for the PI's research program. Our studies on the role of the red wine phytosetrogen resveratrol on breast cancer progression was initiated by a research assistant (Nicolas Azios) who worked on creation of cell lines described in this report and whose salary was funded during the first year of this award. Therefore, this DAMD17-02-1-0582 award is acknowledged in our recent manuscript on the role of resveratrol in regulation of the actin cytoskeleton of breast cancer cells (see Appendix, Azios and Dharmawardhane, 2005. Neoplasia 7:128-140). In this manuscript, we report that resveratrol acts opposite to estrogen and epidermal growth factor (EGF) by decreasing cell migration, focal adhesions, and focal adhesion kinase (FAK) activity, and inducing a rapid global array of actin structures called filopodia. Resveratrol increased EGFR activity even in the presence of an EGFR1 inhibitor. The cytoskeletal responses and EGFR activity in response to E_2 were blocked by EGFR1 inhibitor indicating that E_2 may increase cell migration via crosstalk with EGFR signaling. These data suggest a role for E_2 in promotion and an antiestrogenic role for resveratrol in prevention of breast cancer cell migration.

This project is now funded by a NIH pre-doctoral award to Azios, and NIH/NCI and American Institute of Cancer Research awards to the PI. We are currently investigating the role of resveratrol in regulation of Rac iosforms to modulate actin cytoskeletal changes.

Key Research Accomplishments from May 2002- July 2005

A majority of the proposed experiments have been accomplished.

Task 1. Create stable FP-tagged breast cancer cell lines expressing active and inactive forms of Rac3 and/or the autoinhibitory domain of PAK1.

1. Created RFP-tagged bicistronic mammalian expression vectors containing the following cDNA
   - Rac1 (G12V)
   - Rac3 (G12V)
   - Rac1 (T17N)
   - Rac3 (T17N)
   - Rac3 (F28L)
   - PAK1 (83-149)
   - PAK1 (83-149) (L107F)

2. Created of the following MDA-MB-435 breast cancer variant cell lines stably expressing RFP-tagged Rac mutants
   - MDA-MB-435 Br. vector
   - MDA-MB-435 Br. Rac1 (G12V)
   - MDA-MB-435 Br. Rac3 (G12V)
   - MDA-MB-435 α6HG6. vector
   - MDA-MB-435 α6HG6. Rac1 (T17N)
   - MDA-MB-435 α6HG6. Rac3 (T17N)

Task 2. Analyze the invasive behavior of the cell lines expressing Rac3 and PAK1 mutants in live mouse tumors.

1. Accomplished *in vitro* mutant analysis of actin cytoskeleton, adhesion, invasion, and migration through ECM components of cell lines expressing the Rac mutants listed in (2).
2. Accomplished *in vivo* mutant analysis of cell lines expressing the Rac mutants listed in (2) in the nude mouse model of experimental metastasis.
3. Designed and developed a macroscopic fluorescence imaging system for *in situ* image analysis of FP-tagged breast cancer progression in live mouse models.
4. Designed and adapted an epifluorescence confocal microscope for *in situ* image analysis of FP-tagged breast cancer progression in live mouse models.

Reportable Outcomes

Publications

1. Carlson, A.C, Hoffmeyer, M.R., Wall, K., Richards-Kortum, R., **Dharmawardhane, S.** Development of a macroscopic fluorescence imaging system for *in situ* analysis of human breast cancer progression in murine models. Submitted, *Molecular Imaging.*
2. Baugher, P., Krishnamoorty, L., Price, J. and **Dharmawardhane, S.** 2005. Rac1 and Rac3 regulate breast cancer cell invasion and metastasis in metastatic variants of MB-435 human breast cancer cells. *Breast Cancer Res.*, in press.
3. Azios, N.G., **Dharmawardhane, S.** 2005. Resveratrol and estradiol exert disparate effects on cell migration, cell surface actin structures, and focal adhesion assembly in MDA-MB-231 human breast cancer cells. *Neoplasia* 7:128-140.

Abstracts and Presentations

1. Baugher, P.B., Krishnamoorthy, L., Hoffmeyer, M.R., Lacy, A., Richards-Kortum, R., Price, J.E., **Dharmawardhane**, S. Role of Rac1 and Rac3 in breast cancer metastasis. Era of Hope, Deaprtment of Defense Breast Cancer Research Program Meeting, Philadelphia, PA, June 8-11, 2005.
2. Hoffmeyer, M., Wall, K., Lacy, A., and **Dharmawardhane, S.** *In vivo* imaging of metastatic tumor progression using fluorescent protein-tagged breast cancer cell lines. 96th annual meeting of American Association for Cancer Research, Anaheim, CA. April 16-20, 2005.
3. Baugher, P., Krishnamoorty, L.. **Dharmawardhane, S.**, The role of rac1 and rac3 in the metastatic progression of human breast cancer. Mol. Biol. Cell, 14: 49a. Annual meeting of the American Society of Cell Biology, San Francisco, CA, Dec 13-17, 2003.
4. Azios, NG, Brownson, DM, Dubash, A-D, and **Dharmawardhane**, S. 2003. Cytoskeletal changes in MDA-MB-231 cells mediated by Resveratrol. Proceedings of the American Association for Cancer Research, 44:79.
5. Baugher, P.J., Price, J., and **Dharmawardhane, S.F.** 2002. Rho GTPases in MDA-MB-435 Metastatic Breast Cancer Cell Variants. Mol. Biol. Cell, 13:206.
6. Baugher, P.J., Nahidi, J., Dubash, A., Mack, V., and **Dharmawardhane, S.F.** 2002. Role of the small GTPase Rac3 in breats cancer metastasis. Proceedings of the American Association for Cancer Research, 43:380.

Conclusions

The following are our major findings:

- Metastatic efficiency of MDA-MB-435 breast cancer cell variants can be correlated with increased lamellipodia, focal adhesions, adhesion, invasion, migration and Rac activity.
- Expression of dominant negative Rac1 or Rac3 in the high metastatic variant MDA-MB-435α6HG6 resulted in decreased lamellipodia, focal adhesions, adhesion, invasion, migration, *in vitro*, and metastasis in an *in vivo* nude mouse model.
- Expression of dominant active Rac1 or Rac3 in the low metastatic variant MDA-MB-435.Br resulted in increased lamellipodia, focal adhesions, adhesion, invasion, migration, and metastasis in a nude mouse model.

Therefore, our results validate the hypothesis that Rac3, the closely related Rac1 isoform, is also an important regulator of breast cancer metastasis.

Future Directions

The development and validation of macroscopic and microscopic imaging systems in the third year has enabled a more complete analysis of the Rac1 and Rac3 mutant expressing breast cancer cell lines. We also plan to conduct a similar analysis of the PAK1 mutants that were constructed during this investigation. The *in situ* imaging systems that were developed by the interdisciplinary collaboration between the PI, a cell biologist, Dr. Janet Price, a cancer biologist, and Dr. Rebecca Richards-Kortum, a biomedical engineer has far-reaching consequences in terms of our future investigations of the molecular mechanisms of breast cancer progression. The image analysis methodology developed during the past year will be used not only to investigate an in-depth role for Rac and PAK in breast cancer metastasis but to understand the role of other potential metastasis suppressors and promoters as well as potential breast cancer preventives and therapeutics.

References

1. Woodhouse, E.C., Chuaqui, R.F., and Liotta, L.A. General mechanisms of metastasis. Cancer, *80*: 1529-1537, 1997.
2. Price, J.E. Analyzing the metastatic phenotype. J Cell Biochem, *56*: 16-22, 1994.
   12
3. Fidler, I.J. Seed and soil revisited: contribution of the organ microenvironment to cancer metastasis. Surg Oncol Clin N Am, *10*: 257-270, 2001.
4. Symons, M. and Settleman, J. Rho family GTPases: more than simple switches. Trends Cell Biol, *10*: 415-419, 2000.
5. Evers, E.E., Zondag, G.C., Malliri, A., Price, L.S., ten Klooster, J.P., van der Kammen, R.A., and Collard, J.G. Rho family proteins in cell adhesion and cell migration. Eur J Cancer, *36*: 1269-1274, 2000.
6. Haataja, L., Groffen, J., and Heisterkamp, N. Characterization of RAC3, a novel member of the Rho family. J Biol Chem, *272*: 20384-20388, 1997.
7. Bolis A, Corbetta S, Cioce A, and de Curtis I. Differential distribution of Rac1 and Rac3 GTPases in the developing mouse brain: implications for a role of Rac3 in Purkinje cell differentiation. *Eur J Neurosci* , 18:2417-2424, 2003.
8. Mira, J.P., Benard, V., Groffen, J., Sanders, L.C., and Knaus, U.G. Endogenous,

hyperactive Rac3 controls proliferation of breast cancer cells by a p21-activated kinase-dependent pathway. Proc Natl Acad Sci U S A, *97*: 185-189, 2000.

9. Leung K, Nagy A, Gonzalez-Gomez I, Groffen J, Heisterkamp N, Kaartinen V. Targeted expression of activated Rac3 in mammary epithelium leads to defective postlactational involution and benign mammary gland lesions. Cells Tissues Organs, 175:72-83, 2003.
10. Vadlamudi, RK, and Kumar R. P21-activated kinases in human cancer. Cancer Metastasis Rev.: 22:385-393, 2003.
11. Mukhopadhyay R, Theriault RL, and Price JE. Increased levels of alpha6 integrins are associated with the metastatic phenotype of human breast cancer cells. Clin Exp Metastasis, 17:325-332,1999.
12. Baugher, PJ, Krishnamoorthy, L, Price, JE, and Dharmawardhane, S.Rac1 and Rac3 isoform activation is involved in the invasive and metastatic phenotype of human breast cancer cells. Breast Cancer Res., in press, 2005.
13. Watts, AM, and Kennedy, RC, Quantitation of tumor foci in an experimental murine tumor model using computer-assisted video imaging. Anal Biochem. 256(2):217-219, 1998.
14. Lacy AA, Collier, T, Price, JE, Dharmawardhane, S, Richards-Kortum, R. Near real-time *in vivo* confocal imaging of mouse mammary tumors. Front Biosci. 7:1-7, 2002.

Rac1 and Rac3 isoform activation is involved in the invasive and metastatic phenotype of human breast cancer cells

Paige J. Baugher[a], Lakshmi Krishnamoorthy[a], Janet E. Price[b], Surangani F. Dharmawardhane[a]*

[a]Molecular Cell and Developmental Biology Section and The Institute for Cellular and Molecular Biology,
The University of Texas at Austin,
1 University Station, BIO 311, A6700, Austin, TX 78712

[b]Cancer Biology Department, The University of Texas M. D. Anderson Cancer Center,
1515 Holcombe Blvd, Houston, TX 77030

*To whom correspondence should be addressed
e-mail: surangi@mail.utexas.edu

Paige J. Baugher: p.baugher@mail.utexas.edu
Lakshmi Krishnamoothy: laksh@mail.utexas.edu
Janet E. Price: jprice@mdanderson.org

Abstract

Introduction

The metastatic progression of cancer is a direct result of the disregulation of numerous cellular signaling pathways, including those associated with adhesion, migration, and invasion. The Rac family of small GTPases is known to act as regulators of actin cytoskeletal structures and strongly influence the cellular processes of integrin-mediated adhesion and migration. Even though hyperactivated Rac proteins have been shown to influence metastatic processes, these proteins have never been directly linked to metastatic progression.

Methods

To investigate a role for Rac and Cdc42 in metastatic breast cancer cell invasion and migration, relative endogenous Rac or Cdc42 activity was determined in a panel of metastatic variants of the MDA-MB-435 metastatic human breast cancer cell line using a p21-binding domain-PAK pull down assay. To investigate the migratory and invasive potential of the Rac isoforms in human breast cancer, namely Rac1 and the subsequently-cloned Rac3, we stably expressed either dominant active Rac1 or dominant active Rac3 into the least metastatic cell variant. Dominant negative Rac1 or dominant negative Rac3 were stably expressed in the most metastatic cell variant. Cell lines expressing mutant Rac1 or Rac3 were analyzed using *in vitro* adhesion, migration and invasion assays.

Results

Here, we show that increased activation of Rac proteins directly correlates with increasing metastatic potential in a panel of cell variants derived from the same metastatic breast cancer cell

line (MDA-MB-435), whereas the same correlation could not be found with activated Cdc42. We found not only that this expression resulted in a more invasive and motile morphology, but that it also enhanced the ability of these cells to adhere, migrate, and invade through basal lamina. Moreover, expression of either dominant negative Rac1 or dominant negative Rac3 into the most metastatic cell variant and resulted in a decrease of metastatic properties, as measured *in vitro*.

Conclusions

This study implicates endogenous Rac activity in breast cancer metastasis. Taken together, these results suggest a role for both the Rac1 and Rac3 GTPases in the metastatic progression of human breast cancer.

Introduction

Cancer metastasis is a multi-faceted process requiring the disregulation of numerous signaling pathways, including those associated with cell adhesion and motility. The initial steps of metastasis require the acquisition of a motile phenotype in order to traverse tissue boundaries, while the later stages require dynamic adhesive interactions with the extracellular matrix (ECM) to facilitate the extravasation of malignant cells [1]. Activation of the Rho family GTPases Rac and Cdc42 is a critical event in the integrin and growth factor-mediated regulation of cellular migration and adhesion, implicating the hyperactivation of these proteins in the progression of metastatic disease [2,3].

Activation of Rac and Cdc42 is critical for initiating cell motility and adhesion via the dynamic turnover of cell-substratum contacts (focal adhesions) and the nucleation of actin monomers necessary for the assembly of actin filaments required for cell movement [3]. Activation of the appropriate levels of these proteins, together with temporal and spatial coordination, must be precisely regulated in order to achieve normal cellular function [4]. Aberrant Rac and Cdc42 activities have been recently associated with invasive and malignant behavior in a variety of cell types, including hepatocarcinoma, breast carcinoma, and melanoma [5-7]. However, breast tissue sample analysis has demonstrated that the contribution of the Rac and Cdc42 proteins to tumor cell invasion in breast cancer is not due to genetic mutation, but is due instead to changes in the activity levels of these proteins caused by hyperactivation of upstream activators [4,8]. Yet, a direct correlation between Rac and Cdc42 protein activity states and metastatic progression in human breast cancer remains to be demonstrated.

The Rac subfamily includes Rac1, the myeloid-lineage specific Rac2, and the subsequently cloned Rac3 protein [9]. Exhibiting an 89 and 92% identity to Rac1 and Rac2 respectively, Rac3 differs from other Rac proteins only in the C-terminus, a region essential for subcellular localization and regulatory protein binding [9-10]. In fact, differential localization of Rac1 and Rac3 has been demonstrated in the developing mammalian brain [11]. Moreover, dominant activation of Rac3 in the mammary epithelium has been shown to lead to the formation of mammary lesions [12]. However, a direct role for Rac3 in breast cancer invasion and metastasis has yet to be substantiated.

To further understand the molecular mechanisms of the small GTPases Rac and Cdc42 in human breast cancer, we used a panel of cell variants isolated from the MDA-MB-435 human metastatic breast cancer cell line, and varied in their ability to form secondary pulmonary and cerebral lesions in the nude mouse model of experimental metastasis [13]. Within this panel, we found a direct correlation between the invasive phenotype, enhanced migratory ability, and increased metastatic potential. Moreover, we found that increased Rac, but not Cdc42, activation correlated with increased metastatic potential.

Previously, Rac1 was shown to play a critical role in rat mammary tumor cell growth and metastasis *in vivo* [6]. To establish a role for both Rac1 and Rac3 in human breast cancer, we carried out a comparative study of the invasive capabilities between the two isoforms. Dominant active Rac1 or Rac3 mutants were expressed in the least metastatic cell variant of our panel, while dominant negative Rac1 or Rac3 mutants were expressed in the most metastatic cell variant. Dominant active Rac expression of either isoform resulted in an aggressive phenotype, as well as significant increases in adhesion to ECM, migration, and invasion through basal

lamina. Conversely, dominant negative expression of either isoform resulted in significant decreases in adhesion to ECM, migration, and invasion. Taken together, these data suggest a direct role for both Rac1 and Rac3 protein activation in the metastatic progression of human breast cancer.

Materials and Methods

Cell culture

The human breast cancer cell lines variants MDA-MB-435α6HG6, MDA-MB-435, MDA-MB-435α6LF9, and MDA-MB-435Br1 were cultured in Dulbecco's modified Eagle's medium (DMEM) (Gibco^{TM}, CA) with 10% fetal bovine serum (FBS) (Tissue Culture Biologicals, CA) and cultured in a humidified 5% CO_2 atmosphere at 37°C.

DNA constructs and transfections

Rac1 mutant cDNA (Myc-Rac1(G12V) and Myc-Rac1(T17N)) were generous gifts from Dr. Gary Bokoch of the Scripps Institute (La Jolla, CA). Rac3 mutant cDNA (Myc-Rac3(G12V) and Myc-Rac3(T17N)) were generous gifts from Dr. Ulla Knaus of the Scripps Institute (La Jolla, CA). Mutant Rac cDNAs were digested out of the pRK5myc vector and inserted into the multiple cloning site of the pIRESneo2 vector (Clontech).

pIRESneo2 vector alone, or vectors encoding myc-tagged Rac1(G12V), Rac1(T17N), Rac3(G12V), or Rac3(T17N) were transfected into cell variants using Lipofectamine Plus Reagent (Gibco^{TM}, CA). Maximal expression was achieved 24-48 hours post transfection with a transfection efficiency of ~70% at 48h, as monitored by staining for myc expression. All experiments were conducted at 36 h following trasnfection and confirmed using stable cell lines.

Immunofluorescence microscopy

Cells cultured on glass coverslips were fixed in 3.7% formaldehyde (Sigma Chemical Corp., MO), permeablized with 0.5% Triton X-100 (Sigma, MO), and blocked with 5% goat serum (Gibco^{TM}, CA) and 5% bovine serum albumin (BSA)(Sigma Chemical Corp., MO). Cells were then stained with rhodamine phalloidin (Molecular Probes, OR) to visualize F-actin, and a mouse monoclonal anti-phosphorylated tyrosine antibody, clone 4G10 (Upstate Biotechnology, NY), followed by FITC-conjugated goat anti mouse IgG (ICN Biomedicals Inc., CA) to visualize focal adhesions as is common practice for identifying focal adhesions {15576919 }. Cells were imaged with either an Olympus upright fluorescence microscope or a Zeiss inverted confocal microscope with fluorescence and DIC capabilities. Images were overlayed with Spot Advanced digital camera software (Diagnostic Instruments Inc., MI).

Adhesion assays

Cell adhesion assays were performed according to Klemke, et al. [29]. Briefly, glass coverslips (Fisher Scientific, TX) were coated with laminin (Gibco BRL, MD). Proteins were allowed to bind overnight at 4° before the coverslips were blocked for 1 hour with 1% heat-denatured bovine serum albumin (BSA) (Sigma Chemical Corporation, MO) in 1X PBS. Cells (10^5) were added to the wells and allowed to adhere for 15 minutes. Non-adherent cells were removed, and the adherent cells were fixed in 3.7% formaldehyde (Sigma Chemical Corp., MO). The number of cells per microscopic field for thirty fields per coverslip was counted with an Olympus upright microscope with a 40x phase contrast objective. Nonspecific cell adhesion as measured on BSA-coated coverslips has been subtracted. Effects of the ectopic expression of Rac mutants were assessed 36-48 hours post transfection.

Haptotaxis migration and invasion assays

Cell migration and invasion assays were performed as described in Klemke, et al. [29]. Briefly, modified Boyden chambers (tissue culture treated, 6.5 mm diameter, 10 μm thickness, 8 μm pores, Transwell®, Costar Corp., Cambridge, MA) containing polycarbonate membranes were coated with matrigel (Fisher Scientific, TX) or laminin (Gibco BRL, MD) on the underside of the membrane (migration), or the upperside of the membrane (invasion). For invasion assays, cells chemotracted to media supplemented with 10% fetal bovine serum (FBS) (Tissue Culture Biologicals, CA). Serum starved cells (10^6 cells) were added to the upper surface of each migration chamber and allowed to migrate to the underside of the membrane for 4 hours (migration) or 24 hours (invasion). The non-migratory cells on the upper membrane surface were removed, and the migratory cells attached to the bottom surface of the membrane were stained with propidium iodide (PI) (CalBioChem-Novabiochem Corp., CA). For PI staining, cells were fixed and permeablized in 70% ethanol and then incubated with 40 μg/ml PI in 1X PBS. The number of migratory cells per thirty microscopic fields per membrane was counted with an Olympus upright fluorescence microscope with a 40x objective for migration assays and a 10x objective for invasion assays. Non-specific migration as measured on chambers with no chemoattractant has been subtracted. Effects of the ectopic expression of Rac mutants were assessed 36-48 hours post transfection.

Guanine nucleotide binding

Cell lysates were incubated for 15 min at 30 °C in the presence of 10 mM EDTA and 100 μM GTPγS (Roche, IL) or 1 mM GDP (Sigma, MO) to facilitate nucleotide exchange as described in Knaus, et al. [30]. The loading reaction was stopped by the addition of $MgCl_2$.

Rac and Cdc42 activity assays

Rac and Cdc42 activity assays were performed as described in [19] with minor modifications. Briefly, cells were lysed directly in their 10 cm plates (Fisher Scientific, TX) with ice cold lysis buffer. Lysates were then incubated at 4° with 10 μg of PAK-PBD Protein GST Beads (Cytoskeleton Inc., CO). The bead pellet was washed once with buffer containing 1% Nonidet P-40 (Calbiochem, CA), twice without Nonidet P-40, and suspended in 20 μl Laemelli sample buffer. Proteins from the total cell lysate, as well as the bead pellet, were separated by 10% SDS-PAGE gel, transferred to a nitrocellulose membrane, and blotted for the appropriate GTPase using a monoclonal anti-Rac antibody (clone 32A8, Upstate Biotechnology, NY) or a mouse monoclonal anti-Cdc42 antibody (clone 44, Transduction Laboratories, CA). Immunoblots were detected with the SuperSignal West Femto-Substrate chemiluminescence kit (Pierce Endogen, IL) and Kodak Biomax MR film (Fisher Scientific, TX).

Toxin B Inhibition

Clostridium difficle Toxin B was purchased from Calbiochem (CA) and used as described in {Sliva, 2000 10679229 /id;Woodring, 2002 11864995 /id}. Cells were treated with 2 ng/ml Toxin B for 24 hours before being subjected to haptotaxis assay. These were the conditions required for suppression of all Rho GTPase activity while maintaining 95% cell viability.

Statistical analysis

Data are expressed as means ± SEM. *P*-values were calculated from unpaired (Fig. 2) or paired (Figs. 4-7) t-tests using Microsoft Excel and considered significant at values less than 0.05.

Results

Cytoskeletal and migratory phenotype of MDA-MB-435 metastatic variants correlates with metastatic efficiency.

To understand the role of the Rho GTPases in metastatic breast cancer, we selected variants of the MDA-MB-435 metastatic breast cancer cell line and cycled them through the nude mouse model of experimental metastasis. The variants studied were chosen based on their ability to metastasize from tumors in the mammary fatpad to distant organs, predominantly lungs and lymph nodes. MDA-MB-435α6HG6 variant produced the highest number of distant metastasis from primary mammary tumors, followed by the parental MDA-MB-435, then MDA-MB-435α6LF9, and finally MDA-MB-435Br1. MDA-435Br1 cell line readily forms experimental brain metastases following injection into the intra-carotid artery, yet it shows significantly lower ability to metastasize in the more stringent assay of spontaneous metastasis [13].

An invasive cellular phenotype can be indicative of metastatic behavior [14]. Rac-induced membrane ruffles, or lamellipodia, have been shown not only to be important structures in cellular motility, but have also been shown to play a key role in invasion with respect to metastatic progression [15-16]. Rac-induced lamellipodia contain many cell-substratum contacts, or focal adhesions. Aberrant focal adhesion expression has been associated with malignant progression [17]. Therefore, we investigated the correlation between cytoskeletal phenotype and metastatic efficiency. Our data shows a direct correlation between high lamellipodia expression and increased metastatic efficiency (Figure 1a). The most metastatic variant, MDA-MB-435α6HG6, exhibits a strikingly different phenotype than the other variants,

including an increased number of focal adhesions and a cross-linked actin network. In fact, we found that increased focal adhesion expression correlates with increased metastatic efficiency in all cell variants (Figure 1b). However, individual MDA-MB-435α6HG6 (most metastatic) cells were 1.5 times larger than other variants (data not shown). Thus, the data were compiled as focal adhesions per cell area (Figure 1c). This correlation between lamellipodia, focal adhesions, and metastatic potential strongly suggests an enhanced invasive and motile phenotype correlates with increased metastatic efficiency.

Subsequent to the epithelial to mesenchymal transition, cells must first migrate away from the primary tumor through the basal lamina to begin the process of establishing sites of secondary tumor formation. Therefore, increased cell migration in malignant cells is thought to be closely linked to invasion and metastasis [18]. Upon investigation into the migratory behavior of the cell variants, we found a correlation between increased metastatic potential and increased migration (Figure 2).

Inhibition of Rho GTPase activity suppresses invasive potential of MDA-MB-435 cells

Because the Rho family of small GTPases, namely Rho, Rac, and Cdc42, are essential to cell motility, we used *Clostridium difficile* toxin B to inhibit the Rho family in these cell variants. Toxin B was used as described in {Sliva, 2000 10679229 /id;Woodring, 2002 11864995 /id}. Inhibition of Rho GTPases by incubation in 0.2 ng/ml toxin B for 16 h demonstrated the expected attenuation of Rac-induced lamellipodia in response to *EGF* Subsequent to treatment with toxin B, the most metastatic variant MDA-MB-435α6HG6 exhibited a 50% decrease in migration to basal lamina, while the others exhibited a definite decrease in migration, although

not as striking (Fig. 4a). Therefore, increased migration in the most metastatic variant appears to be regulated in part by the Rho family of small GTPases.

Increased Rac activity can be correlated with MDA-MB-435 metastatic variants

Increases in activity levels of the Rho proteins Rac and Cdc42 have been shown to be accountable for the promotion of tumor cell invasiveness [4,8]. Therefore, we investigated the Rac and Cdc42 activity levels in all MDA-MB-435 metastatic variants. To determine the relative amounts of activated Rac and Cdc42 in the variant panel, we used Rac and Cdc42 activity assays [19]. While total endogenous Rac protein expression remains equal among the cell variants, levels of Rac protein activity ranged from being highest in the most metastatic variant, medium in parental and medium metastatic variant, to least active in the least metastatic variant (Figure 3a). Loading cell lysates with a non-hydrolyzable GTP analog, GTPγS, showed a relatively equal GTP-binding capacity of the Rac protein among the four variants. Therefore, all Rac expressed in the variants of the metastatic panel can potentially be activated to the same extent. Thus, endogenous activators of Rac appear to have increased activity in the more metastatic cell variants. Endogenous Cdc42 protein expression differed slightly among the variants: the more metastatic variants expressed slightly higher levels of endogenous Cdc42 than the less metastatic variants (Figure 3b). However, no active Cdc42 protein could be detected. Again, GTPγS loading showed the ability of the Cdc42 proteins to bind GTP and become active.

Hyperactive Cdc42 has been implicated in tumor cell invasion due to its effects on the actin cytoskeleton [6,20]. To determine a role for Cdc42 in the migration of highly metastatic cells, we expressed vector alone and a dominant negative myc-tagged Cdc42(T17N) construct in the highly metastatic MDA-MB-435α6HG6 cell variant and subjected both to a migration assay.

We found that expression of Cdc42(T17N) did not inhibit migration as compared to the vector alone control (Figure 4a). However, when we expressed vector alone, dominant negative Rac1(T17N), or dominant negative Rac3(T17N), we found a significant inhibition of migration as compared to the vector control (Figure 4b). Therefore, Rac activity appears to be essential for the migration of highly metastatic cells, while Cdc42 activity does not.

Ectopic Rac(G12V) expression augments the invasive phenotype of low metastatic breast cancer cells.

Invasive malignant cell morphology includes an increased number of focal adhesions, as well as an increase in actin structures such as cross-linked actin fibers and membrane ruffles [16]. The morphology of the low metastatic cell variant MDA-MB-435Br1 when expressing vector alone is indicative of a less invasive cell. Actin fibers are not cross-linked, lamellipodia are limited to the proximal and distal ends of the cell, and focal adhesions are few (Figure 5). Conversely, MDA-MB-435Br1 cells expressing myc-tagged Rac1(G12V) or Rac3(G12V) exhibit cross-linked actin fibers, numerous focal adhesions, and lamellipodia expressed ubiquitously around the periphery of the cell (Figure 5). Expression of either myc-tagged Rac1(T17N) or Rac3(T17N) in the highly metastatic MDA-MB-435α6HG6 variant resulted in a slight decrease in focal adhesion number and size of lamellipodia, compared to the vector alone control (data not shown). Expression of dominant negative Cdc42(T17N) in the same cell variant resulted in no significant alteration of phenotype compared to the vector alone control (data not shown).

Rac mutants significantly alter cellular processes essential to metastatic behavior.

Because metastatic progression results from increased migration of malignant cells out of the basal lamina, subsequent adhesion to the extracellular matrix, and final invasion into distant tissues to establish secondary sites of metastasis, we measured the effect of Rac mutants on these processes *in vitro*. For each of these assays, cells expressed equal amounts of activated Rac1 or Rac3 mutant protein (data not shown).

Recent data indicate that changes in cell adhesion play a critical role in tumor progression [21]; thus, we tested the ability of Rac mutants to alter adhesive properties of malignant cells *in vitro*. Expression of dominant active Rac1(G12V) or Rac3(G12V) causes a significant increase in adhesion to basal lamina when expressed in low metastatic MDA-MB-435Br1 as compared to the vector alone control, while dominant negative Rac1(T17N) or Rac3(T17N) cause a significant decrease in adhesion when expressed in high metastatic MDA-MB-435α6HG6 (Fig 6a,d).

A requirement of malignant cells to undergo metastasis is to acquire the ability to penetrate the surrounding extracellular matrix in order to migrate to distant tissues [22]; thus, we tested the effect of Rac mutants on both migration and invasion *in vitro*. Expression of either myc-tagged Rac1(G12V) or Rac3(G12V) caused a significant increase in migration and invasion when expressed in the low metastatic variant (Figure 6b,c). Surprisingly, Rac3(G12V) expressing cells invaded through basal lamina 1.5 times more than cells expressing Rac1(G12V); however, this difference was just a trend and was not statistically significant (Figure 6b). Invasion of high metastatic cells expressing dominant negative Rac1(T17N) or Rac3(T17N) was significantly diminished as compared to the vector alone control (Figure 6e). Furthermore, migration was also significantly reduced in highly metastatic cells expressing dominant negative

mutants of Rac isoforms as compared to vector control (Figure 4b). Taken together, this data establishes the efficacy both Rac1 and Rac3 in human breast cancer progression.

Discussion

The present study demonstrates a strong correlation between the invasive phenotype, increased Rac activity, and the increased metastatic efficiency of the variants of the MDA-MB-435 metastatic human breast cancer cell line. These cell variants reflect the relative ability to form lung metastases from established mammary tumors in the nude mouse of experimental metastasis.

The invasive phenotype, characterized by extensive cross-linked actin networks and increased lamellipodial expression have long been associated with increased motility and invasion [23]. More recently, this specific phenotype has been linked to cells with an inherent ability to metastasize [14]. Our study adds to this field by correlating an increasing aggressive phenotype with an increase of metastatic efficiency in a panel of metastatic cell variants. Oncogenically mutated forms of Rac and Rho proteins have not been found in human cancer cells; instead, it is thought that amplification of Rho family proteins or activation of their upstream regulators such as exchange factors contribute to the ability of these GTPases to influence the transformed phenotype [4, 8, 31]. Therefore, the observed variation in Rac activity of the MDA-MB-435 cell variants is probably due to disparities in the activity of upstream regulators of Rac.

We also show that an increase in focal adhesion number per cell area correlates directly with metastatic efficiency. The physiological significance of this finding is less clear due to discrepancies in the literature on the relative contribution of focal adhesion number to cell

motility. Some studies assert that a simple redistribution or relocalization of focal adhesions is sufficient to alter motility signaling pathways to the point of invasive transformation [24]. Other studies maintain that increased tyrosine phosphorylation and focal adhesion expression are correlated with the progression to an invasive cell phenotype [17]. Our study shows that the increased number of focal adhesions in highly metastatic cells is likely to be located in the lamellipodia, which are also increased in the more highly metastatic variants. Thus, we conclude that an increased number of focal adhesions is correlative with increased invasion. Rac activation can lead to actin polymerization and lamellipodia formation, which in turn can lead to the creation of focal adhesions. Focal adhesion formation can then activate Rac, which creates a positive feedback loop that, when disregulated, can lead to increased motility and invasion [25]. This positive feedback loop is most likely what is being activated in these cell variants to produce the specific phenotype and increased focal adhesion patterns. Supporting this hypothesis is the increased Rac activity found in the more metastatic cell variants.

Surprisingly, we show in this study that Cdc42 is not activated in any of the cell variants, including the variant with the highest metastatic efficiency. This finding is unexpected because Cdc42 is essential to cellular motility via WASP (Wiskott Aldrich Syndrome Protein), Arp2/3 (actin-related protein), and subsequent actin polymerization and filopodia formation [26]. Furthermore, Cdc42 has also been implicated in both transformation and malignant progression of cancer [6,27]. Additionally, we show that blocking all Cdc42 activity cannot prevent the most metastatic variant from haptotaxing to basal lamina. This finding suggests that Cdc42 is not vital to malignant invasion in breast cancer, perhaps because Rac and Cdc42 are redundant in many of the roles they play in cell motility. For example, both Rac and Cdc42 can activate Arp2/3 to

result in actin polymerization. Whereas Cdc42 activates Arp2/3 through WASP, Rac activates Arp2/3 through WAVE (WASP family verprolin homolog) [26].

In this study we also demonstrate the efficacy of both the Rac1 and Rac3 isoforms in the malignant progression of human breast cancer. Because Rac1 and Rac3 both have been implicated in breast cancer [12,28], we carried out a comparative study between the two isoforms. We found that blocking Rac activity by expressing dominant negative mutations of Rac1 or Rac3 significantly curtailed cellular processes critical for metastatic progression *in vitro*. Moreover, we found that augmenting endogenous Rac activity by expressing dominant active Rac1 or Rac3 led to a significant increase in adhesion, migration, and invasion. Taken together, these data substantiate not only a vital role for Rac1 in cell functions relevant for breast cancer metastasis, but also a vital role for Rac3. In fact, expression of a dominant active Rac3 in the MDA-MB-435Br1 low metastatic cell variant increased invasion through basal lamina 1.5 times as compared to expression of dominant active Rac1. This difference suggests an enhanced ability of the cells expressing Rac3(G12V) to invade, perhaps by a more efficient degradation of the extracellular matrix, as compared to the cells expressing Rac1(G12V). Because we found that expression of dominant active Rac1 or Rac3 results in a similar motile phenotype, it is possible that Rac3 is more efficient at activating proteins that degrade extracellular matrix proteins, or matrix metalloproteinases (MMPs), than is Rac1.

Rac1 and Rac3 differ in their C-terminus region which is essential for subcellular localization [9]. Even though protein function is likely partially redundant due to the homology of the downstream effector loops, these proteins have been found to differ in their localization within certain types of cells [11]. Differential subcellular localization can place proteins in the

proximity of different signaling cascades, resulting in differential function. However, more experiments are needed to show that Rac1 actually acts differently than Rac3 with respect to human breast cancer.

Studies have also demonstrated that in addition to the Rac proteins Rho proteins, especially RhoC may contribute to breast cancer cell invasion. RhoC was demonstrated to be overexpressed in the human inflammatory breast cancer (IBC) cell line SUM 149 and transient inhibition of RhoC in IBC cells by treatment with farnesyl transferase inhibitors reduced invasion and motility *in vitro*, while RhoC overexpression in mammary epithelial cells resulted in a significant increase in cell migration {van Golen, K. Merajver.}. Interestingly, the most metastatic MDA-MB-435 variant demonstrated the highest Rho activity (data not shown) and future studies will include an analysis of Rho isoforms to the metastatic phenotype in breast cancer.

Conclusions

We found a direct correlation between increased metastatic potential and increased endogenous Rac activity in a panel of metastatic human breast cancer cells that vary in their ability to form secondary metastases in an *in vivo* model. By using variants of the same cell line, we have minimized genetic variation. However, it remains to be investigated whether or not similar results will be observed in other cell lines with different genetic backgrounds.

The research presented here establishes a direct role for Rac3 in cell functions relevant for breast cancer progression. We found that Rac3 activation alone can significantly increase *in vitro* metastatic properties in human breast cancer cells. Currently, we are testing the hypothesis

that Rac3 activation alone can increase breast cancer metastasis *in vivo* by using the nude mouse model of experimental metastasis.

List of Abbreviations:

ECM: extracellular matrix

Arp2/3: Actin Related Protein 2/3

WASP: Wiskott Aldrich Syndrome Protein

WAVE: WASP family verprolin homolog

Author's Contributions: PB characterized the morphology and motile phenotypes of MDA-MB-435 variants and the dominant active (RacGV) cell lines, carried out activity assays, generated the dominant active stable cell lines, participated in the design of the study, and drafted the manuscript. LK generated the dominant negative stable cell lines and characterized their motility phenotypes. JP provided the cell variants and participated in the coordination of the study. SD conceived of the study, participated in its design, supervised experiments, and helped to draft the manuscript.

Acknowledgements: We wish to thank John Mendenhall of the core facility at the Institute for Cellular and Molecular Biology at the University of Texas at Austin for his expertise with the confocal fluorescent microscope. We would also like to thank Drs. Gary Bokoch and Ulla Knaus of the Scripps Research Institute (La Jolla, CA) for their provision of Rac1 and Rac3 mutant constructs, respectively. We are also grateful to Nicoas G. Azios for editing and statistical analysis of data. This work was funded by grants from Susan G. Komen Breast Cancer Research Foundation to P.B. and NIH/NCI R21 CA83957 and U.S. Army/BRCP DAMD17-02-1-0582 to S.D.

References

1. Sahai E, Marshall CJ: **ROCK and Dia have opposing effects on adherens junctions downstream of Rho.** *Nat Rev Cancer* 2002, **2**:133-142.

2. Miranti CK, Brugge JS: **Sensing the environment: a historical perspective on integrin signal transduction.** *Nat Cell Biol* 2002, **4**:E83-E90

3. Hynes RO: **Integrins: bidirectional, allosteric signaling machines.** *Cell* 2002, **110**:673-687.

4. Price LS, Collard JG: **Regulation of the cytoskeleton by Rho-family GTPases: implications for tumour cell invasion.** *Semin Cancer Biol* 2001, **11**:167-173.

5. Lee TK, Man K, Ho JW, Wang XH, Poon RT, Sun KW, Ng KT, Ng IO, Xu R, Fan ST: **The significance of Rac signaling pathway in HCC cell motility: implication for new therapeutic target.** *Carcinogenesis* 2004, **26(3)**:681-7.

6. Bouzahzah B, Albanese C, Ahmed F, Pixley F, Lisanti MP, Segall JD, Condeelis J, Joyce D, Minden A, Der CJ, Chan A, Symons M, Pestell RG: **Rho family GTPases regulate mammary epithelium cell growth and metastasis through distinguishable pathways.** *Mol Med* 2001, **7**:816-830.

7. Uhlenbrock K, Eberth A, Herbrand U, Daryab N, Stege P, Meier F, Friedl P, Collard JG, Ahmadian MR: **RacGEF Tiam1 inhibits migration and invasion of metastatic melanoma via a novel adhesive mechanism.** *J Cell Sci* 2004, **117**:4863-4871.

8. Fritz G, Brachetti C, Bahlmann F, Schmidt M, Kaina B: **Rho GTPases in human breast tumours: expression and mutation analyses and correlation with clinical parameters.** *Br J Cancer* 2002, **87**:635-644.

9. Haataja L, Groffen J, Heisterkamp N: **Characterization of RAC3, a novel member of the Rho family.** *J Biol Chem* 1997, **272**:20384-20388.

10. Chou MM, Blenis J: **The 70 kDa S6 kinase complexes with and is activated by the Rho family G proteins Cdc42 and Rac1.** *Cell* 1996, **85**:573-583.

11. Bolis A, Corbetta S, Cioce A, de Curtis I: **Differential distribution of Rac1 and Rac3 GTPases in the developing mouse brain: implications for a role of Rac3 in Purkinje cell differentiation.** *Eur J Neurosci* 2003, **18**:2417-2424.

12. Leung K, Nagy A, Gonzalez-Gomez I, Groffen J, Heisterkamp N, Kaartinen V: **Targeted expression of activated Rac3 in mammary epithelium leads to defective postlactational involution and benign mammary gland lesions.** *Cells Tissues Organs* 2003, **175**:72-83.

13. Mukhopadhyay R, Theriault RL, Price JE: **Increased levels of alpha6 integrins are associated with the metastatic phenotype of human breast cancer cells.** *Clin Exp Metastasis* 1999, **17**:325-332.

14. Schmitz AA, Govek EE, Bottner B, Van Aelst L: **Rho GTPases: signaling, migration, and invasion.** *Exp Cell Res* 2000, **261**:1-12.

15. Ridley AJ: **Rho GTPases and cell migration.** *J Cell Sci* 2001, **114**:2713-2722.

16. Condeelis JS, Wyckoff JB, Bailly M, Pestell R, Lawrence D, Backer J, Segall JE: **Lamellipodia in invasion.** *Semin Cancer Biol* 2001, **11**:119-128.

17. Schlaepfer DD, Mitra SK, Ilic D: **Control of motile and invasive cell phenotypes by focal adhesion kinase.** *Biochim Biophys Acta* 2004, **1692**:77-102.

18. Ridley AJ, Schwartz MA, Burridge K, Firtel RA, Ginsberg MH, Borisy G, Parsons JT, Horwitz AR: **Cell migration: integrating signals from front to back.** *Science* 2003, **302**:1704-1709.

19. Benard V, Bohl BP, Bokoch GM: **Characterization of rac and cdc42 activation in chemoattractant- stimulated human neutrophils using a novel assay for active GTPases.** *J Biol Chem* 1999, **274**:13198-13204.

20. Sturge J, Hamelin J, Jones GE: **N-WASP activation by a beta1-integrin-dependent mechanism supports PI3K-independent chemotaxis stimulated by urokinase-type plasminogen activator.** *J Cell Sci* 2002, **115**:699-711.

21. Cavallaro U, Christofori G: **Multitasking in tumor progression: signaling functions of cell adhesion molecules.** *Ann N Y Acad Sci* 2004, **1014**:58-66.

22. Playford MP, Schaller MD: **The interplay between Src and integrins in normal and tumor biology.** *Oncogene* 2004, **23**:7928-7946.

23. Burbelo P, Wellstein A, Pestell RG: **Altered Rho GTPase signaling pathways in breast cancer cells.** *Breast Cancer Res Treat* 2004, **84**:43-48.

24. Guo W, Giancotti FG: **Integrin signalling during tumour progression.** *Nat Rev Mol Cell Biol* 2004, **5**:816-826.

25. Burridge K, Wennerberg K: **Rho and Rac take center stage.** *Cell* 2004, **116**:167-179.

26. Bompard G, Caron E: **Regulation of WASP/WAVE proteins: making a long story short.** *J Cell Biol* 2004, **166**:957-962.

27. Jaffe AB, Hall A: **Rho GTPases in transformation and metastasis.** *Adv Cancer Res* 2002, **84:**57-80.

28. Mira JP, Benard V, Groffen J, Sanders LC, Knaus UG: **Endogenous, hyperactive Rac3 controls proliferation of breast cancer cells by a p21-activated kinase-dependent pathway.** *Proc Natl Acad Sci U S A* 2000, **97:**185-189.

29. Klemke RL, Leng J, Molander R, Brooks PC, Vuori K, Cheresh DA: **CAS/Crk coupling serves as a "molecular switch" for induction of cell migration.** *J Cell Biol* 1998, **140:**961-972.

30. Knaus UG, Heyworth PG, Kinsella BT, Curnutte JT, Bokoch GM: **A cytosolic GTP-binding protein that regulates human neutrophil NADPH oxidase.** *J Biol Chem* 1992, **267:**23575-23582.

31. Rihet S., Vielh P., Camonis J., Goud B., Chevillard S., de Gunzburg J. Mutation status of genes encoding RhoA, Rac1, and Cdc42 GTPases in a panel of invasive human colorectal and breast tumors. J. Cancer Res. Clin. Oncol., *127:* 733-738, 2001.

Figure Legends

Figure 1. Characterization of cytoskeletal structures and focal adhesion distribution in MDA-MB-435 metastatic variants. **(a)** Each of the MDA-MB-435 metastatic variants was plated onto glass coverslips. Actin was visualized with rhodamine phalloidin and focal adhesions were visualized with an anti-p-tyro antibody followed by an FITC conjugated secondary antibody. **(b)** Cell area was measured on 50 individual cells per variant using Spot Digital Camera Software. Focal adhesion number was divided by cell area and plotted on the y-axis. Bars represent (+/-) SEM, and are representative of three independent experiments. Treatments denoted by the same letter indicate no significant difference between those treatments. Treatments denoted by different letters indicate a significant difference between those treatments ($P<0.01$).

Figure 2. Haptotaxis assays of MDA-MB-435 metastatic variants. Each variant was adjusted to 500,000 cells and applied to Transwell chambers in a haptotaxis assay, where the underside of the membrane was coated with matrigel. Cells migrating to the underside of the chamber were stained with PI and counted under (400X). Bars represent (+/-) SEM. Data is representative of three independent experiments. Treatments denoted by the same letter indicate no significant difference between those treatments. Treatments denoted by different letters indicate a significant difference between those treatments ($P<0.01$).

Figure 3. Rac and Cdc42 activity in MDA-MB-435 metastatic variants. Whole cell lysates of all variants were subjected to SDS-PAGE followed by western blot analysis for **(a)** total Rac using an anti-Rac antibody and total **(b)** Cdc42 using an anti-Cdc42 antibody. Rac and Cdc42 activities were assayed using the PAK-PBD activity assay. A non-hydrolyzable GTP analog,

GTPγS, was used as the positive control; GDP alone was used for the negative control. Equal loading of lanes was maintained by performing a total protein assay and is confirmed by western blot analysis for total actin. Results are representative of three to five independent experiments.

Figure4. Inhibition of Rho GTPases, Rac, or Cdc42 in migration of high metastatic MDA-MB-435α6HG6 cell variant. **(a)** MDA-MB-435α6HG6 cells were treated with vehicle or 2 ng/ml Toxin B for 24 h and subjected to a basement membrane haptotaxis assay. Cells migrating to the underside of the membrane were stained with PI and counted under (400X). **(b)** MDA-MB-435α6HG6 cells transiently expressing vector alone or myc-Cdc42(T17N) were subjected to a basement membrane haptotaxis assay. Cells migrating to the underside of the membrane were stained with PI and counted under (400X). Equal loading was confirmed by a total actin blot, myc-Cdc42(T17N) expression confirmed by western blotting with anti-myc. **(c)** MDA-MB-435α6HG6 cells transiently expressing vector alone, myc-Rac1(T17N), or myc-Rac3(T17N) were subjected to a basement membrane haptotaxis assay. Bars represent (+/-) SEM, equal loading was confirmed by total actin blot. Myc-Rac1(T17N) and myc-Rac3(T17N) expression were confirmed by western blotting with anti-myc. Data expressed as mean ± SEM of three independent experiments. A star denotes statistical significance from control ($p<0.05$).

Figure 5. Ectopic dominant active Rac(G12V) expression in low metastatic variant MDA-MB-435Br1. Confocal DIC and fluorescent microscopy was performed on MDA-MB-435Br1 cell variant stably expressing vector alone, myc-Rac1(G12V), or myc-Rac3(G12V). Cells were plated on glass coverslips, fixed in 3.7% formaldehyde and permeablized with 0.2% Triton X-

100. Actin was then visualized with rhodamine phalloidin and focal adhesions were visualized with an anti-p-tyro antibody followed by an FITC conjugate.

Figure6. Effects of mutant Rac isoforms on metastatic properties *in vitro*. MDA-MB-435Br1 cells transiently transfected with vector alone, myc-Rac1(G12V), or myc-Rac3(G12V), were subjected to adhesion **(a)**, haptotaxis **(b)**, and invasion assays **(c)**. MDA-MB-435α6HG6 cells transiently expressing vector alone, myc-Rac1(T17N), or myc-Rac3(T17N), were subjected to adhesion **(d)**, and invasion assays **(e)**. Cells were counted under (200X) for adhesions assays, and (400X) for haptotaxis and invasion assays. Y-axis represents the number of cells/field for at least 20 microscopic fields per variant. Bars represent standard error of the mean, and are representative of at least 3 separate experiments. An asterix indicates a statistically significant difference compared to the control, vector alone, as determined by a Student's *t*-test ($P<0.05$).

Figure 1
Baugher, et al.

a.

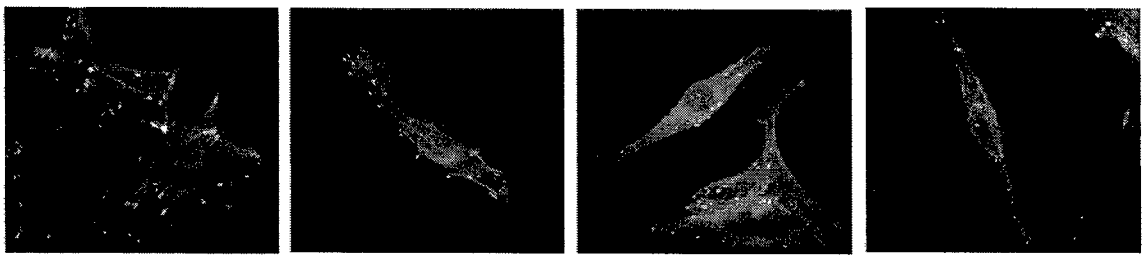

b.

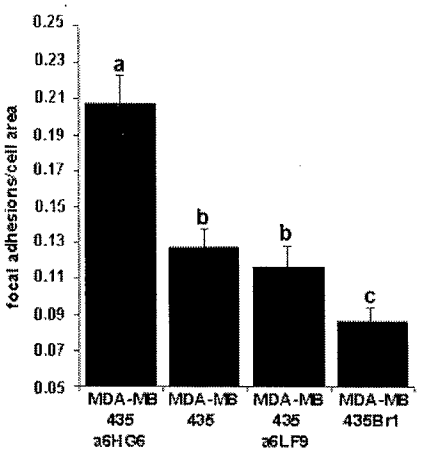

Figure 2
Baugher, et. al.

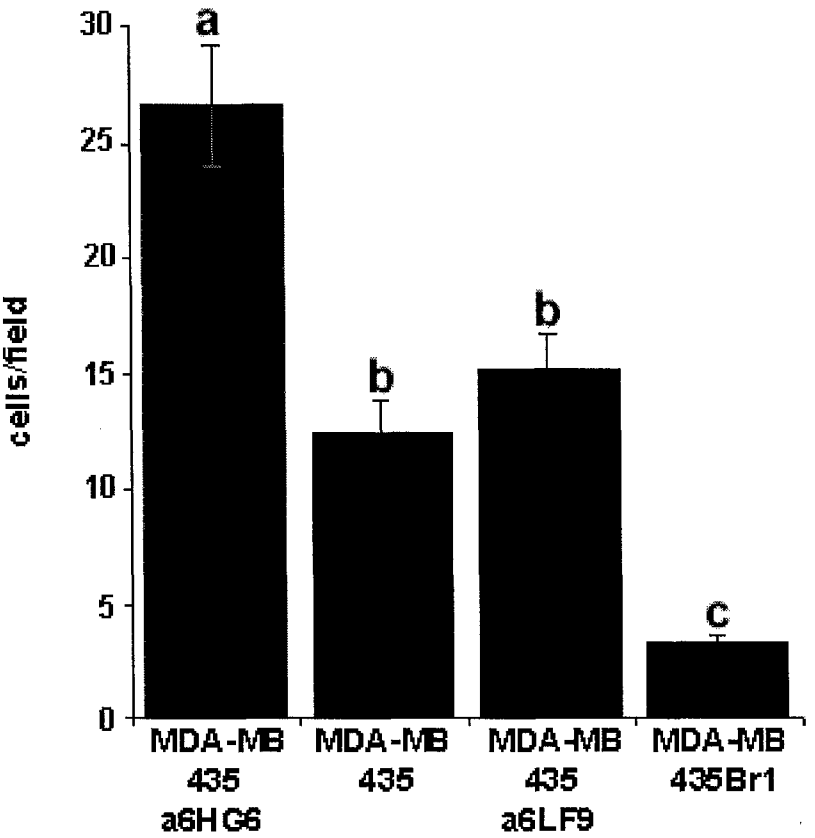

Figure 3
Baugher, et. al.

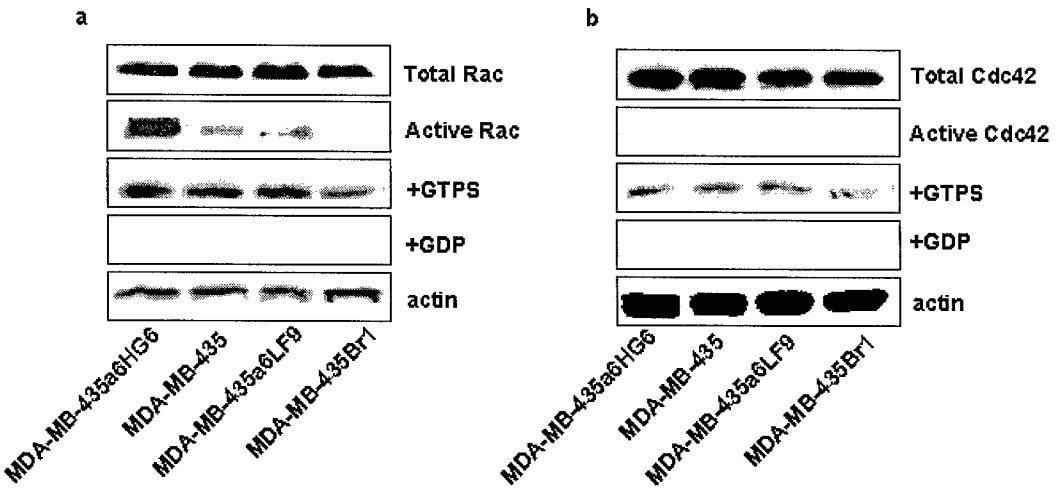

Figure 4
Baugher, et.al.

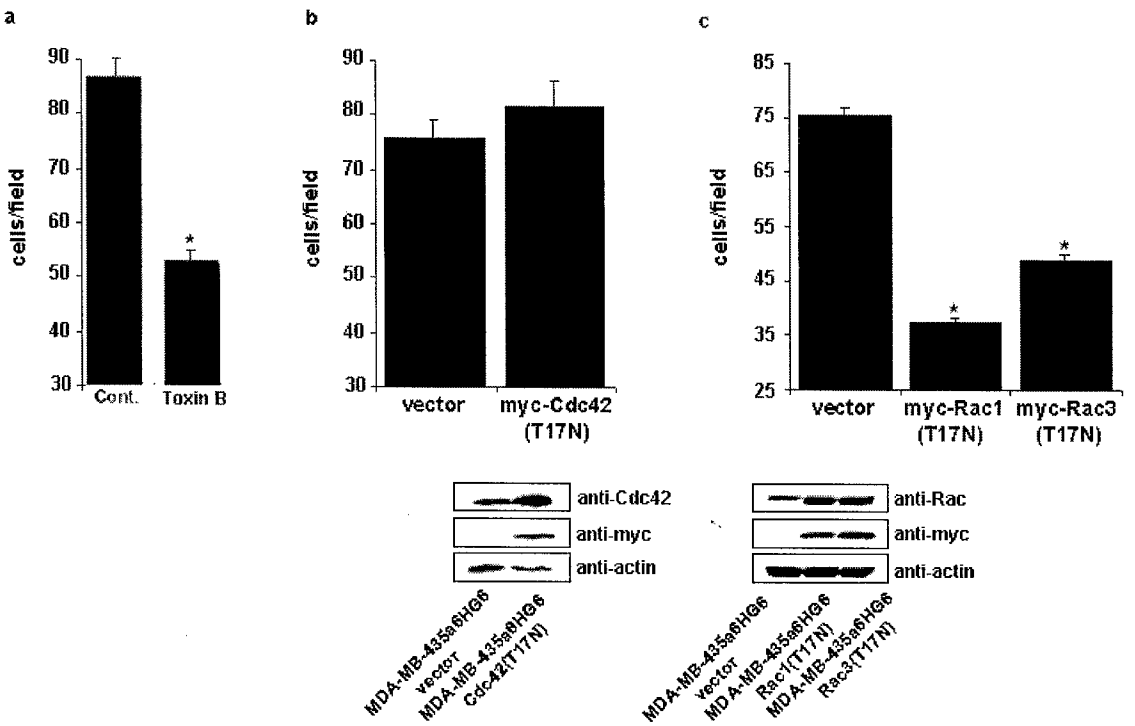

Figure 5
Baugher, et. al.

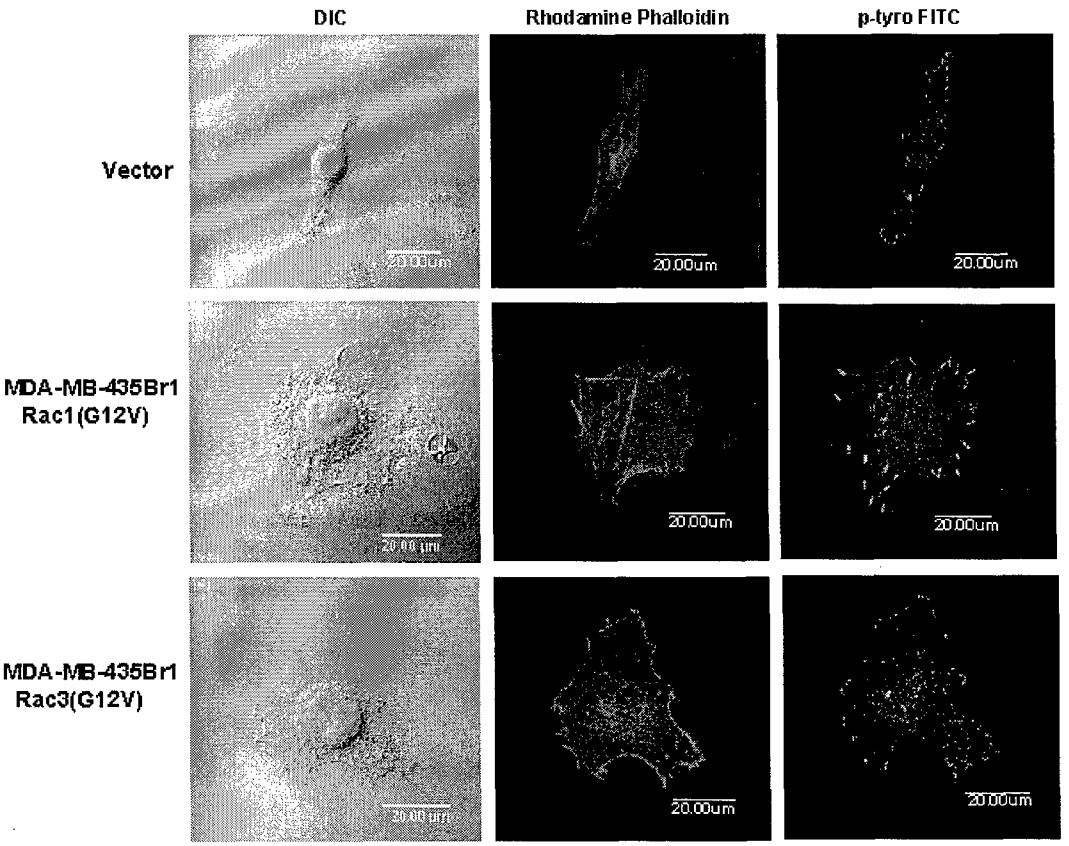

Figure 6
Baugher, et. al.

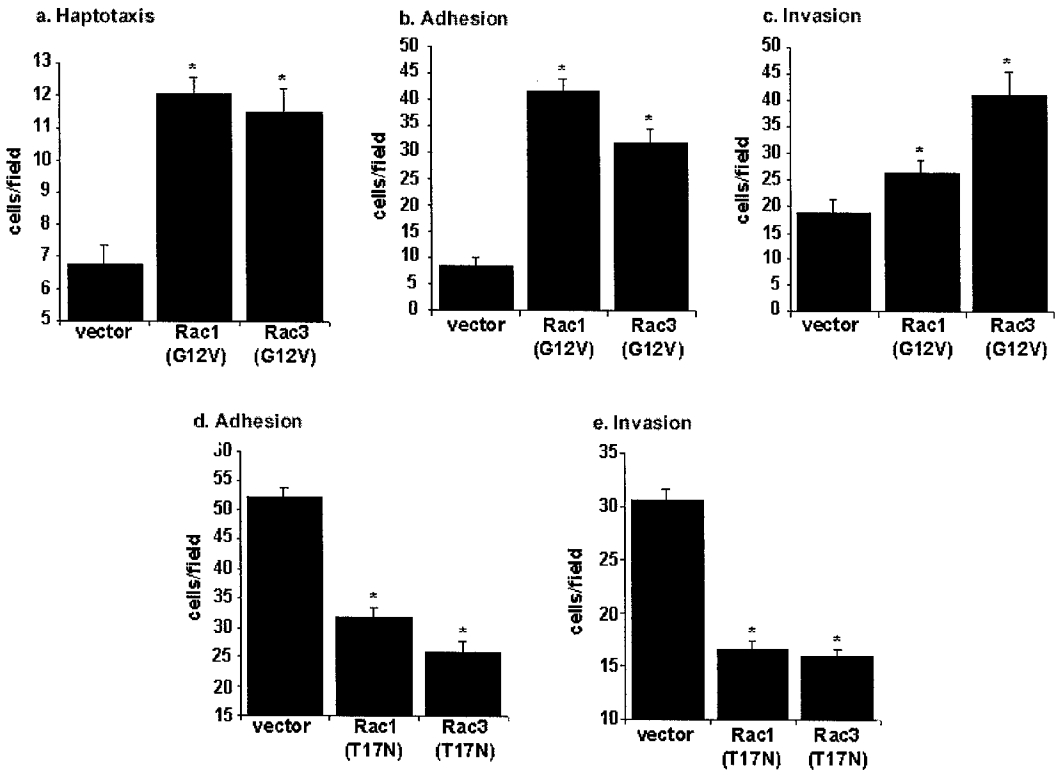

Development of a macroscopic fluorescence imaging system for *in situ* analysis of human breast cancer progression in murine models

Alicia L. Carlson[1#], Michaela R. Hoffmeyer[2#], Kristin M. Wall[1], Paige J. Baugher[2], Rebecca Richards-Kortum[1], and Suranganie F. Dharmawardhane[2*]

Department of Biomedical Engineering[1], Molecular Cell and Developmental Biology Section[2], and Institute for Cellular and Molecular Biology, The University of Texas at Austin, Austin, TX 78712

Running Title: *In situ* image analysis of breast cancer progression

Nonstandard abbreviations: RFP, red fluorescent protein

Keywords: fluorescence imaging, intravital imaging, breast cancer

[#] These authors contributed equally to the manuscript.

[*]To whom correspondence should be addressed:
Current address:
Department of Anatomy and Cell Biology
Universidad Central del Caribe School of Medicine
P.O. Box 60327
Bayamon, PR 00960-6032
Tel: 512-560-1835, 787-798-3001
E-mail: surangi@mail.utexas.edu, surangi@uccaribe.edu

Abstract

Classic studies of breast cancer progression involve analysis of the initial primary tumors and end point metastases, thus limiting a direct evaluation of the multifaceted nature of metastasis. The goal of this study was to develop an inexpensive *in vivo* macroscopic imaging system to monitor fluorescent protein expressing human tumor progression in immunocompromised mice in real-time with no or minimal intervention. This system uses a fiber optic probe to deliver excitation light to the mouse in order to verify successful mammary fat pad tumor take and temporally monitor and quantify tumor progression via fluorescence intensity. This system is also useful for identification of potential distant metastases for further histological analysis. The macroscopic fluorescence imaging system we have designed represents an inexpensive and portable tool to facilitate non-invasive *in situ* cancer detection with the potential to monitor fluorescent tumor formation and progression as well as investigate the efficacy of potential cancer preventatives and therapeutics.

Introduction

Breast cancer is estimated to account for 32% of the new cancer cases in woman in 2005 and is the second major cause of cancer deaths behind lung cancer. Metastatic spread of breast cancer complicates treatment and lowers patient prognosis drastically [1]. Use of mouse models is a common and effective research tool to study breast cancer progression, potential oncogenes and tumor suppressors, and to investigate prospective therapeutics to specifically target metastatic spread [2-5]. Current methods for studying cancer progression and therapeutic agent efficacy include end point analysis of metastases following primary mammary tumor induction in mouse models. Such end point analysis limits investigation of the individual steps in the multi-facetted process of metastasis. Therefore, improved techniques that directly visualize tumor formation, growth, and metastasis in real time are required.

Studies by our laboratory and others with the mouse model of breast cancer have brought to light many limitations. Specifically, mouse mammary fat pad injection does not always lead to 100 percent successful mammary tumor establishment. Post-injection observation for successful tumor establishment requires examination of the injection site for growth over several weeks. Scar tissue formation at the site of injection often obscures successful tumor take. A means to verify successful mammary fat pad tumor implantation and the ability to monitor tumor growth reliably over time is needed. Furthermore, identification of potential metastatic sites for further histological examination is difficult for those not trained in pathology and often must occur after mouse sacrifice. Therefore, a tool to reliably delineate metastatic sites for detailed histological examination would be beneficial. Finally, a reliable and accurate pre-clinical means to test for potential genetic contributors and anti-cancer therapies in the mouse model of human breast cancer is desired. Therefore, a more recent approach has been to develop novel *in situ* imaging modalities to facilitate these needs [6-26].

The goal of this study was to develop an inexpensive *in vivo* macroscopic imaging system for real-time image analysis of tumor formation by red fluorescent protein (RFP) expressing breast cancer cells in mice. This system uses a fiber optic probe to deliver excitation light to the mouse in order to verify successful mammary fat pad tumor take and temporally monitor tumor progression via fluorescence intensity. Additionally, this system can be employed to locate small metastatic lesions via fluorescent signal non-invasively or by minimal invasion using a skin flap. Fluorescent protein emission can also be used by this system to identify potential metastatic areas of interest for further histological analysis. The macroscopic fluorescence imaging system we have designed thus represents an inexpensive and portable tool to facilitate *in situ* cancer detection without the need to anesthetize the animal.

Materials and Methods

Cell Culture

The SUM 149 inflammatory breast cancer (IBC) cell line used for the study was developed from pleural effusions of breast cancer patients [27, 28] and was a generous gift of Dr. Stephen Ethier, The University of Michigan, MI. SUM 149 cells were cultured in F-12 Hams medium (Gibco^{TM}, CA) supplemented with 5% fetal bovine serum (Tissue Culture Biologicals, CA), insulin, and hydrocortisone and cultured in a humidified 5% CO_2 atmosphere at 37°C. The human breast cancer cell line MDA-MB-435α6HG6 was selected according to α6 expression and metastatic efficiency in the nude mouse model as described in [29] and was the kind gift of Dr. Janet E. Price, MD Anderson Cancer Center, Houston, TX. MDA-MB-435α6HG6 cells were cultured in Dulbecco's modified Eagle's medium (DMEM) (Gibco^{TM}, CA) with 10% fetal bovine serum (Tissue Culture Biologicals, CA) and cultured in a humidified 5% CO_2 atmosphere at 37°C.

Vector Construction

SUM 149 cells were transfected with pIRESneo2 DsRed2 (RFP) and the MDA-MB-435 α6HG6 cells were transfected with pIRESpuro3 DsRed2 (RFP) using Lipofectamine as per the manufacture's protocol (Invitrogen, CA). RFP-SUM 149 cells were selected in neomycin and RFP-MDA-MB-435-α6HG6 cells were selected in puromycin. The MDA-MB-435α6HG6 cells stably expressing RFP were further selected via flow cytometry. RFP expression of both cell lines remained stable at ~99% expression in cells that were maintained for two to three months in cell culture and ~95% in cell lines that were restarted following storage in liquid nitrogen for at least a year.

Macroscopic Imaging System

A schematic of the macroscopic imaging system is shown in Figure 1. Light from a 300W Xenon arc lamp with an integrated parabolic reflector (Perkin Elmer, CA) was directed by a cold mirror to the excitation filter wheel (Oriel Instruments, CT). The cold mirror rejected radiation below 300 nm and above 625 nm, preventing ultraviolet and infrared radiation from reaching the excitation filter. A bandpass filter centered at 545 nm was used to select the desired excitation wavelengths (HQ545/30x, Chroma Technology, VT). One filter slot remained open for white light illumination to visualize the position of the mouse. Excitation light was focused onto a flexible fiber optic light guide 5 mm in diameter and 2.5 m long (Multimode Fiber Optics Inc., NJ) for delivery to the mouse. With the 545 nm excitation filter in place, approximately 60 mW of light exited the light guide and diverged rapidly to illuminate a large region of the mouse. Fluorescence emission from the mouse was recorded using a Canon EOS-D30 digital camera equipped with two emission filters, a bandpass filter centered at 610nm (HQ610/75m, Chroma Technology, VT) and a 570nm longpass filter (Schott OG570, Newport Industrial Glass, Inc., CA), attached prior to the camera lens. The filters were easily removed for imaging with white light illumination.

In vivo imaging of RFP expressing cells

All mouse experiments were approved by and preformed in accordance with the Institutional Animal Care and Use Committee (IACUC) at The University of Texas at Austin. For *in vivo* imaging of RFP-SUM 149 breast cancer progression, $1x10^6$ cells suspended in PBS were injected into the mammary fat pad of 6 week old female SCID (severe combined immunodeficiency) mice (CBySmn.CB17-*Prkdc*^{scid}/J , Charles Rivers, MA). For RFP-MDA-MB-435α6HG6 *in vivo* imaging experiments, $2x10^6$ cells suspended in PBS were injected into the mammary fat pad of 6 week old female nude immunocompromised mice (*nu/nu,* Charles Rivers, MA). Mice were manually restrained and imaged under white light illumination. After fitting the camera with the emission filter, the mice were imaged under RFP excitation light. Imaging occurred 2-3 times per week. Digital images were checked for saturation in each color channel and those that were not saturated were then converted to grayscale using Matlab (The MathWorks, Natick, MA). Image intensity was normalized by the camera exposure time prior to analysis. Tumor area was manually traced in each grayscale image using Image J software (freeware provided by the NIH, Bethesda, MD). The mean grayscale value was calculated and the number of pixels was determined and converted to mm^2 for the traced tumor area and plotted versus time.

Results

Image analysis of RFP-expressing breast cancer cells

To verify the expression of RFP and the lack of fluorescence in the parental, non-RFP breast cancer cells, we viewed cell pellets containing $4x10^6$ cells with the macroscopic imaging system prior to mammary fat pad injection (Fig. 2A and B). All of the RFP-tagged breast cancer cells that were used for this study expressed RFP at a 99-100% efficiency. Figure 2A illustrates cell pellets viewed under RFP excitation for SUM 149 (Fig. 2A left) and RFP-tagged SUM 149 (Fig. 2A right) cells. MDA-MB-

435α6HG6 cells were also pelleted (Fig. 2B left) and imaged along side a RFP-tagged MDA-MB-435α6HG6 cell pellet (Fig. 2B right). No fluorescent signal was detected under RFP excitation by our system for either of the parental, non-RFP expressing cell lines. RFP and parental MDA-MB-435α6HG6 cells were also imaged by fluorescence microscopy (Fig. 2C-F). Again, no RFP fluorescence was detected under 100x magnification from the parental cell line (Fig. 4D) while the RFP-tagged MDA-MB-435α6HG6 cells exhibited uniform red fluorescence at a 100% efficiency (Fig. 4F).

Image analysis of RFP-tagged IBC tumors in SCID mice

Figure 3 represents white light and fluorescent images of stably expressing RFP-SUM 149 IBC human breast cancer establishment and progression in the mammary fat pad of female SCID mice. The fluorescent imaging system was easily able to detect $1X10^5$ RFP-tagged breast cancer cells in the syringe prior to injection and underneath the mouse skin following injection at six times more fluorescence intensity than background autofluorescence (data not shown). White light images represent the location and relative size of the mammary tumor. Nodules, such as the one observed in the white light image at three days after mammary fat pad injection, may represent scar tissue or inflammation rather than an actual tumor. Using our macroscopic fluorescence imaging system to excite RFP fluorescence, we were able to visualize the site of breast cancer cell injection in the mammary fat pad and tumor take at and survival in the SCID mouse host at day 3 in the fluorescent image. At day 35, the white light image of the same mouse showed a clearly discernable mammary tumor. This tumor at day 35 showed a substantial increase in red fluorescence signal.

In parallel, female SCID mice were also injected in the mammary fat pad with non-RFP expressing SUM 149 human breast cancer cells. Two days post injection, a region of potential mammary tumor formation by the injected non-fluorescent breast cancer cells was perceived in the white light image and, as expected, there was no detectable fluorescence signal under RFP excitation illumination. By day 34, a non-RFP expressing SUM 149 tumor was clearly visible under white light in the mammary fat pad

of the SCID mouse. As expected, no RFP emission was detected under fluorescence imaging. Interestingly, the tumor exhibited diminished background fluorescence. This was possibly due to the displacement of fluorescent connective tissue components, such as collagen, by the growing tumor within the mouse.

Using the macroscopic fluorescence imaging system, we monitored RFP-tagged SUM 149 mammary tumor growth in SCID mice over time by analyzing changes in tumor fluorescence intensity. Fluorescent images of the RFP-tagged SUM 149 tumors were converted to grayscale and the fluorescent tumor area traced. Mean grayscale pixel value within the traced tumor area was plotted for each image. An increase in fluorescence intensity was evident with increased mammary tumor size. A small, initial decrease in fluorescence intensity was observed near day 6. This is possibly due to the death of some of the injected RFP expressing cancer cells that did not successfully take within the mammary tissue. After this initial decrease, the fluorescent intensity steadily increased as the RFP-tagged tumor grew in size. The autofluorescence from the non-RFP expressing tumor was substantially low compared to the RFP-tagged tumor (Fig. 4A).

In addition to measuring the increase in fluorescence intensity, the size of the RFP-tagged SUM 149 mammary tumor over time was also determined by analyzing the number of pixels within the detectable RFP signal in the fluorescence images. The area in pixels^2, as determined using the Image J software, was converted to mm^2 and plotted versus time. This analysis demonstrates a slight decrease in area of the fluorescence region at day 6, corresponding to the decrease in fluorescence intensity and the expected death of some of the injected RFP expressing cancer cells that did not successfully take within the mammary tissue. Beyond day 6, the size of the tumor increased as a function of time, exhibiting exponential growth after ~ day 35 (Fig. 4B).

Tumor growth was also determined for both RFP-tagged and non-RFP-expressing tumors by a more conventional method, using caliper measurements. The fluorescence imaging system clearly detected RFP-SUM 149 cells from day 0. However, the tumor size could not be determined by caliper measurements until day 30 when the tumors reached a mean area of 3x3 mm^2, illustrating the utility of the imaging system for early tumor detection. These data also demonstrate that the low fluorescence in the non-RFP tumor was not due to a decrease in tumor size because at 48 days following inoculation, the RFP-tagged tumor was 5.75 x 5.2 mm^2 in size while the non-RFP expressing tumor measured at 6.4 x 5.8 mm^2 (Fig. 4C).

Here, we have demonstrated that the macroscopic imaging system enabled a direct analysis of tumor growth over time by monitoring the increase in fluorescence signal. We also demonstrated that the RFP-expressing SUM 149 cell line successfully maintained fluorescence in a mouse over an extended period of time. Non-RFP expressing SUM 149 mammary tumors showed no increase in fluorescence signal as the tumor increased in size over time, as expected. The low background fluorescence measured was autofluorescence signal from the skin and hair of the SCID mouse. Interestingly, a modest decrease in autofluorescence intensity was seen in the non-RFP SUM 149 tumor. This may have been due to the displacement of fluorescent connective tissue components that contribute to the autofluorescence of SCID mouse skin or host-formed fibrous protein encapsulation of the tumor.

Image analysis of RFP-tagged mammary tumors in nude mice

A similar set of experiments was preformed using a highly metastatic RFP-tagged human breast cancer cell line in a different immunocompromised mouse strain to illustrate the versatility of our system. Figure 5 presents white light and fluorescent images of stably expressing RFP-MDA-MB-435α6HG6 human breast tumors in the mammary fat pad of female athymic, nude mice. In the day 7 fluorescent image, RFP emission was obvious at the site of injection, indicating successful MDA-MB-435α6HG6

tumor cell take and survival in the nude mouse host. At day 71, the white light image of the same mouse showed a clearly discernable mammary tumor. The image of this tumor under RFP excitation on day 71 showed a substantial increase in fluorescence signal. In parallel, female nude mice were also injected in the mammary fat pad with non-RFP expressing MDA-MB-435α6HG6 human breast cancer cells which emitted no fluorescence above background autofluorescence of the skin.

We monitored RFP-tagged MDA-MB-435α6HG6 mammary tumor growth in nude mice over time by analyzing increases in tumor fluorescence intensity. As demonstrated in Figure 6, an increase in fluorescence intensity was evident with increased mammary tumor size. Therefore, the macroscopic fluorescence imaging system can be used conveniently to non-invasively quantify fluorescent tumor progression of a metastatic breast cancer cell line.

Figure 7 presents images of distant fluorescent metastases. We were able to detect areas of distant metastases by whole-body imaging; however, intravital imaging where a skin flap is opened over the areas of interest, as described in [14], is necessary for a complete analysis of metastatic lesions by our system in the current configuration. Following necropsy, red fluorescence signal from distant lung metastases was easily detected by our system. This verified the existence of metastatic lesions, since such lesions were not obvious to the untrained, naked eye. Therefore our system can be easily used to detect and quantify metastases without prior histopathology.

Discussion

Here in, we have detailed the development and utilization of a macroscopic fluorescence imaging system to monitor fluorescent protein expressing human tumor progression in immunocompromised mice in real-time with no or minimal intervention. Using our system, we can determine if RFP expressing human breast cancer cells have successfully established a mammary tumor in the mouse at a much earlier

time than visualizing tumor growth at approximately 1-2 weeks post-injection as a means to verify successful implantation. Furthermore, our system can be used to monitor tumor growth over time by measuring an increase in fluorescence intensity from the RFP-tagged tumor. Finally, this system can successfully locate the fluorescence signal from metastatic tumors and thus facilitate identification of regions of interest for further examination by histopathology.

The development and optimization of this system was not without complication. The mouse chow (Harlan Teklab, IN) was found to fluoresce under excitation for RFP and can be seen in the intestinal tract of many of the mouse images (data not shown). While this did not hinder analysis of tumor take and tumor growth over time, this can easily be reduced by feeding mice corn-based chow devoid of the chlorophyll responsible for this background fluorescence. Also, we found it necessary to use the SCID mouse for RFP-SUM 149 experiments because we had limited success establishing tumors with this cell line in nude mice. To avoid the strong fluorescence signal of the hair of the SCID mice, we shaved them prior to imaging. However, even with this complication, we could still successfully detect tumor take and monitor tumor growth over time. With the highly metastatic human breast cancer cell line RFP-MDA-MB-435α6HG6, we could utilize nude mice and successfully monitored tumor take and progression with results similar to those obtained with the RFP-SUM 149 tumors in SCID mice. Therefore, we believe this system can be successfully employed with many different mouse strains.

We used DsRed as the fluorescent tag in these studies because DsRed can be excited by 488 nm argon lasers and fluoresces outside the range of autofluorescence of media, glassware and cellular components, thus resulting in higher signal to noise ratios. Moreover, since DsRed fluoresces at a longer wavelength than other autofluorescent proteins the tissues should absorb less energy at this wavelength. The sensitivity of our system to detect a minimum of $1x10^5$ RFP-tagged cells *in situ* was moderate at 6-7

times over the autofluorescence signal, but this may be improved by the use of GFP tags as previously described [6-22] or improved RFP constructs.

An interesting and unexpected result of this study was a decrease in background fluorescence over time from the non-RFP mouse tumor. In mice, host response to tumor growth can result in the formation of a fibrous tissue cap surrounding established tumors [3, 30-32]. The observed decrease in fluorescence could be a result of fibrous cap formation or possibly from displacement of autofluorescent skin and connective tissue components as the tumor grew in size.

Imaging of optically-tagged cancer cells in mice has been successfully utilized to study the growth and metastatic spread of a variety of cancers and to test the efficacy of potential chemotherapies [6-26]. Hoffman *et a*l. employs a light box system with fiber optic probe delivery of blue light for low resolution, whole body imaging of surgically implanted orthtopic (SOI) green fluorescent protein tagged-tumors in mice. This system is similar to our own but employs a cooled charge-coupled device (CCD) camera for detection [6-17]. The *in vivo* bioluminescence imaging system developed by Contag *et al.* detects light emitted from bioluminescent cells within mice with a CCD camera and has been utilized to evaluate cancer therapies [10-12]. Image analysis of bioluminescently-tagged tumor cells usually involves more manipulation than analysis of fluorescent cells. In order to bioluminesce, the cells need access to oxygen to be metabolically active and require external luciferin as a substrate unless engineered to produce it *in situ* [23]. Furthermore, some of the previously mentioned intravital imaging modalities also require anesthetization of the animal and are invasive, requiring a skin flap opening in the animal [14, 16, 17, 19-22]. Our system will allow examination of a primary tumor of the breast over time and its natural clonal selection *in vivo* leading to tumor metastasis.

Finally, the macroscopic fluorescence imaging system described herein is inexpensive and easy to assemble. We utilized a consumer-grade digital SLR camera to obtain images which can be purchased for

less than $800. Although we used a filtered arc lamp as a source of excitation, several inexpensive alternatives could be used. For example, excitation light can be provided by a Helium Neon laser, a diode pumped solid state (DPSS) laser, or a Light Emitting Diode (LED). HeNe and DPSS lasers provide very narrow linewidth excitation. For lower powers, a HeNe laser costs as little as $500 (Melles Griot) and a DPSS laser can be purchased for as little at $800 (Midwest Laser). Recently, a blue LED flashlight was used as an inexpensive alternative for whole-body imaging of GFP- or RFP-tagged tumors in nude mice [18]. An LED, yielding 60 mW of power, with driver and necessary accessories costs approximately $80 (TheLEDLight.com). The total cost of our system was under $4000, including the camera. However, if a LED is used as the excitation source rather than the arc lamp, the cost of the system decreases to under $1850, making this a very inexpensive intravital imaging modality.

Clearly, the mouse model of breast cancer in conjunction with advances in intravital imaging affords many advantages over traditional *in vitro* and *in vivo* assays in the study of metastatic breast cancer progression. Intravital imaging can be performed with simple tools, and affords the ability to follow tumor progression over time in a single animal. Thus, future studies can be carried out with fewer animals reducing artifacts due to biological variability. Further, this macroscopic imaging system can be used to monitor fluorescent tumor formation and progression, and can be used in future applications to investigate the efficacy of potential anti-cancer preventatives and therapies.

Acknowledgements

We wish to thank Vivian Mack for expert technical assistance. This research was funded by NSF/IGERT Fellowships to M.H. and A.C.; DOD/BCRP Pre-Doctoral Fellowship #BC031906 to M.H.; NIH/NCI R01CA103830 to R.R.K.; and DOD/BCRP #DAMD17-02-1-0582, AICR 03-31-06, and Whitaker Foundation/UT Austin Biomedical Engineering Department Seed Grant to S.D.

References

[1] Jemal A, Murray T, Ward E, Samuels A, Tiwari RC, Ghafoor A, Feuer EJ, and Thun MJ (2005). Cancer Statistics, 2005. *CA Cancer J Clin* **55**, 10-30.

[2] Killion JJ, Radinsky R, and Fidler IJ (1999). Orthotopic models are necessary to predict therapy of transplantable tumors in mice. *Cancer Metastasis Rev* **17**, 279-284.

[3] Price JE (1994). Analyzing the metastatic phenotype. *J Cell Biochem* **56**, 16-22.

[4] Price JE (1996). Metastasis from human breast cancer cell lines. *Breast Cancer Res Treat* **39**, 93-102.

[5] Price JE, and Zhang RD (1990). Studies of human breast cancer metastasis using nude mice. *Cancer Metastasis Rev* **8**, 285-297.

[6] Chishima T, Miyagi Y, Wang X, Yamaoka H, Shimada H, Moosa AR, and Hoffman RM (1997). Cancer invasion and micrometastasis visualized in live tissue by green fluorescent protein expression. *Cancer Res.* **57**, 2042-2047.

[7] Yang M, Baranov E, Jiang P, Sun FX, Li XM, Li L, Hasegawa S, Bouvet M, Al-Tuwaijri M, Chishima T, Shimada H, Moossa AR, Penman S, and Hoffman RM (2000). Whole-body optical imaging of green fluorescent protein-expressing tumors and metastases. *Proc Natl Acad Sci U S A.* **97**, 1206-1211.

[8] Yang M, Baranov E, Moossa AR, Penman S, and Hoffman RM (2000). Visualizing gene expression by whole-body fluorescence imaging. *Proc Natl Acad Sci USA* **97**, 12278-12282.

[9] Rashidi B, Yang M, Jiang P, Baranov E, An Z, Wang X, Moossa AR, and Hoffmam RM (2000). A highly metastatic Lewis lung carcinoma orthotopic green fluorescent protein model. *Clin Exp Metastasis* **18**, 57-60.

[10] Hoffman RM (2000). Orthotopic metastatic mouse models for anticancer drug discovery and evaluation: a bridge to the clinic. *Invest New Drugs* **17**, 343-359.

[11] Yang M, Baranov E, Moossa AR, Penman S, and Hoffman RM (2000). Visualizing gene expression by whole-body fluorescence imaging. *Proc Natl Acad Sci USA* **97**, 12278-12282.

[12] Zhao M, Yang M, Baranova E, Wang X, Penman S, Moossa AR, and Hoffman RM (2001). Spatial-temporal imaging of bacterial infection and antibiotic response in intact animals. *Proc Natl Acad Sci USA* **98**, 9814-9818.

[13] Yang M, Baranov E, Li XM, Wang JW, Jiang P, Li L, Moossa AR, Penman S, and Hoffman RM (2001). Whole-body and intravital optical imaging of angiogenesis in orthopically implanted tumors. *Proc Natl Acad Sci USA* **98**, 2616-2621.

[14] Yang M, Baranov E, Wang JW, Jiang P, Wang X, Sun FX, Bouvet M, Moossa AR, Penman S, and Hoffman RM (2002). Direct external imaging of nascent cancer, tumor progression, angiogenesis, and

metastasis on internal organs in the fluorescent orthotopic model. *Proc Natl Acad Sci USA* **99**, 3824–3829.

[15] Schmitt CA, Fridman JS, Yang M, Baranov E, Hoffman RM, and Lowe SW (2002). Dissecting p53 tumor suppressor function in vivo. *Cancer Cell* **1**, 289-298.

[16] Yamamoto N, Yang M, Jiang P, Tsuchiya H, Tomita K, Moossa AR, and Hoffman RM (2003). Real-time GFP imaging of spontaneous HT-1080 fibrosarcoma lung metastases. *Clin Exp Metastasis* **20**, 181–185.

[17] Amoh Y, Li L, Yang M, Jiang P, Moossa AR, Katsuoka K, and Hoffman RM (2005). Hair follicle-derived blood vessels vascularize tumors in skin and are inhibited by Doxorubicin. *Cancer Res* **65**, 2337-2343.

[18] Yang M, Luiken G, Baranov E, and Hoffman RM (2005). Facile whole-body imaging of internal fluorescent tumors in mice with an LED flashlight. *BioTechniques* **39**:170-172.

[19] Wyckoff JB, Jones JG, Condeelis JS, and Segall JE (2000). A critical step in metastasis: i*n vivo* analysis of intravasation at the primary tumor. *Cancer Res* **60**, 2504-2511.

[20] Wang W, Wyckoff JB, Frohlich VC, Oleynikov Y, Huttelmaier S, Zavadil J, Cermak L, Bottinger EP, Singer RH, White JG, Segall JE, and Condeelis JS (2002). Single cell behavior in metastatic primary mammary tumors correlated with gene expression patterns revealed by molecular profiling. *Cancer Res* **62**, 6278-6288.

[21] Ahmed F, Wyckoff J, Lin EY, Wang W, Wang Y, Hennighausen L, Miyazaki JI, Jones J, Pollard JW, Condeelis JS, and Segall JE (2002). GFP expression in the mammary gland for imaging of mammary tumor cells in transgenic mice. *Cancer Res* **62**, 7166–7169.

[22] Wyckoff JB, Wang W, Lin EY, Wang Y, Pixley F, Stanley ER, Graf T, Pollard JW, Segall JE, and Condeelis JS (2004). A paracrine loop between tumor cells and macrophages is required for tumor cell migration in mammary tumors. *Cancer Res* **64**, 7022-7029.

[23] Rehemtulla A, Stegman LD, Cardozo SJ, Gupta S, Hall DE, Contag CH, and Ross BD (2000). Rapid and quantitative assessment of cancer treatment response using in vivo bioluminescence imaging. *Neoplasia 2,* 491-495.

[24] Edinger M, Cao YA, Verneris MR, Bachmann MH, Contag CH, and Negrin RS (2003). Revealing lymphoma growth and the efficacy of immune cell therapies using in vivo bioluminescence imaging. *Blood* **101**, 640-648.

[25] Mandl SJ, Mari C, Edinger M, Negrin RS, Tait JF, Contag CH, and Blankenberg FG (2004). Multi-modality imaging identifies key times for Annexin V imaging as an early predictor of therapeutic outcome. *Mol Imaging* **3**, 1-8.

[26] Doyle TC, Burns SM, and Contag CH (2004). *In vivo* bioluminescence imaging for integrated studies of infection. *Cell Microbio* **6**, 303-317.

[27] Ethier SP, Kokeny KE, Ridings JW, and Dilts CA (1996). erbB family receptor expression and growth regulation in a newly isolated human breast cancer cell line. *Cancer Res* **56**, 899-907.

[28] Ethier SP (1996). Human breast cancer cell lines as models of growth regulation and disease progression. *J Mammary Gland Biol Neoplasia* **1**, 111-121.

[29] Mukhopadhyay R, Theriault RL, and Price JE (1999). Increased levels of alpha6 integrins are associated with the metastatic phenotype of human breast cancer cells. *Cell Exp Metastasis* **17**, 325-332.

[30] Astoul P, Colt HG, Wang X, Boutin C, and Hoffman RM (1994). "Patient-like" nude mouse metastatic model of advanced human pleural cancer. *J Cell Biochem* **56**, 9-15.

[31] Kubota T (1994). Metastatic models of human cancer xenografted in the nude mouse: The importance of orthotopic transplantation. *J Cell Biochem* **56**, 4-8.

[32] Lacy AA, Collier T, Price JE, Dharmawardhane S, and Richards-Kortum R (2002). Near real-time in vivo confocal imaging of mouse mammary tumors. *Front Biosci* 7, 1-7.

Figure Legends

Figure 1. Schematic of macroscopic fluorescence imaging system. Light from a Xenon arc lamp is directed by mirror to the excitation filter wheel with a bandpass filter centered at 545 nm. Excitation light enters a flexible fiber optic light guide for delivery to the mouse. Fluorescence emission from the mouse is recorded using a digital camera fitted with two emission filters, a bandpass filter centered at 610 nm and a 570 nm longpass filter.

Figure 2. Verification of red fluorescence of human breast cancer cells stably expressing RFP. **A,** Fluorescence images of cell pellets ($4x10^6$ cells) of non-RFP (left tube) or RFP-tagged (right tube) SUM 149 cells taken with the macroscopic imaging system. **B**, Fluorescence images of cell pellets ($4x10^6$) of non-RFP (left tube) and RFP-tagged (right tube) MDA-MB-435α6HG6 cells. **C,** Bright field micrograph at 100x magnification. **D,** Fluorescence micrograph of non-RFP MDA-MB-435α6HG6 cells. **E**, Bright field micrograph at 100x magnification. **F**, Fluorescence micrograph of RFP-tagged MDA-MB-435α6HG6 cells.

Figure 3. Images of RFP- or non-RFP- expressing SUM 149 mammary tumors in female SCID mice. A, Tumors created from RFP-tagged SUM-149 cells. Top row, images under white light; bottom row, images at 580nm. Left column, 3 days; right column, 35 days following injection. **B**, Tumors created from non-RFP SUM 149 cells. Top row, images under white light; bottom row, images at 580nm excitation. Left column, 2 days; right column, 34 days following injection. Arrows indicate tumor site.

Figure 4. Fluorescence intensity and area of RFP- or Non-RFP- expressing SUM 149 mammary tumors in SCID mice as a function of time. A, SCID mice with RFP and non-RFP tagged SUM 149

mammary tumors were imaged under RFP excitation using the macroscopic imaging system. Images were converted to grayscale and mean grayscale pixel value from the traced tumor area was plotted versus time. **B**, Area of the RFP-tagged SUM 149 mammary tumor was measured from the fluorescence images and converted to mm^2. The tumor area is plotted versus time. **C**, The areas of same RFP and non-RFP tagged SUM 149 mammary tumors were measured using calipers starting at day 30 following injection when the tumors were quantifiable by caliper measurements.

Figure 5. Images of RFP- or non-RFP-expressing MDA-MB-435α6HG6 mammary tumors in female athymic, nude mice. Left column, images under white light; right column, images at 580nm. Top row, non-RFP-tagged MDA-MB-435α6HG6 mammary tumors. Middle row, RFP-tagged MDA-MB-435α6HG6 mammary tumor at day 7, post-mammary cancer cell injection. Bottom row, RFP-tagged MDA-MB-435α6HG6 mammary tumor at day 71.

Figure 6. Fluorescence intensity RFP- or non-RFP-expressing MDA-MB-435α6HG6 mammary tumors in nude mice as a function of time. RFP- or non-RFP-expressing MDA-MB-435α6HG6 cells were injected into the mammary fat pads of two female athymic, nude mice. Tumor growth was monitored via fluorescent image analysis using the macroscopic imaging system. Images were converted to grayscale and the mean grayscale pixel value for the traced tumor area was plotted versus time.

Figure 7. Images of lung metastases from RFP-tagged MDA-MB-435α6HG6 mammary tumors. RFP- tagged MDA-MB-435α6HG6 human breast cancer cells were injected into the mammary fat pad of female, nude athymic mice. The mammary tumor was allowed to grow for 71 days. Left column, images under white light; right column, images at 580nm. Top row, mouse with open chest cavity. Bottom row,

excised lung with metastases seen as white nodules (black arrows) under white light and RFP expressing metastatic lesions verified by fluorescent imaging at 580 nm (white arrows).

Fig. 1, Carlson, et al.

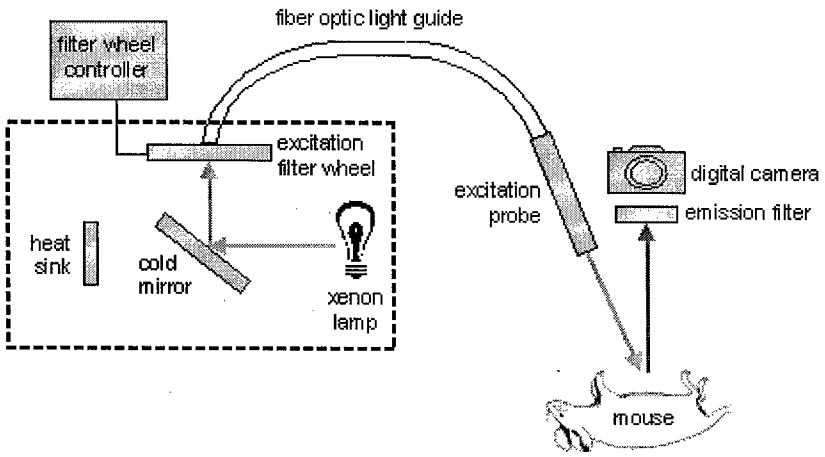

Fig. 2, Carlson, et al.

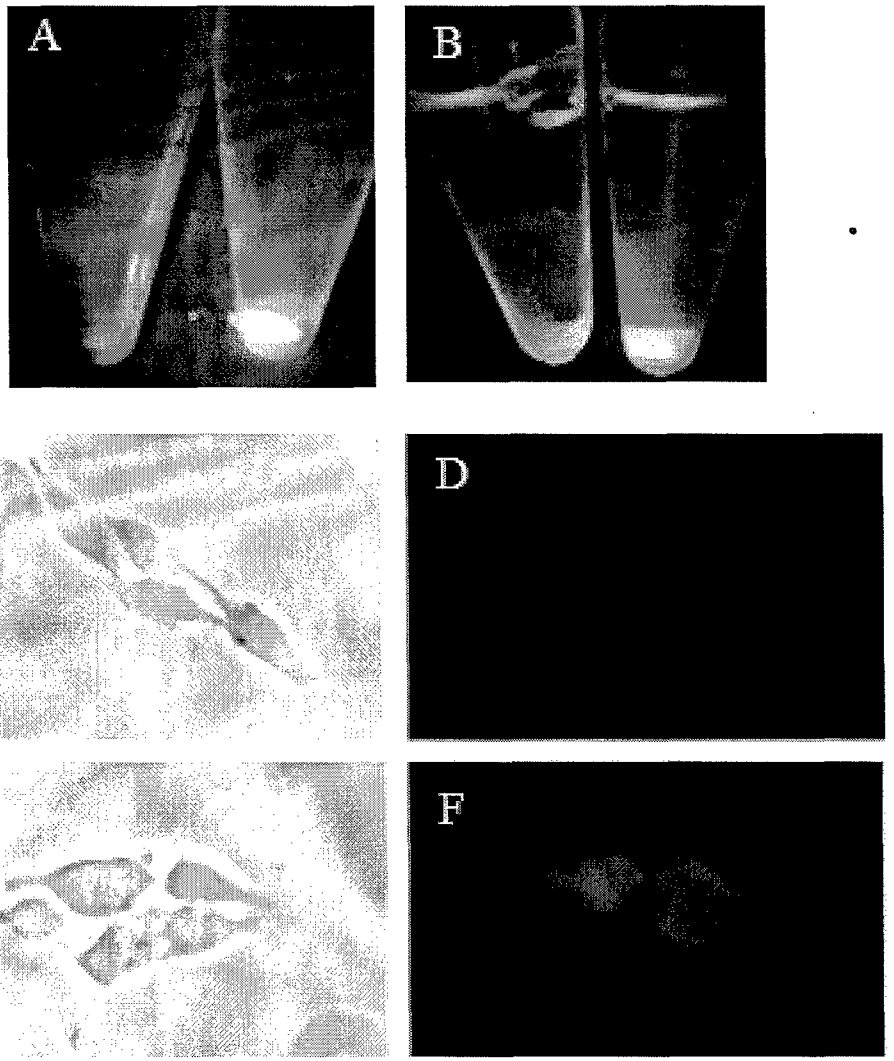

Fig. 3, Carlson, etal.

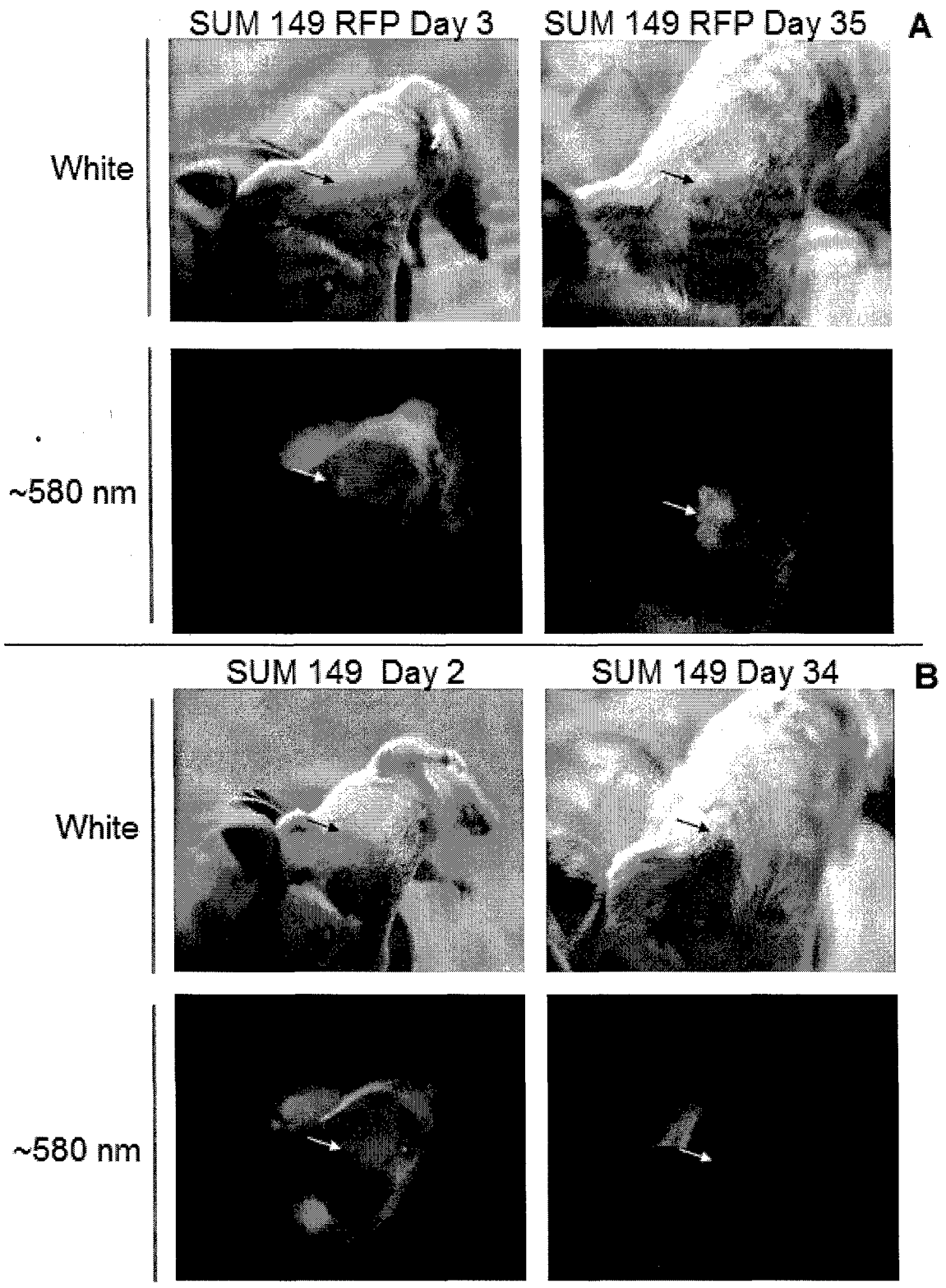

Fig. 4, Carlson, et al.

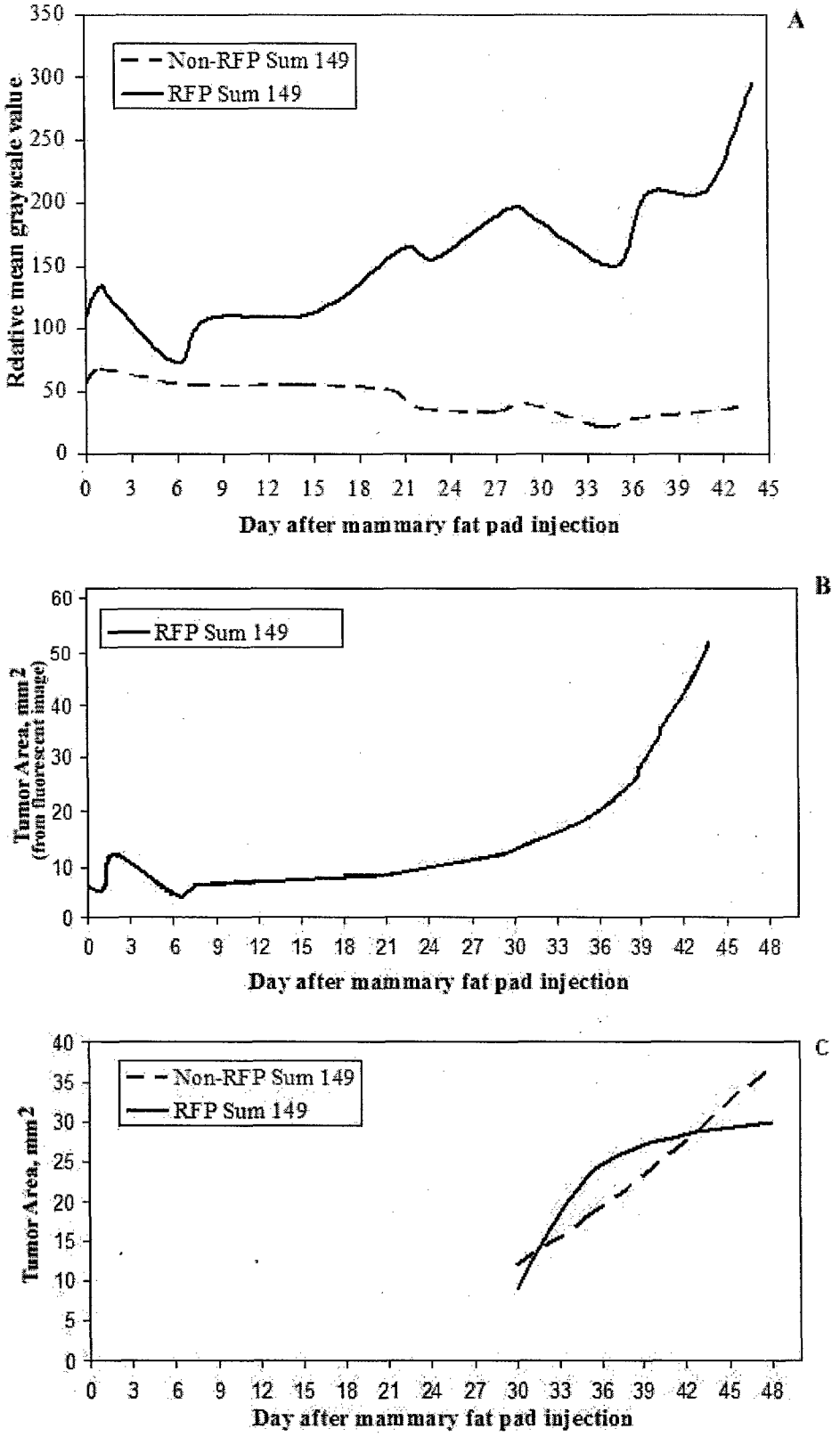

Fig. 5, Carlson, et al.

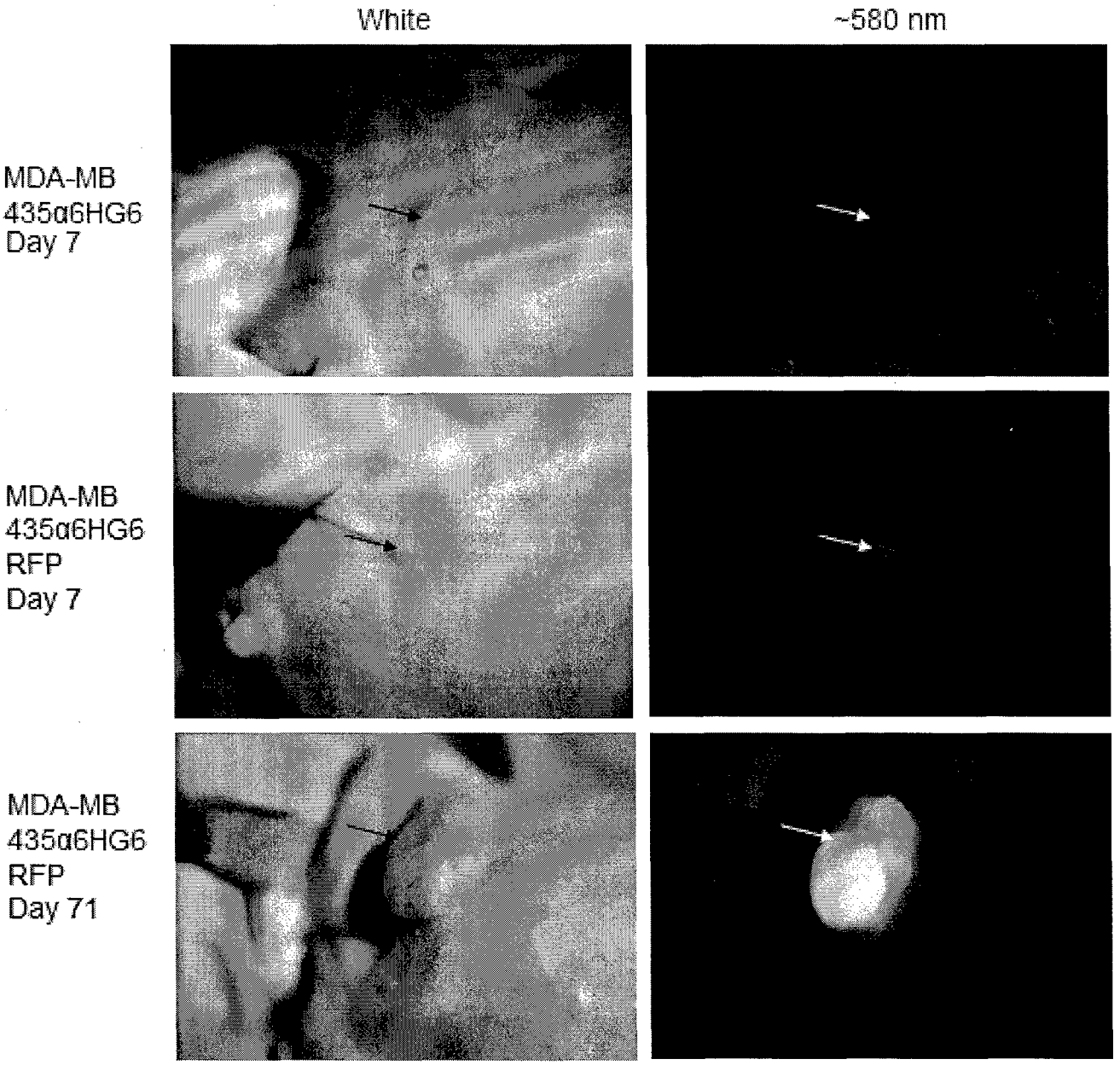

Fig. 6, Carlson, et al.

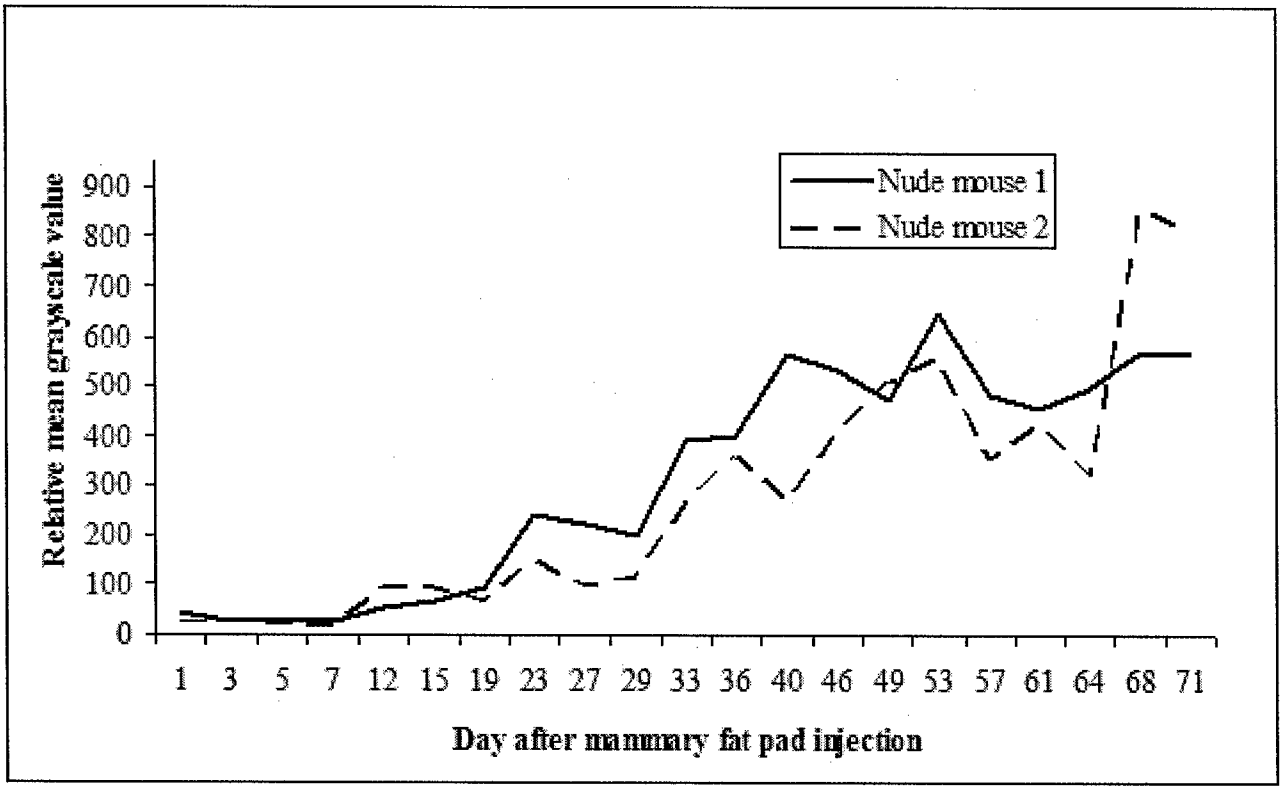

Fig. 7, Carlson, et al.

White

~ 580nm

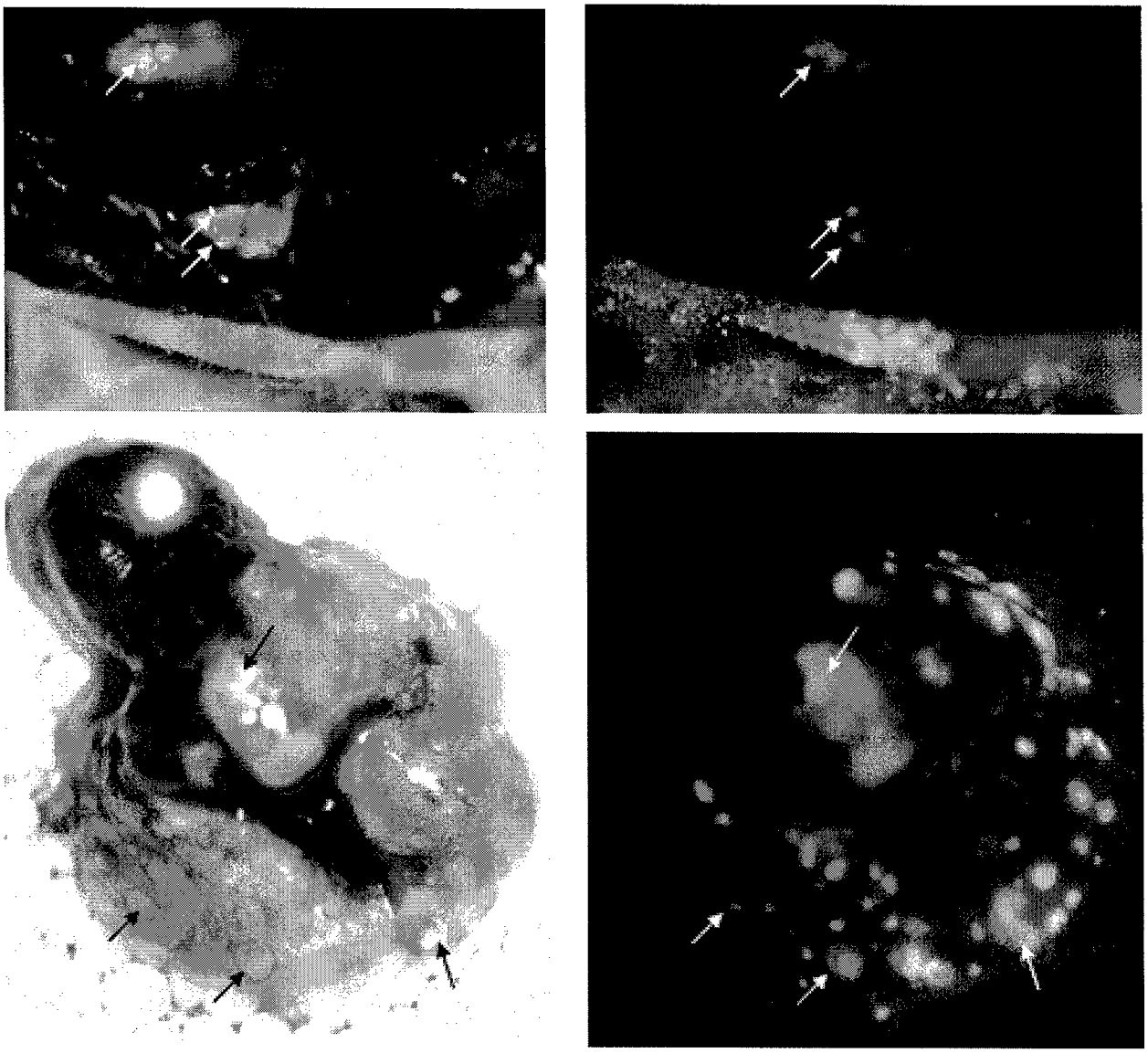

RESEARCH ARTICLE

Neoplasia • Vol. 7, No. 2, February 2005, pp. 128–140 128

www.neoplasia.com

Resveratrol and Estradiol Exert Disparate Effects on Cell Migration, Cell Surface Actin Structures, and Focal Adhesion Assembly in MDA-MB-231 Human Breast Cancer Cells[1]

Nicolas G. Azios and Suranganie F. Dharmawardhane

Molecular Cell and Developmental Biology Section and Institute for Cellular and Molecular Biology, The University of Texas at Austin, Austin, TX 78712, USA

Abstract

Resveratrol, a grape polyphenol, is thought to be a cancer preventive, yet its effects on metastatic breast cancer are relatively unknown. Since cancer cell invasion is dependent on cell migration, the chemotactic response of MDA-MB-231 metastatic human breast cancer cells to resveratrol, estradiol (E_2), or epidermal growth factor (EGF) was investigated. Resveratrol decreased while E_2 and EGF increased directed cell migration. Resveratrol may inhibit cell migration by altering the cytoskeleton. Resveratrol induced a rapid global array of filopodia and decreased focal adhesions and focal adhesion kinase (FAK) activity. E_2 or EGF treatment did not affect filopodia extension but increased lamellipodia and associated focal adhesions that are integral for cell migration. Combined resveratrol and E_2 treatment resulted in a filopodia and focal adhesion response similar to resveratrol alone. Combined resveratrol and EGF resulted in a lamellipodia and focal adhesion response similar to EGF alone. E_2 and to a lesser extent resveratrol increased EGFR activity. The cytoskeletal changes and EGFR activity in response to E_2 were blocked by EGFR1 inhibitor indicating that E_2 may increase cell migration via crosstalk with EGFR signaling. These data suggest a promotional role for E_2 in breast cancer cell migration but an antiestrogenic, preventative role for resveratrol.

Neoplasia (2005) **7,** 128–140

Keywords: Resveratrol, estradiol, filopodia, focal adhesions, cell migration.

Introduction

Estrogen (E_2) acts by regulating gene transcription through two major intracellular estrogen receptors (ERs), ERα and ERβ, to play a critical role in the establishment and maintenance of female reproductive function as well as in the initiation and progression of breast and gynecologic cancers [1,2]. Consequently, inhibition of ERα has become a major strategy for the prevention and treatment of breast cancer [3]. However, this approach is limited to the treatment of metastatic breast cancer because ERα expression is often lost during breast cancer progression to the metastatic state [4]. These ERα(−) cancers may still retain the more recently identified ERβ as well as membrane-bound forms of ER, and more studies are necessary to understand the role of these ER isoforms in breast cancer malignancy. In addition to the well-established long-term (genomic) effects of E_2 on gene transcription [5], E_2 also induces short-term (nongenomic) effects. Such nonclassic effects of E_2 have been reported from a variety of cell types including breast cancer cells and are thought to be modulated by plasmamembrane ERs that can cross-activate a variety of signaling cascades [6,7].

Recent reports on the rapid, nongenomic action of E_2 from a variety of cell types and tissues have demonstrated novel roles for E_2 in the regulation of a variety of cell functions relevant to cancer progression [8–11]. E_2 cross-activates heterotrimeric G proteins to stimulate adenylate cyclase and phospholipase C, thus inducing protein kinase A (PKA), protein kinase C (PKC), and intracellular Ca^{2+} fluxes [12,13]. Moreover, E_2-bound ERα has been shown to associate with Src tyrosine kinase as well as the regulatory subunit of phosphoinositide 3-kinase (PI3-K) to regulate signaling pathways implicated in cell proliferation, survival, and migration [14,15]. Activation of membrane ERs by E_2 has been shown to transactivate epidermal growth factor receptors (EGFRs) potentially through a G protein–coupled pathway [11,16]. EGFRs are tyrosine kinase–type integral membrane receptors that regulate signaling relevant to both genomic effects on cell proliferation and survival as well as nongenomic signaling to affect migration and invasion [17,18]. Interestingly, loss of ERα in breast cancer is associated with overexpression of EGFRs that contribute to tumor malignancy and poor prognosis [19]. Therefore, there is a pressing need to investigate the nongenomic aspects of E_2 signaling and how it relates to metastatic breast cancer.

Abbreviations: E_2, 17β-estradiol; EGF, epidermal growth factor; ER, estrogen receptor; FAK, focal adhesion kinase

Address all correspondence to: Suranganie F. Dharmawardhane, Molecular Cell and Developmental Biology Section, The University of Texas at Austin, BIO 311, A6700, 1 University Station, Austin, TX 78712. E-mail: surangi@mail.utexas.edu

[1]This investigation was supported by NIH/NCI grants CA83957-01A1 and DAMD17-02-1-0582 (to S.D.) and the Hispanic Scholarship Fund and Sigma Xi (to N.A.).

Received 26 May 2004; Revised 17 July 2004; Accepted 19 July 2004.

DOI 10.1593/neo.04346

Phytoestrogens are naturally occurring estrogen-like plant compounds that act as agonists or antagonists of E_2 and may have protective action against some cancers as well as prevent the undesirable symptoms of menopause [20]. Resveratrol (*trans*-3,4′,5 trihydroxystilbene), a phytoestrogen present in grape skin and red wine, is known to have cancer-preventive and cardioprotective properties [21,22]. Resveratrol binds to and activates ERs (α and β) to exert both estrogenic and antiestrogenic effects [23,24]. Resveratrol acts as a cancer-preventive agent due to its antioxidant, proapoptotic, and antigrowth properties [21,25,26]. Resveratrol may also be important for breast cancer prevention because it inhibits breast cancer cell growth in ERα(+) and ERα(−) cells [23,27,28]. We have previously demonstrated that in ER(+) breast cancer cells, resveratrol reduces the activity of Akt, a regulator of cell survival, and increases Akt activity in ERα(−) ERβ(+) breast cancer cells [29]. A recent report demonstrated that resveratrol could directly inhibit Akt activity of ER(+) breast cancer cells through an ERα-associated PI3-K pathway [30].

Resveratrol has also been shown to prevent angiogenesis and wound healing of endothelial cells, and such antiangiogenic properties of resveratrol make it a good candidate for the prevention of cancer progression [31–34]. Resveratrol has been demonstrated to reduce hepatoma cell invasion in response to hepatocyte growth factor *in vitro* and hepatoma and Lewis lung carcinoma invasion in mice [31,35]. Resveratrol was recently shown to inhibit phorbol myristate acetate–induced cervical cancer cell invasion [36]. Although the role of resveratrol in the inhibition of cancer cell growth is well established, the role and mechanisms by which resveratrol may act to prevent cancer metastasis remain to be investigated.

Directed cell migration is an integral component of cancer cell invasion during metastasis. Metastatic cancer cells break cell–cell adhesions and initiate movement out of the primary tumor into surrounding tissues and blood vessels [37]. Cancer cell invasion is regulated by growth factors that can rapidly activate cell surface receptors to induce actin polymerization and reorganization into actin-based extensions such as filopodia (thin needle–shaped structures with parallel actin bundles) and lamellipodia (flat cell surface protrusions with cross-linked actin). Extension of lamellipodia and dynamic turnover of focal adhesions at the leading edge are thought to drive forward migration [37–40]. Filopodia are not essential for cell migration and are considered to function as environmental sensors [39].

Focal adhesions are multimolecular complexes formed by the interaction of integrin receptors with the extracellular matrix (ECM). Focal adhesions contain both structural and signaling components with numerous tyrosine-phosphorylated proteins such as focal adhesion kinase (FAK) and Src as well as actin-binding proteins that anchor focal adhesions to the actin cytoskeleton. FAK is recruited to the membrane in response to integrin as well as growth factor receptor activation. FAK is activated by autophosphorylation at multiple sites that in turn interact with adapter and structural proteins facilitating the modulation of cell proliferation, survival, migration, and cancer cell invasion [41].

Although ERα is commonly lost in metastatic breast cancer [4], these cells still retain the ERβ isoform, which has been shown to interact with resveratrol [42]. Therefore, as a first step toward investigating a role for resveratrol in breast cancer metastasis, we monitored directed cell migration and accompanying changes in the cytoskeleton in response to resveratrol or E_2 in the ERα(−) ERβ(+) MDA-MB-231 [43] human metastatic breast cancer cell line. For the first time, the present data demonstrate that resveratrol may inhibit breast cancer cell migration by modulating the actin cytoskeleton to form a global array of filopodia and by decreasing focal adhesion assembly and FAK activity. Conversely, E_2 increases cell migration and accompanying lamellipodia extension and focal adhesion assembly. Thus, these data indicate that resveratrol may prevent, whereas E_2 may advance, metastatic breast cancer in ERα(−) ERβ(+) tumors.

Materials and Methods

Reagents

All culture media components were from Life Technologies/Gibco (Rockville, MD). EGF was obtained from Upstate Biotechnology, Inc. (Charlottesville, VA). 17β-Estradiol (E_2) was obtained from Sigma (St. Louis, MO). *trans*-Resveratrol was from LKT Laboratories (St. Paul, MN). All chemoattractants were dissolved in DMSO. Rhodamine phalloidin was purchased from Molecular Probes (Eugene, OR). Anti-phosphotyrosine and anti-ERα antibodies were from Santa Cruz Biotechnology (Santa Cruz, CA). Anti-ERβ, anti-EGFR, and anti-phosphoEGFR antibodies were from Upstate Biotechnology, Inc. FITC-conjugated goat antimouse antibody was from Cappel (West Chester, PA). Tyrphostin AG1478 was purchased from Calbiochem (San Diego, CA).

Cell Culture

Human breast cancer cell lines were cultured in Dulbecco's modified Eagle's medium (DMEM) supplemented with 10% fetal bovine serum (FBS) at 37°C in 5% CO_2.

Migration Assay

Migration assays were conducted according to Ref. [44]. MDA-MB-231 cells were serum-starved in phenol red–free DMEM for 24 hours. Cells were then trypsinized, recovered with trypsin inhibitor (0.5 mg/ml), and seeded at 1×10^5 cells per chamber in the upper well of Costar wells (VWR, Suwanee, GA) containing membranes with 8-μm–diameter pores. DMSO (control), E_2 (0.1 μM), EGF (50 ng/ml), or resveratrol (50 μM) was added as a chemoattractant to the bottom wells for 8 hours. For experiments where the effect of resveratrol was analyzed in combination with E_2 or EGF, resveratrol was added to the bottom well for 10 minutes followed by E_2 or EGF for the duration of the experiment. Cells on the upper surface of the membrane were removed, and cells that had moved through to the other side of the

membrane were stained with propidium iodide and quantified. For statistical purposes, the total number of cells migrated in 10 microscopic fields per well were counted for at least three separate experiments.

Immunofluorescence Microscopy

Cells were seeded at 1.5×10^5 cells per cover slip and grown overnight in DMEM in six-well plates. Cells were serum-starved in phenol red–free DMEM for 24 hours. Cells were then treated for 10 minutes with DMSO (control), E_2 (0.1 μM), EGF (50 ng/ml), or resveratrol (10, 50, or 100 μM). For experiments where the effect of resveratrol was analyzed in combination with E_2 or EGF, cells were preincubated in resveratrol for 10 minutes and incubated with E_2 or EGF for a further 10 minutes. For experiments using tyrphostin AG1478 to inhibit EGFR activity, cells were preincubated in 50 μM tyrphostin AG1478 for 15 minutes as described in Ref. [15]. Cells were fixed with 3.7% formaldehyde in PBS for 15 minutes, permeabilized with 0.2% Triton X-100 for 20 minutes, and blocked with 5% bovine serum albumin (BSA). Cells were then probed with rhodamine phalloidin to visualize F-actin and anti-phosphotyrosine followed by FITC-conjugated secondary antibody to visualize focal adhesions, as described in Ref. [45]. Micrographs at ×600 magnification were digitally captured using a SpotII digital camera and software (Diagnostic Instruments, Inc., Sterling Heights, MI). Cells in 10 microscopic fields per treatment were counted for three separate experiments.

Analysis of ER Expression and FAK and EGFR Activity

Cells were disrupted in lysis buffer [20 mM Tris–HCl (pH 7.5), 150 mM NaCl, 1 mM EGTA, 1 mM EDTA, 2.5 mM sodium pyrophosphate, 50 mM sodium fluoride, 10% glycerol, 1% NP-40, 1 mM DTT, 0.5% deoxycholate, and protease inhibitors] on ice. Lysates were centrifuged at 14,000 rpm, and the supernatant mixed with Laemmli sample buffer, equally loaded, and separated on 10% SDS-PAGE gels. Proteins were transferred to PVDF membranes, blocked with 5% BSA, and probed with specific primary antibodies. Positive bands were detected using a horseradish peroxidase (HRP)–conjugated secondary antibody and developed with Super Signal West Fempto Substrate (Pierce Biotechnology, Rockford, IL). For analysis of ER isoform or EGFR expression, cell lysates containing equal amounts of protein, as determined by total protein assays (Bio-Rad, Hercules, CA), were loaded and specific ER isoforms detected using monoclonal antibodies to ERα, ERβ, EGFR, or phosphoEGFR.

For analysis of FAK activity, anti-FAK (against the N-terminus) and anti-phosphoFAK (Tyr-397) antibodies were used as probes. The densities of positive bands were quantified using Scion Image software. The relative FAK activity was calculated as the ratio of the density of phosphoFAK in stimulated cell lysates to the density of FAK in stimulated cell lysates divided by the ratio of the density of phosphoFAK in unstimulated cell lysates to the density of FAK in unstimulated cell lysates, as described in Ref. [29]. In our previously published results, FAK activity was quantified using a C-terminal anti-FAK antibody to detect total FAK levels. Herein, this assay has been improved by the use of a total anti-FAK antibody that detects the N-terminus of FAK, thus including all of the proteins detected by an anti-phosphoFAK tyr-397 antibody. The results are representative of three separate experiments.

For the analysis of EGFR activity, cells were pretreated with tyrphostin AG1478 (50 μM) for 15 minutes as described in Ref. [15]. Cells were then treated with 50 ng/ml EGF or vehicle for 10 minutes, lysed, and Western-blotted as described above using an antibody against phospho-EGFR (Y1173).

Statistical Analysis

Data are expressed as mean ± S.E.M. *P* values were calculated from unpaired *t*-tests using Microsoft Excel and considered significant at values less than .05.

Results

To determine the effect of resveratrol on cell functions relevant to cancer cell invasion, we investigated the changes in cell migration, cell surface actin structures, focal adhesion assembly, and FAK and EGFR activity induced by 10-minute exposure to resveratrol (50 μM) compared to DMSO (control), E_2 (0.1 μM), or EGF (50 ng/ml). The concentration of resveratrol used is comparable to the range of concentrations used to demonstrate interactions with ER [24] and signal transduction through modulation of gene expression [36]. The concentration for resveratrol used is well within the published range for resveratrol action, where different cell types, including breast cancer cells, were incubated in concentrations of resveratrol ranging from 1 to 100 μM for over 24 hours [30,34,46–48]. E_2 concentration is in the range used for the demonstration of nongenomic effects in breast cancer cells [15,49]. The concentration of EGF is in the range used to activate EGFR and elicit effects on the actin cytoskeleton and invasion of breast cancer cells [50,51].

Resveratrol Decreases Migration Whereas E_2 Increases Migration of MDA-MB-231 Cells

As shown in Figure 1, the role of E_2 and resveratrol as chemoattractants in directed cell migration was analyzed in ERα(–) β(+) MDA-MB-231 metastatic human breast cancer cells. E_2 and EGF treatments both significantly increased cell migration by 50% and 30%, respectively, compared to control. Resveratrol treatment resulted in significantly decreased cell migration by 26% compared to control. To investigate the ability of resveratrol to inhibit E_2 or EGF action, cells were treated with resveratrol prior to E_2 (Res/E_2) or EGF (Res/EGF). Combined treatment of Res/E_2 or Res/EGF was significantly decreased from unstimulated control by 33% and 41%, respectively, but were not significantly different from resveratrol-treated cells alone. In Res/E_2 treatments, the number of cells that migrated was significantly reduced by 55% when compared to E_2 alone. In Res/EGF treatments, the number of cells that migrated was also significantly reduced by 55% when compared to EGF alone.

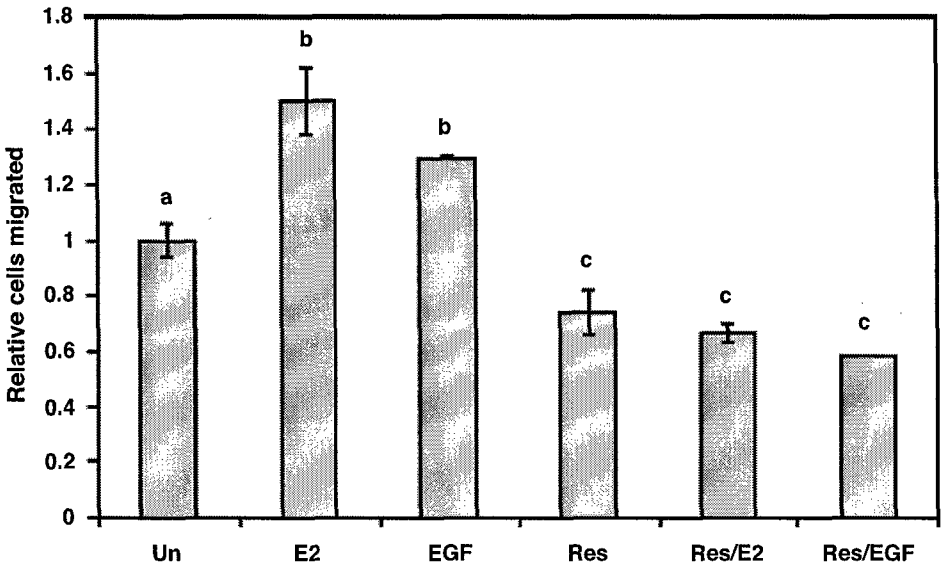

Figure 1. *Effects of E_2, EGF, and trans-resveratrol on directed cell migration of MDA-MB-231 cells. Cells were serum-starved in phenol red–free media for 24 hours and migration assays were conducted using the following as chemoattractants for 8 hours: DMSO as control (Un); 0.1 μM E_2 (E_2); 50 ng/ml EGF (EGF); 50 μM resveratrol (Res), pretreated with Res for 10 minutes followed by E_2 for 10 minutes (Res/E_2), or pretreated with Res for 10 minutes followed by EGF for 10 minutes (Res/EGF). The number of cells that migrated through the upper chamber of Costar wells was quantified and made relative to DMSO control. Data are expressed as mean cells migrated ± SEM of at least three independent experiments. Treatments denoted by the same letter indicate no significant difference between those treatments. Treatments denoted by different letters indicate a significant difference between those treatments at $P < .05$.*

Thus, resveratrol effectively inhibited cell migration even in the presence of E_2 or EGF, both stimulators of directed cell migration.

Resveratrol, But Not E_2, Induces Filopodia Extension in ER(+) Breast Cancer Cells

To investigate a structural mechanism for the migratory response of ERα(−) β(+) MDA-MB-231 to resveratrol and E_2, we monitored the effect of these compounds on the actin cytoskeleton of ERα(+) T47D, ERα(−) β(+) MDA-MB-231, and ERα(−) β(−) SKBR3 human breast cancer cell lines. The ER α and β protein expression status of all three cell lines was confirmed by Western blot analysis with monospecific antibodies (Figure 2*B*). As shown in Figure 2*A*, addition of resveratrol or E_2 to quiescent T47D and MDA-MB-231 human breast cancer cell lines resulted in rapid reorganization of the actin cytoskeleton. However, the actin cytoskeletal response to resveratrol compared to E_2 was structurally very different. Treatment with resveratrol resulted in a dynamic global extension of filopodia, which contain bundles of actin filaments; whereas treatment with E_2 resulted in extension of lamellipodia, which contain cross-linked networks of actin filaments. In the ERα(−) β(+) MDA-MB-231 cells, we have observed significant increases in filopodia extension from 5 to 30 minutes following resveratrol treatment at concentrations ranging from 10 to 100 μM with saturation at 50 μM resveratrol (data not shown). Resveratrol-induced increases in filopodia were also observed for the ERαβ(+) T47D cells (Figure 2*A*). However, E_2 or resveratrol did not affect the actin cytoskeleton of the ERαβ(−) metastatic breast cancer cell line, SKBR3 (Figure 2*A*). As confirmed in Figure 2*B*, the SKBR3 cell line is known to be deficient in ER mRNA expression [52]. Therefore, these effects of E_2 and resveratrol on the actin cytoskeleton may be ER-dependent but not specific to ERα.

Because we investigate a role for E_2 and resveratrol in crosstalk with EGFR signaling, expression of EGFR was also confirmed in these breast cancer cell lines (Figure 2*B*). Although the EGFR antibody was not sensitive enough to detect the low expression of EGFR in T47D cells, Western blot analysis of lysates from cells grown in serum with a phospho-specific EGFR antibody detected activated EGFR in T47D cells as well as in MDA-MB-231 and SKBR3 cells. Therefore, the observed lack of an actin cytoskeletal response following E_2 or resveratrol in SKBR3 cells is not due to lack of EGFR function but probably due to their ER(−) status.

Stimulation of ERα(−) β(+) MDA-MB-231 cells with EGF resulted in lamellipodia formation, as has been reported in other breast cancer cell lines [37]. Interestingly, E_2 exerted a similar, but not as pronounced, effect as EGF by inducing lamellipodia. This has previously been shown in ERαβ(+) MCF-7 breast cancer cells [38]. The number of filopodia extended in cells treated with E_2 or EGF did not differ significantly from controls (Figures 2–4). These parallel cytoskeletal responses to E_2 or EGF suggest that E_2 may exert effects on the actin cytoskeleton through EGFR.

As shown in Figure 3, the number of filopodia extended in response to 50 μM resveratrol was significantly increased by ~4.5-fold compared to control, E_2, or EGF. To evaluate the role of resveratrol as an inhibitor of E_2 or EGF action on the cytoskeleton, the number of filopodia was quantified in cells preincubated with resveratrol and subsequently stimulated

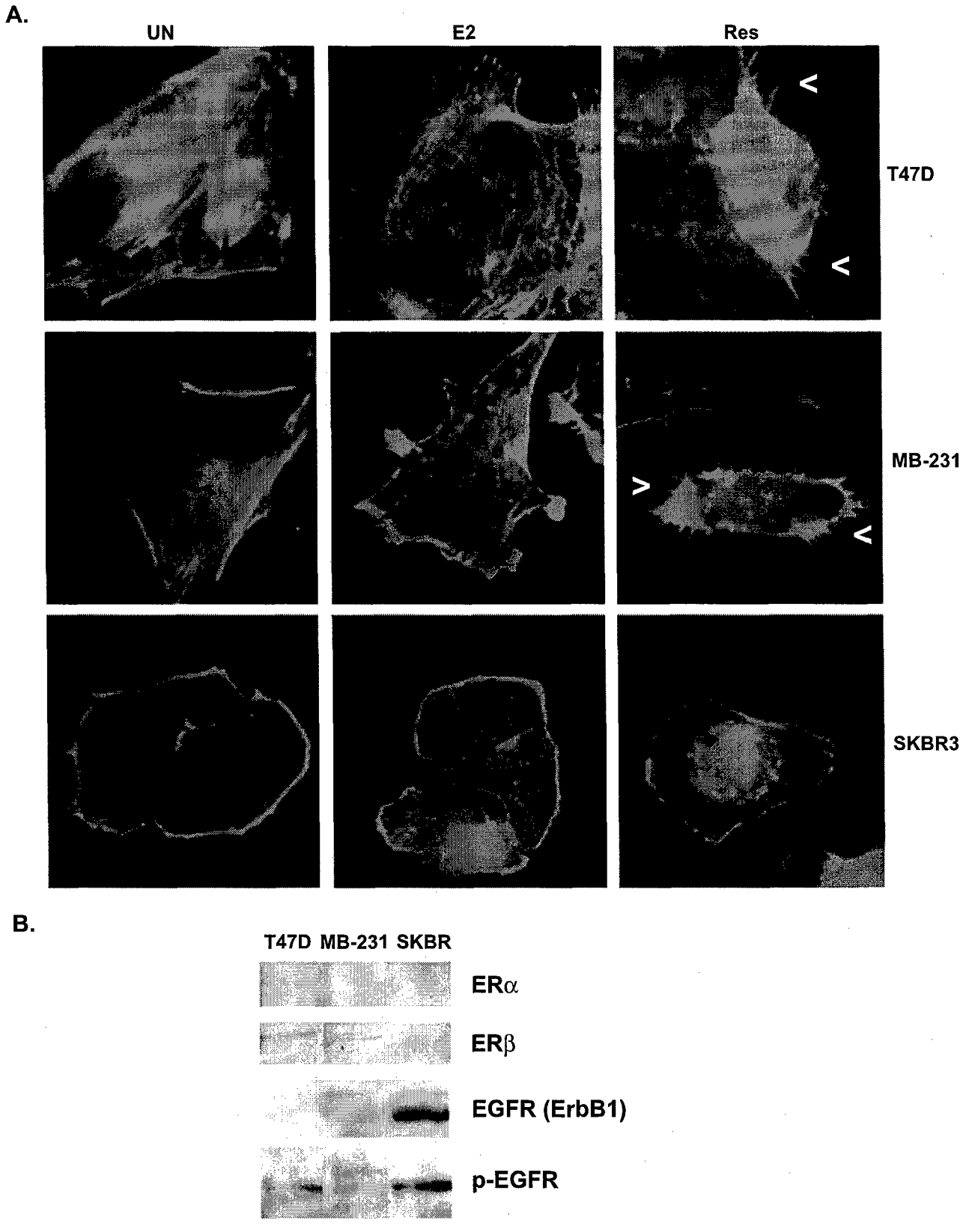

Figure 2. *Effect of E_2 and trans-resveratrol on the actin cytoskeleton of ER (+) and (−) cells. (A) Micrographs of T47D, MDA-MB-231, and SKBR3 cells at ×600 magnification. Cells were serum-starved in phenol red–free media for 24 hours and stimulated for 10 minutes with DMSO as control (Un), E_2 (0.1 μM), or 50 μM resveratrol (Res). Cells were stained with rhodamine phalloidin to visualize F-actin. Arrowheads (<) indicate a filopodium. (B) Western blot of whole cell lysates of T47D, MDA-MB-231, and SKBR3. Equal amounts of proteins from cell lysates were loaded on SDS-PAGE and Western-blotted using anti-ERα (65 kDa band) or anti-ERβ (53 kDa band). Equal amounts of cell lysates were also probed with anti-EGFR1 (185 kDa) or anti-phosphoEGFR (Y1173) (185 kDa).*

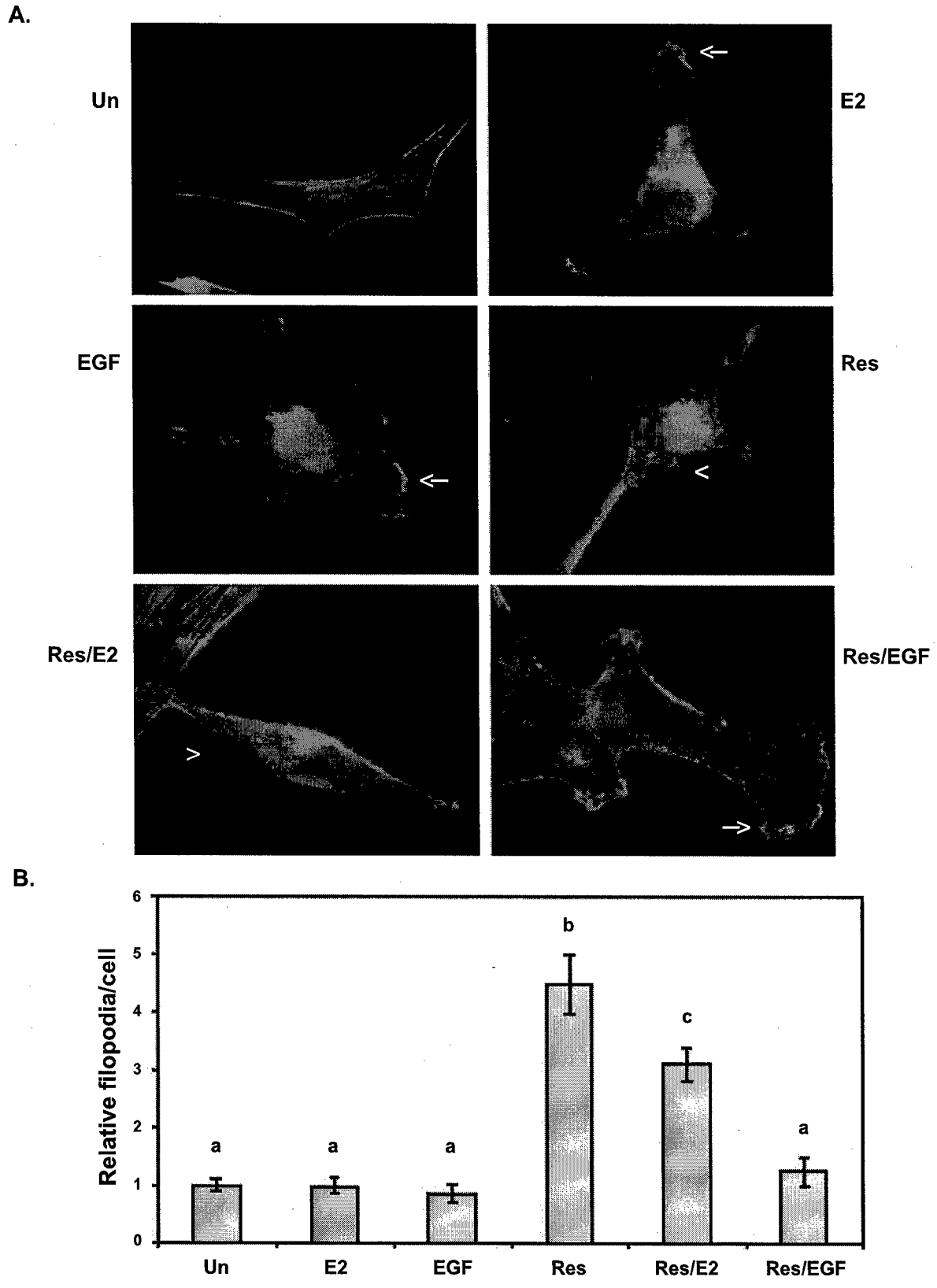

Figure 3. *Effect of E_2, EGF, or trans-resveratrol on the actin cytoskeleton of MDA-MB-231 cells. Cells were serum-starved in phenol red–free media for 24 hours and stimulated for 10 minutes with DMSO as control (Un); 0.1 μM E_2 (E_2); 50 ng/ml EGF (EGF); and 50 μM resveratrol (Res), pretreated with Res for 10 minutes followed by E_2 for 10 minutes (Res/E_2), or pretreated with Res for 10 minutes followed by EGF for 10 minutes (Res/EGF). Cells were stained with rhodamine phalloidin to visualize F-actin. (A) Micrographs at ×600 magnification. Arrowheads (<) indicate a filopodium; arrows (←) indicate a lamellipodium. (B) Filopodia number was quantified for at least 10 microscopic fields per treatment per experiment and made relative to DMSO control (Un). Data expressed as mean filopodia ± SEM of three independent experiments. Treatments denoted by the same letter indicate no significant difference between those treatments. Treatments denoted by different letters indicate a significant difference between those treatments at $P < .05$.*

with E_2 (Res/E_2) or EGF (Res/EGF). In Res/E_2 treatments, the number of filopodia was significantly greater than unstimulated control or E_2 alone by ~3-fold. However, the number of filopodia extended in this Res/E_2 combined treatment was still significantly less (31%) when compared to resveratrol alone. Resveratrol pretreatment followed by EGF (Res/EGF) did not significantly increase filopodia number when compared to EGF alone. Thus, these results demonstrate that resveratrol may counteract the effect of E_2 on the actin cytoskeleton. In the presence of EGF, resveratrol did not affect direct EGF signaling to the actin cytoskeleton, indicating that resveratrol may not directly compete with EGF to alter EGFR signaling.

Resveratrol and E_2 Effects on the Actin Cytoskeleton of MDA-MB-231 Cells Are Modulated by EGFR Inhibitor

Plasmamembrane ERs have been implicated in the cross-activation of tyrosine kinase-type growth factor receptors, such as EGFR [7,11]. To further evaluate the role of EGFR on resveratrol-mediated effects on the actin cytoskeleton, we investigated the effect of tyrphostin AG1478, an EGFR1 specific inhibitor. As shown in Figure 4*A*, treatment of unstimulated cells with AG1478 (Un^+) resulted in a significant increase in the number of filopodia when compared to unstimulated control (Un^-). This increase may be due to a nonspecific effect of AG1478 treatment or inhibition of intrinsic EGFR activity.

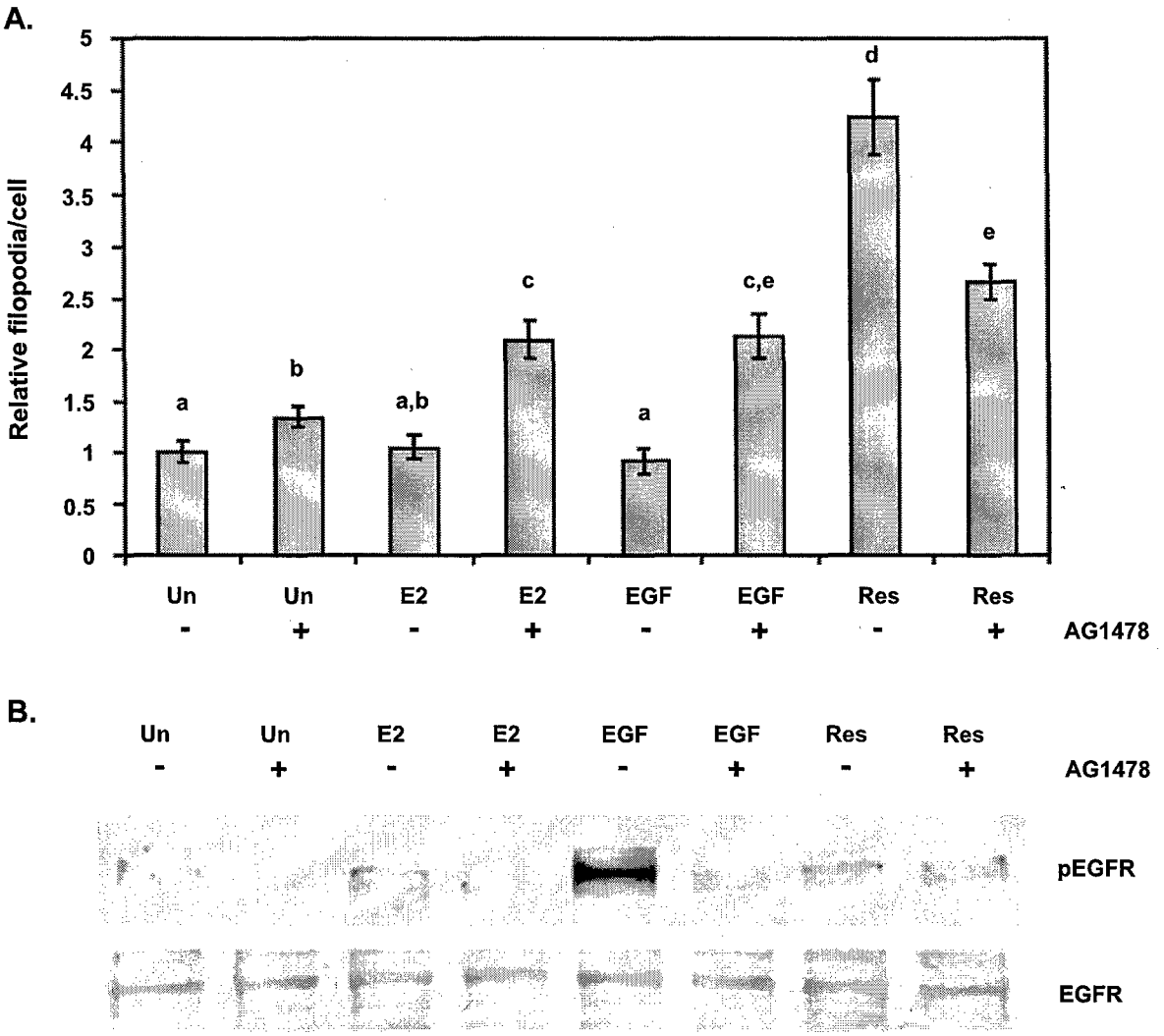

Figure 4. *Effect of tyrphostin AG1478 on filopodia formation in MDA-MB-231 cells. (A) Cells were serum-starved in phenol red–free media for 24 hours and pretreated with vehicle (–AG1478) or tyrphostin AG1478 (+AG1478) for 15 minutes then treated with DMSO as control (Un), 0.1 μM E_2 (E_2), 50 ng/ml EGF (EGF), or 50 μM resveratrol (Res) for 10 minutes. Cells were stained with rhodamine phalloidin to visualize F-actin. Filopodia number was quantified for at least 10 microscopic fields per treatment per experiment and made relative to DMSO control (Un). Data expressed as mean filopodia ± SEM of three independent experiments. Treatments denoted by the same letter indicate no significant difference between those treatments. Treatments denoted by different letters indicate a significant difference between those treatments at $P < .05$. (B) Quiescent cells were pretreated with DMSO (–AG1478) or tyrphostin AG1478 (+AG1478) for 15 minutes then treated with DMSO as control (Un), 0.1 μM E_2 (E_2), 50 ng/ml EGF (EGF), or 50 μM resveratrol (Res) for 10 minutes. Cells were immediately lysed and equal amounts of protein were separated on SDS-PAGE and Western-blotted for activated EGFR using an anti-phosphoEGFR (Y1173) antibody. The result is representative of two separate experiments.*

When E_2- or EGF-treated cells were pretreated with AG1478 (E_2^+ or EGF^+, respectively), the filopodia number increased significantly compared to unstimulated plus AG1478 (Un^+) treatment. There was a significant ~2-fold increase of filopodia in cells treated with E_2 in the presence of AG1478 (E_2^+) compared to those treated with E_2 in the absence of AG1478 (E_2^-), or in cells treated with EGF in the presence of AG1478 (EGF^+) compared to those treated with EGF in the absence of AG1478 (EGF^-). These increases may also be a direct result of inhibition of EGFR activity or a nonspecific effect of AG1478.

Conversely, AG1478 treatment partially reduced the number of filopodia extended in response to resveratrol (Res^+) by ~1.4-fold when compared to resveratrol alone (Res^-). The number of filopodia in resveratrol-treated cells in the presence of AG1478 (Res^+) was still significantly higher than the number of filopodia in unstimulated cells in the presence of AG1478 (Un^+) (~2-fold) and in E_2-stimulated cells in the presence of AG1478 (E_2^+) (27%), and nearly significant for EGF-stimulated cells in the presence of AG1478 (EGF^+) (24%; $P = .06$). Thus, EGFR signaling appears to play a partial role in resveratrol signaling to the actin cytoskeleton.

To determine the effect of E_2 or resveratrol on EGFR activation, EGFR activity was detected by a monospecific antibody to the phosphotyrosine residue 1173 of EGFR, which is autophosphorylated upon receptor occupation. Our results are limited by the sensitivity of the phosphoEGFR (Y1173) antibody and by the fact that EGFR is phosphorylated on several other phosphotyrosine residues upon activation [19]. As shown in Figure 4*B*, there was a very low intrinsic EGFR activity in quiescent MDA-MB-231 cells. As expected, EGF stimulation resulted in a marked increase in phosphoEGFR levels, which was abolished by AG1478 treatment. Similarly, E_2 induced EGFR activity, but to a lesser degree than EGF, and was inhibited by AG1478. Interestingly, resveratrol also increased EGFR activity but to a lesser degree than E_2. This activity did not appear to be attenuated by AG1478. These results reveal a potential resveratrol-induced AG1478-insensitive fraction of EGFR signaling.

Resveratrol Decreases, Whereas E_2 Increases, Focal Adhesion Number in MDA-MB-231 Cells

Because focal adhesions are commonly associated with cell surface actin structures such as filopodia and lamellipodia [38], cells stimulated with E_2, EGF, or resveratrol were examined for focal adhesions. As shown in Figure 5*b*, EGF increased the number of focal adhesions per cell compared to unstimulated controls in a statistically significant manner by ~2-fold. Increased focal adhesion assembly in response to E_2 was more moderate at 20% but still statistically significant when compared to controls, again demonstrating a similar but not as pronounced effect on the cytoskeleton as EGF. Moreover, the focal adhesions extended in response to E_2 or EGF were observed to be smaller and distributed in lamellipodia, and thus characteristic of motile cells.

Resveratrol treatment resulted in significantly reduced focal adhesion assembly by 36% compared to control (Figure 5). Resveratrol-induced filopodia did not appear to be associated with focal adhesions. To investigate the ability of resveratrol to inhibit E_2 or EGF action, focal adhesion number was quantitated in E_2- or EGF-treated cells after resveratrol treatment. When cells were treated with resveratrol prior to E_2 (Res/E_2), focal adhesions per cell were significantly reduced by 29% when compared to E_2 alone. There was also a 29% reduction in focal adhesion number observed for cells treated with resveratrol prior to EGF (Res/EGF) when compared to EGF alone ($P = .07$). However, focal adhesions in Res/E_2 and Res/EGF treatments were still significantly higher than resveratrol alone by ~1.6- and ~2.8-fold, respectively. These results indicate at least a partial role for ER in resveratrol-mediated inhibition of focal complex assembly.

As shown in Figure 6, AG1478 treatment did not significantly alter the amount of focal adhesions in unstimulated cells. Compared to E_2 alone (E_2^-), treatment with AG1478 (E_2^+) reduced the number of focal adhesions significantly by 41%. The number of focal adhesions per cell in response to EGF (EGF^-) also decreased significantly in the presence of tyrphostin AG1478 (EGF^+) by 56%. The decrease in focal adhesion number in the presence of AG1478 in E_2-treated (E_2^+) or EGF-treated (EGF^+) cells was significantly lower than that of unstimulated cells in the presence of AG1478 (Un^+) by 13% and 9%, respectively. We did not observe a significant reduction in focal adhesion number in the presence of tyrphostin AG1478 (Res^+) in resveratrol-treated cells (Res^-). This result demonstrates that the increased focal adhesions in both E_2- and EGF-treated cells are probably due to EGFR activity.

Resveratrol Decreases FAK Activity in MDA-MB-231 Cells

Because FAK is a signaling intermediate that is recruited to focal adhesions immediately following integrin activation and is also regulated by growth factor receptor stimulation, we determined FAK activity in response to resveratrol. FAK activity in response to resveratrol was determined by analysis of autophosphorylation of FAK following a range of resveratrol concentrations as described in Ref. [29]. In MDA-MB-231 cells, resveratrol at 10 minutes slightly increased FAK activity at 1 and 10 μM. Endogenous FAK activity decreased when treated with 25 μM resveratrol by 34%, at 50 μM by 52%, and at 100 μM by 84% (Figure 7). Thus, the decreased FAK activity in response to resveratrol corresponds to the decreased focal adhesion assembly by resveratrol.

Discussion

Overall, the data presented demonstrate that although E_2 and EGF increase directed cell migration, lamellipodia extension, and focal adhesion assembly, resveratrol exerts an opposite effect by inhibiting cell migration, increasing filopodia formation, and decreasing the number of focal adhesions and FAK activity. Thus, rapid resveratrol signaling to the

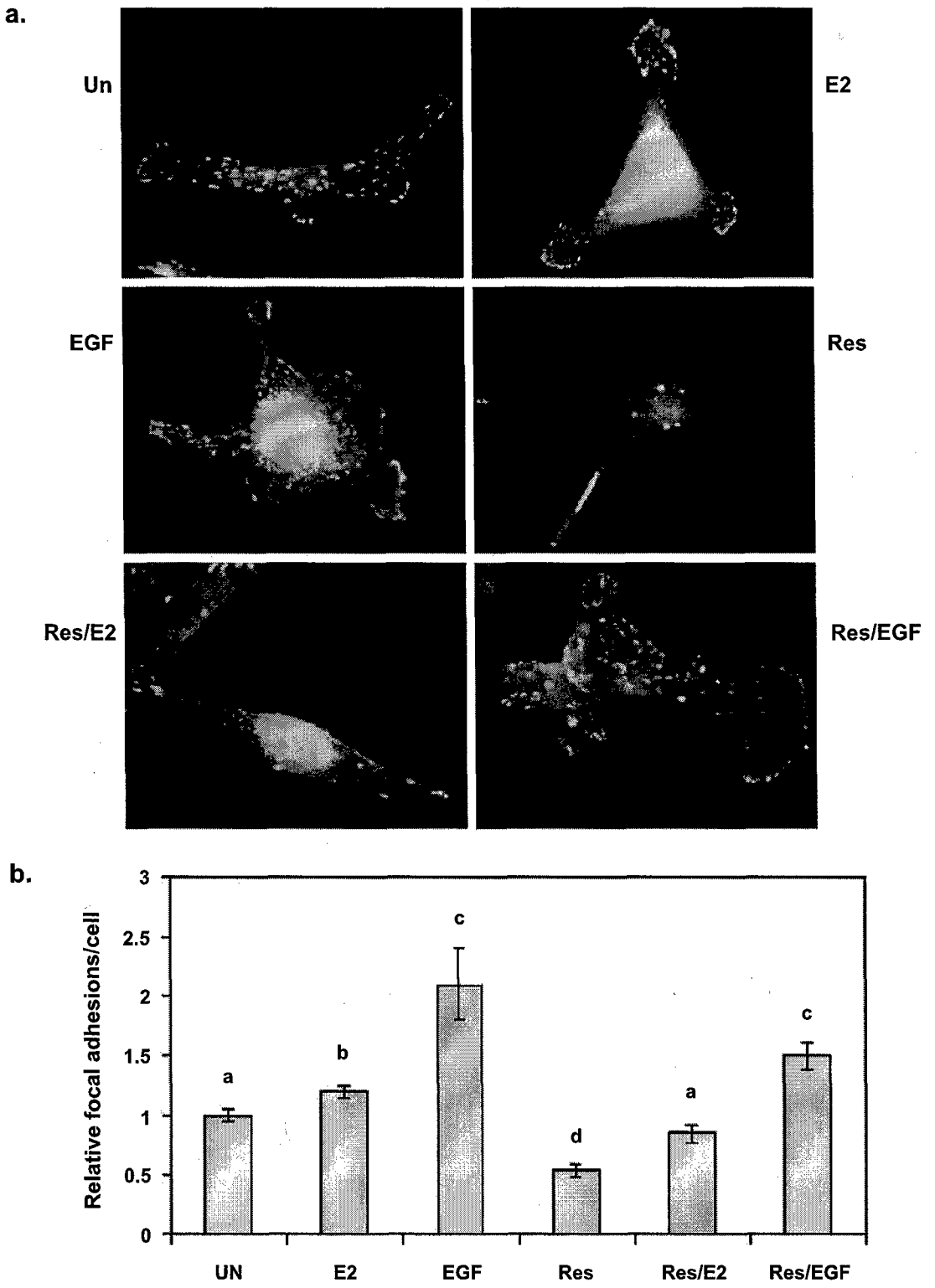

Figure 5. *Effect of E_2, EGF, or trans-resveratrol on focal adhesion assembly in MDA-MB-231 cells. Cells were serum-starved in phenol red–free media for 24 hours and stimulated for 10 minutes with DMSO as control (Un); 0.1 μM E_2 (E_2); 50 ng/ml EGF (EGF); 50 μM resveratrol (Res), pretreated with Res for 10 minutes followed by E_2 for 10 minutes (Res/E_2), or pretreated with Res for 10 minutes followed by EGF for 10 minutes (Res/EGF). Cells were probed with anti-phosphotyrosine primary antibody and FITC-conjugated secondary antibody to visualize focal adhesions. (a) Micrographs at ×600 magnification. (b) Focal adhesion number per cell was quantified for at least 10 microscopic fields per treatment per experiment and made relative to DMSO control (Un). Data expressed as mean focal adhesions ± SEM of three independent experiments. Treatments denoted by the same letter indicate no significant difference between those treatments. Treatments denoted by different letters indicate a significant difference between those treatments at $P < .05$.*

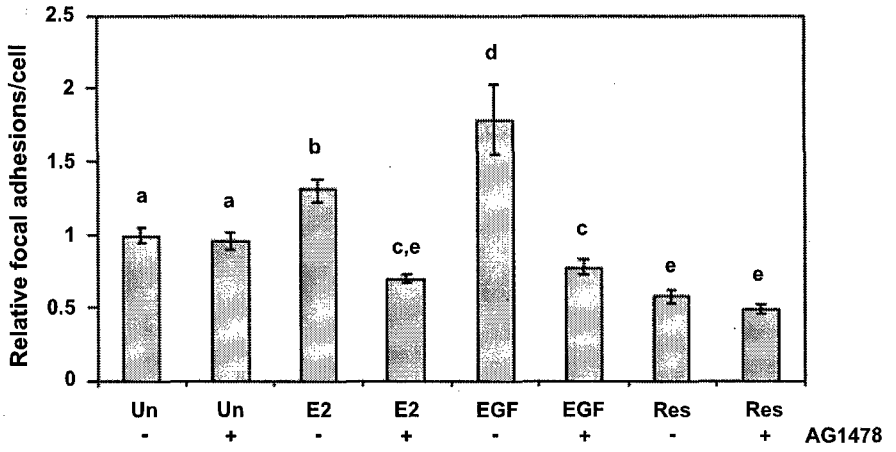

Figure 6. *Effect of tyrphostin AG1478 on focal adhesion assembly in MDA-MB-231 cells. Cells were serum-starved in phenol red–free media for 24 hours and pretreated with vehicle (–AG1478) or tyrphostin AG1478 (+AG1478) for 15 minutes then treated with DMSO as control (Un), 0.1 μM E_2 (E_2), 50 ng/ml EGF (EGF), or 50 μM trans-resveratrol (Res) for 10 minutes. Cells were probed with an anti-phosphotyrosine antibody followed by FITC secondary antibody to visualize focal adhesions. Focal adhesion number was quantified for at least 10 microscopic fields per treatment per experiment and made relative to DMSO control (Un). Data expressed as mean focal adhesions ± SEM of three independent experiments. Treatments denoted by the same letter indicate no significant difference between those treatments. Treatments denoted by different letters indicate a significant difference between those treatments at P < .05.*

cytoskeleton of ERα(–) ER β(+) MDA-MB-231 breast cancer cells appears to function in an antiestrogenic manner.

Cell migration is crucial for cancer cell invasion and metastasis. Herein, we report that resveratrol inhibits cell migration, whereas E_2 acts similar to EGF, a known promoter of cell migration. This resveratrol-induced inhibitory effect on cell migration was still evident when cells were pretreated with resveratrol followed by EGF or E_2. The demonstrated inhibitory effect of resveratrol on directed cell migration is also substantiated by previous studies, which reported that resveratrol blocked the wound healing response of epithelial cells [33,34] and invasion of phorbol myristate acetate–induced cervical cancer cell invasion [36]. This inhibitory effect of resveratrol on directed cell migration could be accounted for by its reported antiproliferative and proapoptotic properties. However, the short exposure times of our experiments (10 minutes for detection of filopodia and focal adhesion assembly and 8 hours for migration) makes this possibility highly unlikely. We have examined the cells (by propidium iodide staining of nuclei) at the end of our experiments and they appear to be viable. Previous reports on the role of resveratrol in apoptosis, where the authors incubated cells for over 24 hours in micromolar concentrations of resveratrol, support our inference that we are monitoring rapid signaling effects and not effects of resveratrol on cell growth [31,53–56].

In fibroblast-like cells such as MDA-MB-231 breast cancer cells, directed motility in response to a chemoattractant is driven by cell polarization, polymerization of actin, and incorporation of cross-linked actin filaments into leading-edge lamellipodia and filopodia that are stabilized by making focal adhesions with the ECM [39,57]. Lamellipodia are considered to be essential for directed cell migration, whereas filopodia are not essential for cell migration but considered to serve as environmental sensors. Filopodia are often reorganized to form leading-edge lamellipodia during cell migration [39]. Thus, the observed cytoskeletal response to resveratrol—where cells appear relatively unpolarized and extend large numbers of unorganized peripheral filopodia that are not associated with focal adhesions and do not get converted to lamellipodia—is hypothesized to be directly responsible for the inhibition of cell migration by resveratrol.

FAK is one of the first signaling intermediates recruited to nascent focal adhesions. FAK-mediated increases in cell proliferation, motility, and invasion have been correlated with tumor malignancy [41,58]. Therefore, the observed reduced FAK activity in response to resveratrol at concentrations of 25 μM and above may also contribute to the inhibitory effect of resveratrol on cell migration. This result coincides with our reported decrease of focal adhesion number with resveratrol at 50 μM. Reduction in focal contacts with the ECM is known to activate apoptosis [58]; thus, the resveratrol-mediated decreased FAK activity and focal adhesion number may represent another pathway by which resveratrol can induce apoptosis.

Rapid E_2 effects have been shown to be mediated through EGFR signaling [11]. EGFR activity is known to regulate pathways leading to actin reorganization by nongenomic mechanisms [50]. EGFR signaling activates the Rho family GTPases, Rac and Cdc42, that regulate extension of cell surface actin structures such as filopodia and lamellipodia [38,59]. Our results show that E_2 acts similarly to EGF and activates EGFR, increases directed cell migration, lamellipodia extension, and focal adhesion assembly. Thus, E_2 and EGF may promote directed cell migration by similar mechanisms that involve extension of lamellipodia with multiple dynamic focal adhesions that support protrusion and traction at the cell front during motility. Recent data have demonstrated that EGF-induced filopodia are always associated with basal focal adhesions and the filopodia that contain shaft adhesions (focal adhesions inside the filopodia) are useful for directed motility by conversion into lamellipodia

[60]. Interestingly, the filopodia extended in response to resveratrol were not associated with basal or shaft adhesions. Thus, the filopodia and focal adhesions assembled in resveratrol-treated cells may be structurally and functionally different from those assembled in response to E_2 or EGF.

The effects of E_2 and resveratrol on the cytoskeleton were only evident in cells that expressed a functional ER isoform and not in the ERαβ(−) SKRB3 cell line. When ERβ(+) MDA-MB-231 breast cancer cells were preincubated in resveratrol and subsequently treated with E_2, the cytoskeletal response of increased filopodia and decreased focal adhesions was similar to that of resveratrol alone, indicating that resveratrol probably exerts its effects on the actin cytoskeleton through ER. The slightly reduced cytoskeletal response of resveratrol combined with E_2, when compared to resveratrol alone, may be due to the lower binding affinity of resveratrol for ERβ compared to E_2 [61]. However, resveratrol has been shown to exert potentially ER-independent effects on modulation of enzymes such as cyclooxygenases and PKC isoforms [25,26]. Thus, some of the effects of resveratrol on the actin cytoskeleton may indicate an ER-independent alternate pathway that blocks or overpasses ER action.

To investigate the potential role of EGFR signaling on resveratrol and E_2 effects on the cytoskeleton, we evaluated the effect of inhibiting the kinase activity of EGFR1 with tyrphostin AG1478. As expected, we observed an AG1478-sensitive EGFR phosphorylation response to both E_2 and EGF. We also observed a reduction in lamellipodia and the number of focal adhesions assembled in response to EGF or E_2 in the presence of AG1478. According to recent reports, E_2 acts through G proteins to activate EGFR-mediated signaling to MAPK and Akt activity pathways that regulate cell proliferation and survival [11,15,62]. The present study has elucidated a novel role for E_2 in rapid signaling to the actin cytoskeleton to promote directed migration that may represent another relevant E_2/EGFR–mediated signaling pathway.

When cells were treated with resveratrol prior to EGF, resveratrol did not directly interfere with EGF for signaling to EGFR to exert effects on the cytoskeleton. However,

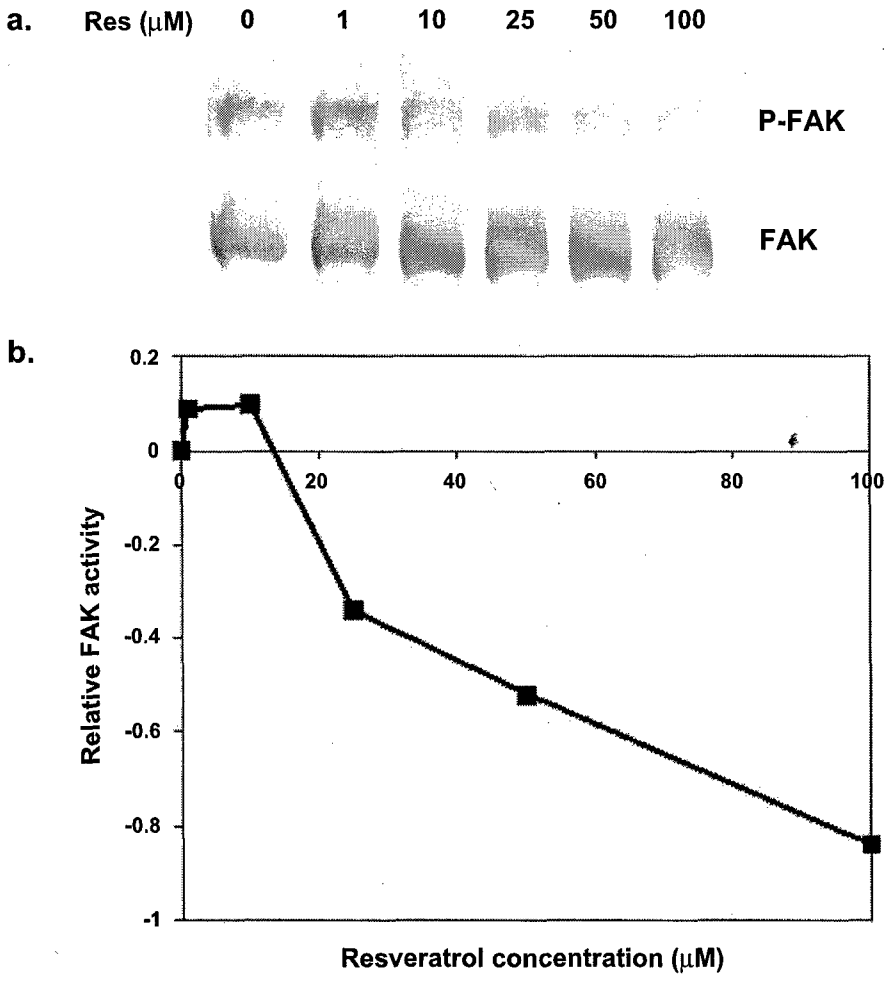

Figure 7. *Effect of resveratrol on FAK activity in MDA-MB-231 cells. Cells were starved for 24 hours in phenol red– and serum-free media and treated with DMSO as vehicle (0) or resveratrol (1, 10, 25, 50, or 100 μM) for 10 minutes. (a) Equal amounts of protein were run on SDS-PAGE and Western-blotted using FAK (N-terminus) or phosphoFAK (tyr-397) antibodies. (b) The integrated density of phosphoFAK and FAK bands from Western blots was quantified. Relative activity is the difference between the ratio of phosphoFAK to total FAK with stimulation, and the ratio of phosphoFAK to FAK without stimulation. The result is representative of three separate experiments.*

addition of AG1478 inhibited a portion of the filopodia extended in response to resveratrol. Thus, at least some of the resveratrol-mediated effects on the actin cytoskeleton are regulated by EGFR signaling. It is also possible that the filopodia extended by resveratrol in the presence of AG1478 may still be under EGFR regulation because resveratrol-induced autophosphorylation of EGFR could not be inhibited by AG1478. This interesting result may be due to an AG1478- insensitive resveratrol-mediated EGFR activation. This possibility is substantiated by a recent report that demonstrates an AG1478-independent activation of EGFR phosphorylation through Src activity [63].

Interestingly, treatment of unstimulated cells with AG1478 (Un^+) resulted in a significant increase in the number of filopodia when compared to unstimulated control (Un^-). This implies that EGFR activity was necessary to prevent filopodia formation on unstimulated cells (Un^-). Moreover, when E_2- or EGF-treated cells were pretreated with AG1478, there was also a significant increase in filopodia formation compared to E_2 or EGF alone. These perplexing results may be explained if EGFR activity is important for the conversion of filopodia into lamellipodia, as previously reported [64]. In our microscopy studies, we have observed that when MDA-MB-231 cells were stimulated with EGF, they responded initially (at 5 minutes) by filopodia extension. These filopodia then merged into lamellipodia, which were completely formed by 10 minutes. Based on this observation, it is possible that AG1478-sensitive EGFR signaling is important for the conversion of filopodia to lamellipodia, which may be regulated by EGF or E_2 through EGFR1 signaling. Thus, in the presence of AG1478, the fraction of filopodia induced by AG1478-insensitive alternate EGFR signaling may remain as filopodia instead of reorganizing into lamellipodia.

The present study makes a significant contribution to the field of nongenomic signaling of E_2 and related compounds by investigation of a novel role for E_2 and resveratrol in cancer cell migration through rapid reorganization of the actin cytoskeleton. For the first time, we demonstrate that resveratrol inhibits cell migration in response to E_2 or EGF. This inhibitory effect of resveratrol on cell migration may be due to rapid filopodia formation without accompanying cell polarization or attachment to the ECM. Taken together, these findings indicate that resveratrol may have the potential to play a preventive role in the progression of ERα(−) ERβ(+) metastatic breast cancers that express EGFR. A growing body of literature suggests that moderate red wine consumption may have several health benefits, including a lowered risk of breast cancer. The data presented implicate an additional beneficial role for resveratrol in the prevention of breast cancer cell invasion and metastasis.

Acknowledgements

We wish to thank Kristen Wall and Drs. Mona Mehdy and Michelle Lane for editorial assistance and Adi Dubash and Lakshmi Krishnamoorthy for technical assistance. We also thank Dr. Delia Brownson for her technical and intellectual contributions to the conception of this project.

References

[1] McDonnell DP and Norris JD (2002). Connections and regulation of the human estrogen receptor. *Science* **296,** 1642–1644.

[2] Cavalieri EL and Rogan EG (2002). A unified mechanism in the initiation of cancer. *Ann NY Acad Sci* **959,** 341–354.

[3] Salih AK and Fentiman IS (2001). Breast cancer prevention: present and future. *Cancer Treat Rev* **27,** 261–273.

[4] Shen Q and Brown PH (2003). Novel agents for the prevention of breast cancer: targeting transcription factors and signal transduction pathways. *J Mammary Gland Biol Neoplasia* **8,** 45–73.

[5] Katzenellenbogen BS, Choi I, Delage-Mourroux R, Ediger TR, Martini PG, Montano M, Sun J, Weis K, and Katzenellenbogen JA (2000). Molecular mechanisms of estrogen action: selective ligands and receptor pharmacology. *J Steroid Biochem Mol Biol* **74,** 279–285.

[6] Nicholson RI, Hutcheson IR, Harper ME, Knowlden JM, Barrow D, McClelland RA, Jones HE, Wakeling AE, and Gee JM (2002). Modulation of epidermal growth factor receptor in endocrine-resistant, estrogen-receptor–positive breast cancer. *Ann NY Acad Sci* **963,** 104–115.

[7] Levin ER (2002). Cellular functions of plasma membrane estrogen receptors. *Steroids* **67,** 471–475.

[8] Belcher SM and Zsarnovszky A (2001). Estrogenic actions in the brain: estrogen, phytoestrogens, and rapid intracellular signaling mechanisms. *J Pharmacol Exp Ther* **299,** 408–414.

[9] Gray GA, Sharif I, Webb DJ, and Seckl JR (2001). Oestrogen and the cardiovascular system: the good, the bad and the puzzling. *Trends Pharmacol Sci* **22,** 152–156.

[10] Coleman KM and Smith CL (2001). Intracellular signaling pathways: nongenomic actions of estrogens and ligand-independent activation of estrogen receptors. *Front Biosci* **6,** D1379–D1391.

[11] Levin ER (2003). Bidirectional signaling between the estrogen receptor and the epidermal growth factor receptor. *Mol Endocrinol* **17,** 309–317.

[12] Winter DC, Taylor C, O'S C, and Harvey BJ (2000). Mitogenic effects of oestrogen mediated by a non-genomic receptor in human colon. *Br J Surg* **87,** 1684–1689.

[13] Driggers PH and Segars JH (2002). Estrogen action and cytoplasmic signaling pathways: Part II. The role of growth factors and phosphorylation in estrogen signaling. *Trends Endocrinol Metab* **13,** 422–427.

[14] Castoria G, Migliaccio A, Bilancio A, Di Domenico M, de Falco A, Lombardi M, Fiorentino R, Varricchio L, Barone MV, and Auricchio F (2001). PI3-kinase in concert with Src promotes the S-phase entry of oestradiol-stimulated MCF-7 cells. *EMBO J* **20,** 6050–6059.

[15] Razandi M, Pedram A, Park ST, and Levin ER (2003). Proximal events in signaling by plasma membrane estrogen receptors. *J Biol Chem* **278,** 2701–2712.

[16] Pietras RJ (2003). Interactions between estrogen and growth factor receptors in human breast cancers and the tumor-associated vasculature. *Breast J* **9,** 361–373.

[17] Laskin JJ and Sandler AB (2004). Epidermal growth factor receptor: a promising target in solid tumours. *Cancer Treat Rev* **30,** 1–17.

[18] Wells A, Kassis J, Solava J, Turner T, and Lauffenburger DA (2002). Growth factor–induced cell motility in tumor invasion. *Acta Oncol* **41,** 124–130.

[19] Mendelsohn J and Baselga J (2000). The EGF receptor family as targets for cancer therapy. *Oncogene* **19,** 6550–6565.

[20] Herrington D (2000). Role of estrogens, selective estrogen receptor modulators and phytoestrogens in cardiovascular protection. *Can J Cardiol* **16,** 5E–9E.

[21] Burns J, Yokota T, Ashihara H, Lean ME, and Crozier A (2002). Plant foods and herbal sources of resveratrol. *J Agric Food Chem* **50,** 3337–3340.

[22] Jang M, Cai L, Udeani GO, Slowing KV, Thomas CF, Beecher CW, Fong HH, Farnsworth NR, Kinghorn AD, Mehta RG, Moon RC, and Pezzuto JM (1997). Cancer chemopreventive activity of resveratrol, a natural product derived from grapes. *Science* **275,** 218–220.

[23] Bhat KP, Lantvit D, Christov K, Mehta RG, Moon RC, and Pezzuto JM (2001). Estrogenic and antiestrogenic properties of resveratrol in mammary tumor models. *Cancer Res* **61,** 7456–7463.

[24] Gehm BD, McAndrews JM, Chien PY, and Jameson JL (1997). Resveratrol, a polyphenolic compound found in grapes and wine, is an agonist for the estrogen receptor. *Proc Natl Acad Sci USA* **94,** 14138–14143.

[25] Bhat KP and Pezzuto JM (2002). Cancer chemopreventive activity of resveratrol. *Ann NY Acad Sci* **957,** 210–229.

[26] Aziz MH, Kumar R, and Ahmad N (2003). Cancer chemoprevention by resveratrol: *in vitro* and *in vivo* studies and the underlying mechanisms (review). *Int J Oncol* **23,** 17–28.

[27] Lu R and Serrero G (1999). Resveratrol, a natural product derived from

grape, exhibits antiestrogenic activity and inhibits the growth of human breast cancer cells. *J Cell Physiol* **179,** 297–304.

[28] Hsieh TC, Burfeind P, Laud K, Backer JM, Traganos F, Darzynkiewicz Z, and Wu JM (1999). Cell cycle effects and control of gene expression by resveratrol in human breast carcinoma cell lines with different metastatic potentials. *Int J Oncol* **15,** 245–252.

[29] Brownson DM, Azios NG, Fuqua BK, Dharmawardhane SF, and Mabry TJ (2002). Flavonoid effects relevant to cancer. *J Nutr* **132,** 3482S–3489S.

[30] Pozo-Guisado E, Lorenzo-Benayas MJ, and Fernandez-Salguero PM (2004). Resveratrol modulates the phosphoinositide 3-kinase pathway through an estrogen receptor alpha-dependent mechanism: relevance in cell proliferation. *Int J Cancer* **109,** 167–173.

[31] Kozuki Y, Miura Y, and Yagasaki K (2001). Resveratrol suppresses hepatoma cell invasion independently of its anti-proliferative action. *Cancer Lett* **167,** 151–156.

[32] Cao Y, Cao R, and Brakenhielm E (2002). Antiangiogenic mechanisms of diet-derived polyphenols. *J Nutr Biochem* **13,** 380–390.

[33] Brakenhielm E, Cao R, and Cao Y (2001). Suppression of angiogenesis, tumor growth, and wound healing by resveratrol, a natural compound in red wine and grapes. *FASEB J* **15,** 1798–1800.

[34] Igura K, Ohta T, Kuroda Y, and Kaji K (2001). Resveratrol and quercetin inhibit angiogenesis *in vitro*. *Cancer Lett* **171,** 11–16.

[35] De LV, Monvoisin A, Neaud V, Krisa S, Payrastre B, Bedin C, Desmouliere A, Bioulac-Sage P, and Rosenbaum J (2001). *trans*-Resveratrol, a grapevine-derived polyphenol, blocks hepatocyte growth factor–induced invasion of hepatocellular carcinoma cells. *Int J Oncol* **19,** 83–88.

[36] Woo JH, Lim JH, Kim YH, Suh SI, Min DS, Chang JS, Lee YH, Park JW, and Kwon TK (2004). Resveratrol inhibits phorbol myristate acetate–induced matrix metalloproteinase-9 expression by inhibiting JNK and PKC delta signal transduction. *Oncogene* **23,** 1845–1853.

[37] Condeelis JS, Wyckoff JB, Bailly M, Pestell R, Lawrence D, Backer J, and Segall JE (2001). Lamellipodia in invasion. *Semin Cancer Biol* **11,** 119–128.

[38] Song RX, Barnes CJ, Zhang Z, Bao Y, Kumar R, and Santen RJ (2004). The role of Shc and insulin-like growth factor 1 receptor in mediating the translocation of estrogen receptor α to the plasma membrane. *Proc Natl Acad Sci* **101,** 2076–2081.

[39] Ridley AJ, Schwartz MA, Burridge K, Firtel RA, Ginsberg MH, Borisy G, Parsons JT, and Horwitz AR (2003). Cell migration: integrating signals from front to back. *Science* **302,** 1704–1709.

[40] Hood JD and Cheresh DA (2002). Role of integrins in cell invasion and migration. *Nat Rev Cancer* **2,** 91–100.

[41] Schlaepfer DD and Mitra SK (2004). Multiple connections link FAK to cell motility and invasion. *Curr Opin Genet Dev* **14,** 92–101.

[42] Kuiper GG, Lemmen JG, Carlsson B, Corton JC, Safe SH, van der Saag PT, van der Burg B, and Gustafsson JA (1998). Interaction of estrogenic chemicals and phytoestrogens with estrogen receptor beta. *Endocrinology* **139,** 4252–4263.

[43] Tong D, Schuster E, Seifert M, Czerwenka K, Leodolte S, and Zeillinger R (2002). Expression of estrogen receptor beta isoforms in human breast cancer tissues and cell lines. *Breast Cancer Res Treat* **71,** 249–255.

[44] Leng J, Klemke RL, Reddy AC, and Cheresh DA (1999). Potentiation of cell migration by adhesion-dependent cooperative signals from the GTPase Rac and Raf kinase. *J Biol Chem* **274,** 37855–37861.

[45] Dharmawardhane S, Schurmann A, Sells MA, Chernoff J, Schmid SL, and Bokoch GM (2000). Regulation of macropinocytosis by p21-activated kinase-1. *Mol Biol Cell* **11,** 3341–3352.

[46] Kaneuchi M, Sasaki M, Tanaka Y, Yamamoto R, Sakuragi N, and Dahiya R (2003). Resveratrol suppresses growth of Ishikawa cells through down-regulation of EGF. *Int J Oncol* **23,** 1167–1172.

[47] Niles RM, McFarland M, Weimer MB, Redkar A, Fu YM, and Meadows GG (2003). Resveratrol is a potent inducer of apoptosis in human melanoma cells. *Cancer Lett* **190,** 157–163.

[48] Pozo-Guisado E, Alvarez-Barrientos A, Mulero-Navarro S, Santiago-Josefat B, and Fernandez-Salguero PM (2002). The antiproliferative activity of resveratrol results in apoptosis in MCF-7 but not in MDA-MB-231 human breast cancer cells: cell-specific alteration of the cell cycle. *Biochem Pharmacol* **64,** 1375–1386.

[49] Tsai EM, Wang SC, Lee JN, and Hung MC (2001). Akt activation by estrogen in estrogen receptor–negative breast cancer cells. *Cancer Res* **61,** 8390–8392.

[50] Chan AY, Raft S, Bailly M, Wyckoff JB, Segall JE, and Condeelis JS (1998). EGF stimulates an increase in actin nucleation and filament number at the leading edge of the lamellipod in mammary adenocarcinoma cells. *J Cell Sci* **111** (Part 2), 199–211.

[51] Lotz M, Wang HH, Cance W, Matthews J, and Pories S (2003). Epidermal growth factor stimulation can substitute for c-Src overexpression in promoting breast carcinoma invasion. *J Surg Res* **109,** 123–129.

[52] Skliris GP, Munot K, Bell SM, Carder PJ, Lane S, Horgan K, Lansdown MR, Parkes AT, Hanby AM, Markham AF, and Speirs V (2003). Reduced expression of oestrogen receptor beta in invasive breast cancer and its re-expression using DNA methyl transferase inhibitors in a cell line model. *J Pathol* **201,** 213–220.

[53] Shih A, Davis FB, Lin HY, and Davis PJ (2002). Resveratrol induces apoptosis in thyroid cancer cell lines *via* a MAPK- and p53-dependent mechanism. *J Clin Endocrinol Metab* **87,** 1223–1232.

[54] Hsieh CT and Wu JM (1999). Differential effects on growth, cell cycle arrest, and induction of apoptosis by resveratrol in human prostate cancer cell lines. *Exp Cell Res* **249,** 109–115.

[55] Bove K, Lincoln DW, and Tsan MF (2002). Effect of resveratrol on growth of 4T1 breast cancer cells *in vitro* and *in vivo*. *Biochem Biophys Res Commun* **291,** 1001–1005.

[56] Damianaki A, Bakogeorgou E, Kampa M, Notas G, Hatzoglou A, Panagiotou S, Gemetzi C, Kouroumalis E, Martin PM, and Castanas E (2000). Potent inhibitory action of red wine polyphenols on human breast cancer cells. *J Cell Biochem* **78,** 429–441.

[57] Small JV, Stradal T, Vignal E, and Rottner K (2002). The lamellipodium: where motility begins. *Trends Cell Biol* **12,** 112–120.

[58] Schaller MD (2001). Biochemical signals and biological responses elicited by the focal adhesion kinase. *Biochim Biophys Acta* **1540,** 1–21.

[59] Burridge K and Wennerberg K (2004). Rho and Rac take center stage. *Cell* **116,** 167–179.

[60] Steketee MB and Tosney KW (2002). Three functionally distinct adhesions in filopodia: shaft adhesions control lamellar extension. *J Neurosci* **22,** 8071–8083.

[61] Bhat KP and Pezzuto JM (2001). Resveratrol exhibits cytostatic and antiestrogenic properties with human endometrial adenocarcinoma (Ishikawa) cells. *Cancer Res* **61,** 6137–6144.

[62] Stoica GE, Franke TF, Moroni M, Mueller S, Morgan E, Iann MC, Winder AD, Reiter R, Wellstein A, Martin MB, and Stoica A (2003). Effect of estradiol on estrogen receptor-alpha gene expression and activity can be modulated by the ErbB2/PI3-K/Akt pathway. *Oncogene* **22,** 6054–6067.

[63] Sato K, Nagao T, Iwasaki T, Nishihira Y, and Fukami Y (2003). Src-dependent phosphorylation of the EGF receptor Tyr-845 mediates Stat–p21waf1 pathway in A431 cells. *Genes Cells* **8,** 995–1003.

[64] Steketee MB and Tosney KW (2002). Three functionally distinct adhesions in filopodia: shaft adhesions control lamellar extension. *J Neurosci* **22,** 8071–8083.